

Towards a fitting procedure for deeply virtual Compton scattering at next-to-leading order and beyond

K. Kumerički^{a,b}, D. Müller^{b,c,d}, and K. Passek-Kumerički^{b,e}

^a*Department of Physics, Faculty of Science, University of Zagreb
P.O.B. 331, HR-10002 Zagreb, Croatia*

^b*Institut für Theoretische Physik, Universität Regensburg
D-93040 Regensburg, Germany*

^c*Department of Physics and Astronomy, Arizona State University
Tempe, AZ 85287-1504, USA*

^d*Institut für Theoretische Physik II, Ruhr-Universität Bochum
D-44780 Bochum, Germany*

^e*Theoretical Physics Division, Rudjer Bošković Institute
P.O.Box 180, HR-10002 Zagreb, Croatia*

Abstract

Combining dispersion and operator product expansion techniques, we derive the conformal partial wave decomposition of the virtual Compton scattering amplitude in terms of complex conformal spin to twist-two accuracy. The perturbation theory predictions for the deeply virtual Compton scattering (DVCS) amplitude are presented in next-to-leading order for both conformal and modified minimal subtraction scheme. Within a conformal subtraction scheme, where we exploit predictive power of conformal symmetry, the radiative corrections are presented up to next-to-next-to-leading order accuracy. Here, because of the trace anomaly, the mixing of conformal moments of generalized parton distributions (GPD) at the three-loop level remains unknown. Within a new proposed parameterization for GPDs, we then study the convergence of perturbation theory and demonstrate that our formalism is suitable for a fitting procedure of DVCS observables.

PACS numbers: 11.25.Db, 12.38.Bx, 13.60.Fz

Keywords: deeply virtual Compton scattering, next-to-next-to-leading order corrections, fitting procedure, generalized parton distributions, conformal symmetry

Contents

1	Introduction	3
2	Compton scattering tensor and Compton form factors	7
2.1	General formalism	7
2.2	Analyticity and dispersion relations	9
3	Operator product expansion to twist-two accuracy	11
3.1	General form of the operator product expansion at twist-two level	12
3.2	Employing the dispersion relation	15
3.2.1	Mellin–Barnes representation for CFFs	15
3.2.2	Discussing the subtraction constant	17
3.3	Representation of CFFs in terms of conformal moments	20
3.3.1	Lessons from a toy example	21
3.3.2	Complex conformal partial wave expansion	23
3.3.3	Mellin–Barnes representation of conformal GPD moments	25
4	DVCS amplitude up to next-to-next-to-leading order	26
4.1	Conformal OPE prediction and beyond	27
4.2	Perturbative expansion of Compton form factors	30
4.2.1	Flavor nonsinglet Wilson coefficients	32
4.2.2	Flavor singlet Wilson coefficients	33
4.2.3	Expansion of the evolution operator	35
4.3	$\overline{\text{MS}}$ results up to NLO order	37
5	Parameterization of GPDs	40
5.1	SO(3) partial wave decomposition of conformal GPD moments	41
5.2	Ansatz for SO(3) partial wave amplitudes	44
5.3	Modelling of conformal GPD moments	47
6	Perturbative corrections of the DVCS cross section	52
6.1	A simplified generic ansatz for conformal GPD moments	53
6.2	Compton form factors to LO accuracy	55
6.3	Size of NLO radiative corrections: $\overline{\text{CS}}$ versus $\overline{\text{MS}}$ scheme	57
6.3.1	Flavor nonsinglet sector	59
6.3.2	Flavor singlet sector	65
6.4	Radiative corrections beyond NLO	68

7	Fitting procedure of experimental data	73
7.1	Setting the scene	74
7.2	Lessons from fits	76
7.3	Comparison and partonic interpretation of the results	79
8	Conclusions	82
A	Normalization of Wilson coefficients and anomalous dimensions	84
B	Bases in the flavor singlet sector	87
C	Momentum fraction representation versus conformal moments	88
C.1	Evaluation of conformal moments	88
C.2	Conformal moments for the gluon part	89

1 Introduction

The partonic content of the nucleon, other hadrons, and nuclei has been studied within hard inclusive processes over almost four decades. Since partons are confined by the strong force, their response to, e.g., an electromagnetic probe cannot be directly accessed in experiments; the long-range interaction in their environment remains essential. Fortunately, based on factorization theorems [1], the short- and the long-distance interaction can often be separated. The former depends on the specific process and can be systematically computed using perturbation theory, while the latter is encoded in process-independent nonperturbative quantities, e.g., parton densities. These densities have a semiclassical interpretation within the parton picture, which is, however, not independent of the conventions used in the evaluation of short-distance physics. Together with an increasing amount of experimental data, the perturbative factorization approach leads to a deeper and more precise insight into the hadronic world, which is essential even for the search of new physics.

Most importantly, the factorization approach is a tool that relates observables measured in various inclusive processes and thus has a predictive power. The improvement of quantitative predictions requires, besides precise experimental measurements, also a refinement of the theoretical approach. This includes both the perturbative evaluation of radiative corrections to the short-distance physics at higher orders and an understanding of the so-called power suppressed corrections, which alter the factorization theorems. In particular, the effort in the perturbative sector, which reached the three-loop level, led to a quantitative understanding of the inclusive QCD physics at the level of a few percent. In practice, parton densities have for a long time been extracted via a theoretically motivated functional ansatz, see, e.g., Ref. [2], depending on a number of parameters, that is globally fitted to experimental data [3, 4, 5, 6, 7, 8, 9, 10]. In such fits, based on traditional χ^2 minimization, the error estimation using the hypothesis of linear error propagation has become standard in the last few years [3, 4, 5, 8]. To overcome drawbacks of this traditional method, alternative frameworks of statistical inference [11] and neural network parameterization [12, 13] have been proposed.

In contrast to inclusive processes, the understanding and the theoretical description of exclusive ones remain poor. In general, there is a lack of experimental data and so the underlying theoretical framework, e.g., the factorization of hadronic amplitudes in terms of distribution amplitudes [14, 15, 16, 17, 18], cannot be quantitatively tested. Moreover, the theoretical framework at the next-to-leading order (NLO) is developed for only a few processes and the applicability of the factorization approach at accessible scales is controversially discussed in the literature [19, 20, 21]. The old problem of whether all valence partons take part in the short-distance process or only the active one (Feynman mechanism) remains open. A way out of this theoretical dilemma might be

provided by the use of light-cone sum rules [22, 23].

Some years ago a new nonperturbative generalized distribution amplitude¹ was proposed as a means to access the partonic content of hadrons [24, 25]. In particular, it was theoretically studied in connection with deeply virtual Compton scattering (DVCS), where the partonic content of a hadron is probed by two photons. To leading order, the underlying picture portrays a parton which is probed by a virtual photon, travels near the light cone, emits a real photon, and remains a constituent of the probed hadron. The partonic probability amplitude for such a process is given by the generalized parton distribution (GPD) [26, 27, 28]. It has soon been realized that diffractive vector meson electroproduction [29], measured in the collider experiments H1 and ZEUS at DESY (see, e.g., Refs. [30, 31, 32]), can be described in terms of GPDs [33, 34], too. The usefulness of the GPDs has also been widely realized in connection with the spin problem, since they encode the angular momentum carried by the individual parton species, as explicated by the Ji's sum rule [26]. During the last decade they have become an attractive object for theoretical and experimental investigations. Today, they are considered as a new concept that provides a link between different fields: exclusive and inclusive processes, perturbative and nonperturbative physics (e.g., lattice simulations [35, 36, 37, 38, 39, 40] and model building [41, 42, 43, 44, 45, 46, 47, 48, 49]). For comprehensive reviews, see Refs. [50, 51].

In contrast to parton densities, which depend on the longitudinal momentum fraction of the probed parton and on the resolution scale, GPDs encode also transversal degrees of freedom. This allows a three-dimensional probabilistic interpretation of the parton distribution either in the infinite momentum [52, 53, 54, 55, 56] or in the rest frame [57]. Indeed, to some extent this information can already be extracted from present experiments. The main theoretical complication arises from the fact that GPDs depend on two longitudinal momentum fractions: x and skewness η , which are related to the s - and t -channel exchanges, respectively. The former one is either integrated out during the convolution (in the real part of the scattering amplitude) or identified with the latter one (in the imaginary part of the scattering amplitude). Even if we precisely knew the modulus and the phase of hard exclusive leptonproduction scattering amplitudes², a complete reconstruction of the GPD would not be uniquely possible, except with ideal data and employing evolution. We note that it was pointed out that already the Fourier transform of the DVCS

¹This notion, proposed in Ref. [24], stood for expectation values of light-ray operators sandwiched between vacuum and final hadronic or between initial and final hadronic states. Today, it denotes the distribution corresponding to the former expectation value, while the distribution corresponding to the latter one is called generalized parton distribution.

²We remark that the scan of the GPD shape in a certain region of the momentum fraction plane is possible only in the so-called double DVCS process [58, 59, 60] by variation of the incoming photon virtuality and the lepton pair mass.

amplitude with respect to the skewness parameter provides an image of the target with respect to the longitudinal degrees of freedom [61, 62]. The problem of deconvolution can be overcome to some extent either by a realistic model, which we at present do not have, or by a hypothesis about the form of skewness dependence. In the case of those GPDs that in the forward kinematics reduce to parton densities, such a hypothesis can be tested by statistical analysis of inclusive and exclusive data, e.g., by means of the χ^2 criteria. Certainly, if the skewness problem could be solved, the extrapolation to the $\eta \rightarrow 0$ case would be simple and would be a step towards the experimental access of both Ji's spin sum rule and a three-dimensional picture of the proton.

Among processes which enable us to access GPDs at present experiments, the DVCS is considered the theoretically cleanest one. Indeed, the first experimental DVCS data on the beam spin asymmetry in fixed target experiments [63, 64], or the cross section, measured by the H1 and ZEUS collaborations [65, 66, 67], could be successfully understood even in terms of oversimplified GPD ansätze [68]. In contrast, the normalization of the cross sections of vector-meson electroproduction, predicted to LO in the collinear factorization approach, in general overshoots the H1 and ZEUS data. This process is widely believed to be affected by power-suppressed contributions. They are mainly related to the transversal size of the meson and appear so separately as factorized contributions, which might be modelled by themselves [69, 70]. On the other hand, perturbative higher-order corrections for this process are large and reduce the size of the predicted cross sections [71]. However, to the best of our knowledge, a global NLO analysis of all available experimental data has not been achieved so far. In our opinion, this is the only possible way of confronting the collinear approach with experimental findings and before this is done, a judgement about this approach can hardly be drawn.

With increasing amount and precision of experimental DVCS data [72, 73, 74, 75], there arises a need for a better theoretical understanding of this process. Certainly, for the phenomenology of GPDs it is essential to include and estimate perturbative and power-suppressed contributions as well as to introduce a flexible parameterization of them. Besides a qualitative or a semianalytic understanding of observables in dependence on GPDs, see here, for instance, Refs. [68, 76], also fast and stable numerical routines are needed for a fitting procedure.

So far the perturbative contributions to the DVCS have been worked out to NLO accuracy [77, 78, 79, 80, 81], including the evolution [82, 83, 84]. There exist numerical routines in the momentum fraction space [85, 86, 87]. In this space the GPD ansatz is given in terms of a spectral function [24, 88]. Here one has to model the functional dependencies on two momentum fraction variables and the momentum transfer squared. Alternatively, one can work with the conformal moments of GPDs [89], which diagonalize the LO evolution equation. This offers the possibility of a flexible GPD parameterization, which covers the complete set of degrees of freedom and

makes direct contact with lattice results. The problem here is rather to find an appropriate and physically motivated truncation in the parameter space. A partial wave expansion with respect to the angular momentum, the so-called dual GPD parameterization, has been proposed [90], where the partial wave amplitudes are those of the mesonic exchanges in the t -channel with given angular momentum. This also allows one to use the angular momentum as an expansion parameter [91] and Regge phenomenology as a guideline towards realistic GPD ansätze.

Unfortunately, if one works with discrete conformal moments, the GPDs are expanded in terms of (mathematical) distributions, which live only in the so-called central region ($-\eta \leq x \leq \eta$) of the whole support ($-1 \leq x \leq 1$). This is quite analogous to the expansion of parton densities with respect to the Dirac function and its derivatives, which live at the point $x = 0$. A variety of approaches have been proposed to resum this formal series and thus to restore the correct support of GPDs: smearing the expansion [89, 90], an integral transformation [92, 93], Fourier transformation in the light-cone position space [94, 95, 96, 97], and a Sommerfeld–Watson transformation [98]. Note that all these approaches should be mathematically equivalent and, in particular, those of Refs. [96] and [98] lead to essentially the same representation. So far only the smearing method has been extended to NLO accuracy in the $\overline{\text{MS}}$ scheme; however, speed and stability remain restricted [99, 100].

We believe that the GPD formalism that is based on the Sommerfeld–Watson transformation and Mellin–Barnes integral representation [98] is suitable to satisfy the requirements which we spelled out. Moreover, we can employ the power of conformal symmetry to investigate the convergence of the perturbative series up to NNLO [101, 102]. Therefore, the fivefold goal of this article is

- to present a detailed derivation, based on analyticity and short-distance operator product expansion, of the Mellin–Barnes integral representation for the twist-two Compton form factors (CFFs),
- to present the radiative corrections up to NNLO obtained using the predictive power of conformal symmetry, as well as to present the radiative corrections in the standard $\overline{\text{MS}}$ scheme up to NLO accuracy, including the evolution,
- to propose an intuitive ansatz for conformal GPD moments,
- to investigate the convergency properties of the perturbative expansion,
- to demonstrate the usefulness of the GPD fitting procedure based on this formalism, as well as to discuss the requirements for a GPD ansatz.

The outline is as follows. In Sect. 2 we introduce the Compton scattering tensor and its decomposition in leading twist-two Compton form factors (CFFs). Employing their analytic properties, we derive dispersion relations for CFFs. In Sect. 3 these dispersion relations together with the short-distance operator product expansion are used to represent the CFFs as Mellin–Barnes integrals. To diagonalize the evolution operator, we then introduce the conformal partial wave expansion of CFFs. In Sect. 4 we employ conformal symmetry in the perturbative QCD sector to find the Wilson coefficients for CFFs, expanded up to NNLO in the coupling. We also employ the conformal partial wave expansion for the representation of the NLO corrections in the $\overline{\text{MS}}$ scheme. An intuitive ansatz for the conformal GPD moments is introduced in Sect. 5. It is based on the internal duality of GPDs and consists of an $\text{SO}(3)$ partial wave expansion in the t -channel. In Sect. 6 we discuss the convergency of the perturbative series. We then demonstrate in Sect. 7 on hand of the DVCS cross section, measured at high energies by the H1 and ZEUS collaborations, that our formalism is suitable for a fitting procedure that is used to extract GPD information from experimental data. Finally, we summarize and conclude. Three appendices contain details on our conventions and the evaluation of conformal moments.

2 Compton scattering tensor and Compton form factors

2.1 General formalism

We are interested in the perturbative description of hard photon leptonproduction off a hadronic target, e.g., a proton. Besides the Bethe-Heitler bremsstrahlungs process, parameterized by electromagnetic form factors, the DVCS process contributes [24, 26, 28]. The amplitude of the latter is expressed by the Compton tensor. This tensor is defined in terms of the time-ordered product of two electromagnetic currents, sandwiched between the initial and final hadronic state,

$$T_{\mu\nu}(q, P, \Delta) = \frac{i}{e^2} \int d^4x e^{ix \cdot q} \langle P_2, S_2 | T j_\mu(x/2) j_\nu(-x/2) | P_1, S_1 \rangle, \quad (1)$$

where $q = (q_1 + q_2)/2$ (μ and q_2 refer to the outgoing real photon), while $P = P_1 + P_2$ and $\Delta = P_2 - P_1$. The incoming photon has a large virtuality $q_1^2 = -Q^2$ and we require that, in the limit $-q^2 = Q^2 \rightarrow \infty$, the scaling variables

$$\xi = \frac{Q^2}{P \cdot q}, \quad \eta = -\frac{\Delta \cdot q}{P \cdot q}, \quad (2)$$

and the momentum transfer squared Δ^2 are fixed. The dominant contributions arise then from the light-cone singularities of the time-ordered product. This kinematics is a generalization of the Bjorken limit, well-known from deep inelastic scattering (DIS). In particular, if the final photon is

on-shell, i.e., for the process we are interested in, the skewness parameter η and the Bjorken-like scaling parameter ξ are equal to twist-two accuracy, i.e., $\eta = \xi + \mathcal{O}(1/Q^2)$. Note that in the following we assume $\Delta \cdot P = P_2^2 - P_1^2 = 0$.

In the generalized Bjorken limit, we can employ the OPE to evaluate the Compton scattering tensor (1). Its dominant part is given by matrix elements of leading twist-two operators. The use of the light-cone expansion, a resummed version of the short-distance operator product expansion, allows a straightforward evaluation [24]. On the other hand, one might employ the short-distance expansion, which yields a Taylor expansion of the Compton scattering tensor with respect to the variable $1/\xi$. Since this expansion converges only in the unphysical region, i.e., $\xi > 1$, we need in addition a dispersion relation that connects the Mellin moments in the physical region with the short-distance expansion. This technique well-known from deep inelastic scattering has been adopted for nonforward kinematics, e.g., in Ref. [103]. Below we use it within a special short-distance OPE, namely, the conformally covariant one.

Let us introduce a parameterization of the Compton tensor in terms of the so-called Compton form factors (CFFs), which has been employed for the evaluation of the differential cross section [104, 68]. To leading twist-two accuracy it reads

$$T_{\mu\nu}(q, P, \Delta) = -\tilde{g}_{\mu\nu}^T \frac{q_\sigma V^\sigma}{P \cdot q} - i\tilde{\epsilon}_{\mu\nu q P} \frac{q_\sigma A^\sigma}{(P \cdot q)^2} + \dots, \quad (3)$$

where $\tilde{g}_{\mu\nu}^T$ and $\tilde{\epsilon}_{\mu\nu q P} \equiv \tilde{\epsilon}_{\mu\nu\alpha\beta} q^\alpha P^\beta$ are the transversal part of the metric³ and the Levi-Civita tensor, respectively, which are contracted $\tilde{X}_{\mu\nu} \equiv \mathcal{P}_{\mu\rho} X^{\rho\sigma} \mathcal{P}_{\sigma\nu}$ with projectors

$$\mathcal{P}^{\alpha\beta} = g^{\alpha\beta} - \frac{q_1^\alpha q_2^\beta}{q_1 \cdot q_2} \quad (4)$$

to ensure current conservation [104]. The ellipsis indicate terms that are finally power suppressed⁴ in the DVCS amplitude, or are determined by the gluon transversity GPD. The latter is a twist-two contribution that enters at NLO, evaluated in [105, 81, 106], and is tied to a specific azimuthal angular dependence in the cross section [107, 68]. Hence, using an appropriate definition of observables, it can be separated from the other twist-two (and twist-three) contributions. For the time being we consider its perturbative corrections beyond NLO more as an academic issue and will not evaluate it here.

In the parity even sector the vector

$$V^\sigma = \overline{U}(P_2, S_2) \left(\mathcal{H} \gamma^\sigma + \mathcal{E} \frac{i\sigma^{\sigma\rho} \Delta_\rho}{2M} \right) U(P_1, S_1) + \dots, \quad (5)$$

³The transversal part of the metric tensor reads $g_{\mu\nu}^T = g_{\mu\nu} - n_\mu n'_\nu - n_\nu n'_\mu$, where $n_\mu = (1, 0, 0, \pm 1)/\sqrt{2}$ and $n'_\mu = (1, 0, 0, \mp 1)/\sqrt{2}$ and at twist-2 we have $n_\mu n'_\nu = q_\mu P_\nu / (q \cdot P)$.

⁴Here we have neglected a further twist-two Compton form factor that can occur for virtual photons that are longitudinal polarized. Obviously, it does not contribute to the DVCS amplitude, where the final photon state is of course transversally polarized.

is decomposed into the target helicity conserving CFF \mathcal{H} and the helicity flip one \mathcal{E} . Analogously, the axial-vector

$$A^\sigma = \overline{U}(P_2, S_2) \left(\tilde{\mathcal{H}} \gamma^\sigma \gamma_5 + \tilde{\mathcal{E}} \frac{\Delta^\sigma \gamma_5}{2M} \right) U(P_1, S_1) + \dots, \quad (6)$$

is parameterized in terms of $\tilde{\mathcal{H}}$ and $\tilde{\mathcal{E}}$, where again higher-twist contributions are neglected. The normalization of the spinors is $\overline{U}(P, S) \gamma^\sigma U(P, S) = 2P^\sigma$.

It is convenient to introduce the nomenclature

$$\mathcal{F} = \{\mathcal{F}^V, \mathcal{F}^A\}, \quad \mathcal{F}^V = \{\mathcal{H}, \mathcal{E}\}, \quad \mathcal{F}^A = \{\tilde{\mathcal{H}}, \tilde{\mathcal{E}}\}, \quad (7)$$

with the following choice of arguments: $\mathcal{F}(\nu, \vartheta, \Delta^2, Q^2)$. The variable

$$\nu = \frac{P \cdot q}{\sqrt{P^2}} = \frac{1}{\xi} \frac{Q^2}{\sqrt{P^2}} = \frac{W^2 - u}{2\sqrt{P^2}} \quad \text{with} \quad W^2 = (P_1 + q_1)^2, \quad u = (P_1 - q_2)^2 \quad (8)$$

is in the Breit frame simply given by q_0 , the conjugate variable of the time x_0 . It is an appropriate generalization of the photon energy in the rest frame for DIS. Instead of the skewness variable η , depending on ν , we will employ the virtual photon mass asymmetry

$$\vartheta = \frac{q_1^2 - q_2^2}{q_1^2 + q_2^2} = \frac{\eta}{\xi} + \mathcal{O}(\Delta^2/Q^2). \quad (9)$$

Obviously, $\vartheta = 0$ in the forward case and $\vartheta = 1$ for DVCS.

2.2 Analyticity and dispersion relations

Based on the analyticity of the Compton tensor (1), now we derive a dispersion relation for the CFFs, introduced in Eqs. (5) and (6). From the definition of the Compton tensor (1), we read off for complex valued q the following properties, see, for instance, Refs. [108, 109],

$$[T_{\mu\nu}(q, P, \Delta; S_1, S_2)]^* = T_{\nu\mu}(q^*, P, -\Delta; S_2, S_1), \quad (10)$$

$$T_{\mu\nu}(q, P, \Delta; S_1, S_2) = T_{\nu\mu}(-q, P, \Delta; S_1, S_2). \quad (11)$$

The former of these equations can be viewed as a generalization of the Schwarz reflection principle, whereas the latter equation stems from crossing symmetry under the Bose exchange $(q_1, q_2, \mu, \nu) \leftrightarrow (-q_2, -q_1, \nu, \mu)$. Furthermore, in the spacelike region, i.e., $0 < Q^2$, and for $0 \leq -\Delta^2 \leq -\Delta_{\text{Max}}^2$, where the upper limit is constrained by kinematics, the Compton tensor is holomorphic in ν except for the branch cuts along the real axis. Its absorptive part

$$T_{\mu\nu}(q, P, \Delta; S_1, S_2) - [T_{\nu\mu}(q, P, -\Delta; S_2, S_1)]^* \equiv 4\pi i W_{\mu\nu}(q, P, \Delta; S_1, S_2), \quad (12)$$

is given by the commutator of the electromagnetic currents

$$W_{\mu\nu} = \frac{1}{4\pi e^2} \int d^4x e^{ix \cdot q} \langle P_2, S_2 | [j_\mu(x/2), j_\nu(-x/2)] | P_1, S_1 \rangle. \quad (13)$$

Finally, using the generalized Schwarz reflection principle (10), we have for the discontinuity, now expressed in terms of the more appropriate variable ν ,

$$\text{Disc } T_{\mu\nu} \equiv T_{\mu\nu}(\nu + i\epsilon, \dots) - T_{\mu\nu}(\nu - i\epsilon, \dots) = 4\pi i W_{\mu\nu}. \quad (14)$$

The spectral representation of the hadronic tensor $W_{\mu\nu}$ and baryon number conservation tell us that this discontinuity does not vanish for $|\nu| \geq \nu_{\text{cut}}$ with $\nu_{\text{cut}} = (4Q^2 + \Delta^2)/4\sqrt{P^2}$, see Fig. 1.

Obviously, these analytic properties hold for the CFFs, too. The crossing relation (11) implies the symmetry relations

$$\mathcal{F}^V(\nu, \dots) = \mathcal{F}^V(-\nu, \dots), \quad \mathcal{F}^A(\nu, \dots) = -\mathcal{F}^A(-\nu, \dots). \quad (15)$$

To fix the form of the dispersion relation, we should estimate the high-energy behavior of the CFFs from the common arguments of Regge phenomenology. The leading meson trajectories give rise to a $\nu^{\alpha_M(\Delta^2)}$ behavior with $\alpha_M(\Delta^2) \leq \alpha_M(0) \simeq 1/2$ for $\Delta^2 < 0$. Thus, for the meson-exchange induced part it is appropriate to use Cauchy's theorem with one subtraction, i.e., cf. Fig. 1(a),

$$\mathcal{F}(\nu, \vartheta, \Delta^2, Q^2) = \frac{1}{2\pi i} \oint_{-\nu_{\text{cut}}+0}^{\nu_{\text{cut}}-0} \frac{d\nu'}{\nu'} \frac{\nu}{\nu' - \nu} \mathcal{F}(\nu', \vartheta, \Delta^2, Q^2) + \mathcal{C}(\vartheta, \Delta^2, Q^2). \quad (16)$$

In the axial-vector case, the subtraction constant $\mathcal{C}(\dots) \equiv \mathcal{F}(\nu = 0, \dots)$ is zero for symmetry reasons, see Eq. (15). In the flavor singlet sector of parity even CFFs \mathcal{F}^V the pomeron exchange appears. It induces a stronger power-like growth with an exponent $\alpha_{\mathbb{P}}(\Delta^2)$, where $\alpha_{\mathbb{P}}(\Delta^2) \leq \alpha_{\mathbb{P}}(0) \simeq 1$. For this contribution a second subtraction should in principle be introduced in Eq. (16), giving rise to a $\nu \mathcal{C}'$ term. However, since a parity even CFFs is a even function in ν , this constant \mathcal{C}' is zero. Hence, the analytic properties allow us to derive a singly subtracted dispersion relation. Inflating the integration path to infinity, pictured in Fig. 1(b), we are left with a path that encircles the cuts on the real axis. Picking up the discontinuity and employing now the symmetry (15), we find for all CFFs and $|\xi| > 1$ the dispersion relation⁵

$$\mathcal{F}(\xi, \vartheta, \Delta^2, Q^2) = \frac{1}{\pi} \int_0^1 d\xi' \left(\frac{1}{\xi - \xi'} \mp \frac{1}{\xi + \xi'} \right) \Im \mathcal{F}(\xi' - i0, \vartheta, \Delta^2, Q^2) + \mathcal{C}(\vartheta, \Delta^2, Q^2). \quad (17)$$

Here, the upper and lower sign belong to the vector (V) and axial-vector (A) case, respectively, where in the latter case the subtraction constant \mathcal{C} vanishes. We have also used the fact that the imaginary part $\Im \mathcal{F}(\xi', \dots)$ has the support $|\xi'| \leq 1/(1 + \Delta^2/4Q^2) \lesssim 1$.

⁵Although the function \mathcal{F} is now expressed in terms of ξ rather than ν , for simplicity we do not introduce a new notation.

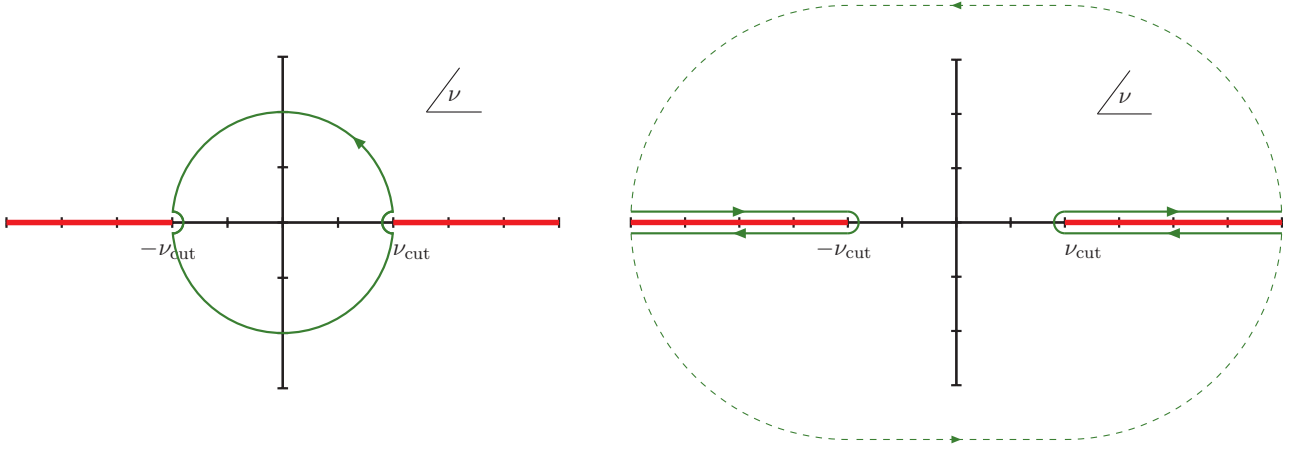


Figure 1: The integration contour used in Eq. (16) and its deformation, employed to derive the dispersion relation (17), are sketched in the left and right panel, respectively. Contribution of dashed segments vanishes.

The dispersion relation (17) will be used to relate the short-distance OPE, given as a Taylor series with respect to the variable $\omega = 1/\xi < 1$, to the imaginary part of the CFFs in the physical region. If we choose to write the Taylor expansion of the CFFs with respect to ω as

$$\mathcal{F}(\xi, \vartheta, \Delta^2, Q^2) = \sum_{j=0}^{\infty} [1 \mp (-1)^j] \omega^{j+1} \mathcal{F}_j(\vartheta, \Delta^2, Q^2) + \mathcal{C}(\vartheta, \Delta^2, Q^2), \quad (18)$$

taking into account the symmetry relation (15), we arrive at

$$\mathcal{F}_j(\cdots) \equiv \frac{1}{2(j+1)!} \frac{d^{j+1}}{d\omega^{j+1}} \mathcal{F}(1/\omega, \cdots) \Big|_{\omega=0} = \frac{1 \mp (-1)^j}{2\pi} \int_0^1 d\xi \xi^j \Im \mathcal{F}(\xi - i0, \cdots). \quad (19)$$

This relation is valid for $0 \leq j$, where the subtraction term does not contribute. The latter enters for $j = -1$, for which the first term in Eq. (17) drops out, and so we have the trivial identity

$$\mathcal{C}(\vartheta, \Delta^2, Q^2) \equiv \mathcal{F}^V(1/\omega, \vartheta, \Delta^2, Q^2) \Big|_{\omega=0}. \quad (20)$$

3 Operator product expansion to twist-two accuracy

Using the conformal OPE, presented in Sect. 3.1, and the dispersion relation, we derive in Sect. 3.2 a Mellin–Barnes representation for CFFs. Then we give a detailed discussion of the subtraction constant, which appears in a certain set of CFFs. On hand of a simple toy GPD model we investigate some mathematical aspects of the Mellin–Barnes representation. In Sect. 3.3 we present the CFFs as conformal partial wave expansion in terms of conformal GPD moments, depending on the complex conformal spin. We also provide the rotation of common Mellin GPD moments to the conformal ones.

3.1 General form of the operator product expansion at twist-two level

The perturbative QCD predictions for the CFFs (7) might be derived by means of the OPE for the time-ordered product of two electromagnetic currents, which is then plugged into the Compton tensor (1). The predictive power of conformal symmetry allows for an economical evaluation and is the key for the perturbative QCD predictions of the DVCS amplitude beyond NLO, which will be presented in Sect. 4. Thus, we choose an operator basis in which this symmetry can be manifestly implemented. The evaluation of the CFFs in this so-called conformal OPE is straightforward and can be found in Refs. [110, 111, 112, 113, 114, 77, 115]. In this section we mainly present our conventions and give a short insight into several aspects of the conformal OPE.

The time-ordered product of two electromagnetic currents is expanded in the basis of so-called conformal operators. The twist-two operators that are built of quark fields read at tree level

$$\left\{ \begin{matrix} {}^q\mathcal{O}^V \\ {}^q\mathcal{O}^A \end{matrix} \right\}_j = \frac{\Gamma(3/2)\Gamma(1+j)}{2^j\Gamma(3/2+j)} (i\partial_+)^j \bar{\psi} \lambda^a \left\{ \begin{matrix} \gamma_+ \\ \gamma_+\gamma_5 \end{matrix} \right\} C_j^{3/2} \left(\frac{\overleftrightarrow{D}_+}{\partial_+} \right) \psi, \quad (21)$$

where, e.g., for three active quarks the nonsinglet and singlet flavor matrices are

$$\lambda^{\text{NS}} = \begin{pmatrix} 2 & 0 & 0 \\ 0 & -1 & 0 \\ 0 & 0 & -1 \end{pmatrix} \quad \text{and} \quad \lambda^{\Sigma} = \begin{pmatrix} 1 & 0 & 0 \\ 0 & 1 & 0 \\ 0 & 0 & 1 \end{pmatrix}. \quad (22)$$

The gluon operators are expressed by the field strength tensor $G_{\mu\nu}^a = \partial_\mu B_\nu^a - \partial_\nu B_\mu^a + g f^{abc} B_\mu^b B_\nu^c$

$$\left\{ \begin{matrix} {}^G\mathcal{O}^V \\ {}^G\mathcal{O}^A \end{matrix} \right\}_j = \frac{\Gamma(5/2)\Gamma(j)}{2^{j-2}\Gamma(3/2+j)} (i\partial_+)^{j-1} G_+^\mu \left\{ \begin{matrix} g_{\mu\nu} \\ i\epsilon_{\mu\nu-+} \end{matrix} \right\} C_{j-1}^{5/2} \left(\frac{\overleftrightarrow{D}_+}{\partial_+} \right) G_\nu^+. \quad (23)$$

The covariant derivatives either in the fundamental or adjoint representation contracted with the light-like vector n are denoted as $\overleftrightarrow{D}_+ = \overrightarrow{D}_+ - \overleftarrow{D}_+$ and $\partial_+ = \overrightarrow{\partial}_+ + \overleftarrow{\partial}_+$ for the total derivative. C_j^ν is the Gegenbauer polynomial of order j with index ν . The “−” component is obtained by contraction with the dual light-like vector n' , i.e., $n \cdot n' = 1$. The operators (21) and (23) are the ground states of conformal multiplets (towers), which are labelled by the conformal spin $j + 2$. Their Lorentz spin is $J = j + 1$ and higher states are obtained by multiplying the ground state with total derivatives $i\partial_+$. Hence, their spin J is increased by the number of total derivatives.

The advantage of such a basis is that in the hypothetical conformal limit conformal symmetry guarantees that the renormalization procedure can be performed in such a way that only operators with the same conformal spin will mix. Beyond LO, this statement is not true in an arbitrary scheme, and in particular not in the $\overline{\text{MS}}$ one. Suppose we rely on a scheme in which the conformal spin is a good quantum number. Then the only mixing problem occurs in the flavor singlet sector,

where quark and gluon operators with the same conformal spin will mix [114]. The 2×2 anomalous dimension matrix can be simply diagonalized by the transformation

$$\begin{pmatrix} +\mathcal{O}^{\text{I}} \\ -\mathcal{O}^{\text{I}} \end{pmatrix}_j = \mathbf{U}_j^{\text{I}}(\alpha_s(\mu)) \begin{pmatrix} \Sigma \mathcal{O}^{\text{I}} \\ \text{G}\mathcal{O}^{\text{I}} \end{pmatrix}_j, \quad (24)$$

where the 2×2 matrices \mathbf{U}_j^{I} are expressed in terms of the anomalous dimensions. Here $\{+, -\}$ labels the eigenfunctions of the renormalization group equation in this sector and $\text{I} \in \{V, A\}$. Consequently, the renormalization group equation for all operators in question is then simply

$$\mu \frac{d}{d\mu} {}^a\mathcal{O}_j^{\text{I}}(\mu) = -a\gamma_j^{\text{I}}(\alpha_s(\mu)) {}^a\mathcal{O}_j^{\text{I}}(\mu) \quad (25)$$

for $a \in \{\text{NS}, +, -\}$. Moreover, if conformal symmetry is implemented in such a manifest way, it can be employed to predict the Wilson coefficients of the OPE [110, 111, 112, 113, 114, 77, 115].

With respect to the mixing properties of operators, it is convenient to perform also a decomposition in flavor nonsinglet (NS) and singlet (S) CFFs and express the latter by the two eigenmodes $a \in \{+, -\}$ of the evolution operator:

$$\mathcal{F} = Q_{\text{NS}}^2 {}^{\text{NS}}\mathcal{F} + Q_{\text{S}}^2 {}^{\text{S}}\mathcal{F}, \quad {}^{\text{S}}\mathcal{F} = {}^{\Sigma}\mathcal{F} + {}^{\text{G}}\mathcal{F} = {}^{+}\mathcal{F} + {}^{-}\mathcal{F}. \quad (26)$$

The fractional charge factors are for three [four] active light quarks⁶

$$Q_{\text{NS}}^2 = \frac{1}{9} \left[\frac{1}{6} \right], \quad Q_{\text{S}}^2 = Q_{\Sigma}^2 = Q_G^2 = Q_{\pm}^2 = \frac{2}{9} \left[\frac{5}{18} \right]. \quad (27)$$

The general form of the short-distance OPE is governed by Lorentz invariance and is given as sum over the irreducible representations of local operators. In our conformal operator basis this expansion leads to the following leading twist approximation of the CFFs

$$\mathcal{F} = \sum_{a=\text{NS}, \pm} Q_a^2 {}^a\mathcal{F}, \quad {}^a\mathcal{F} \simeq \sum_{j=0}^{\infty} [1 \mp (-1)^j] \xi^{-j-1} {}^aC_j^{\text{I}}(\vartheta, Q^2/\mu^2, \alpha_s(\mu)) {}^aF_j(\eta, \Delta^2, \mu^2). \quad (28)$$

Here, they are factorized in the perturbatively calculable Wilson coefficients ${}^aC_j^{\text{I}}(\vartheta, Q^2/\mu^2, \alpha_s(\mu))$ and nonperturbative reduced matrix elements ${}^aF_j(\eta, \Delta^2, \mu^2)$, defined below in Eqs. (31) and (32). These matrix elements carry conformal spin $j+2$ and are nothing but the conformal moments of GPDs (see Appendix C). In Eq. (28) the sum runs over the conformal spin and for $\text{I}=\text{V}$ (A) only its odd (even) values contribute (in the following we will lighten our notation by suppressing the superscript $\text{I} \in \{V, A\}$).

⁶See Appendix A for more details. Basically, the squared fractional charges Q_{NS}^2 and Q_{Σ}^2 are obtained from the decomposition $Q_{\text{NS}}^2 {}^{\text{NS}}\mathcal{F} + Q_{\Sigma}^2 {}^{\Sigma}\mathcal{F} = Q_{\text{u}}^2 {}^{\text{u}}\mathcal{F} + Q_{\text{d}}^2 {}^{\text{d}}\mathcal{F} + Q_{\text{s}}^2 {}^{\text{s}}\mathcal{F} [+Q_{\text{c}}^2 {}^{\text{c}}\mathcal{F}]$.

The $\vartheta = \eta/\xi$ dependence of the Wilson coefficients aC_j encodes information on how operators with the same spin, but a different number of total derivatives, or different conformal spin projection, are arranged⁷. This arrangement is indeed governed in the hypothetical conformal limit by conformal symmetry. For instance, to LO approximation this symmetry predicts the form of the Wilson coefficients, that are expressed by hypergeometric functions, see e.g., Ref. [114], as

$${}^aC_j^{\text{tree}}(\vartheta) = {}^ac_j^{\text{tree}} {}_2F_1 \left(\begin{matrix} (1+j)/2, (2+j)/2 \\ (5+2j)/2 \end{matrix} \middle| \vartheta^2 \right). \quad (29)$$

The normalization ${}^ac_j^{\text{tree}}$ is not fixed. However, crucial for our following results is the fact that it can be borrowed from deeply inelastic scattering. Namely, setting $\vartheta = 0$, we realize that ${}^ac_j^{\text{tree}}$ coincides with the forward Wilson coefficients

$${}^ac_j^{\text{tree}} \equiv {}^aC_j^{\text{tree}}(\vartheta = 0) = 1 \quad \text{for } a = u, d, s, (c). \quad (30)$$

Such correspondence is also valid in all orders of perturbation theory, see next section and Appendix A.

The conformal moments $F_j = \{H_j, E_j, \tilde{H}_j, \tilde{E}_j\}$ arise from the form factor decomposition of the matrix elements of conformal operators (21) and (23). The reduced matrix elements

$$\frac{1}{P_+^j} \langle P_2, S_2 | {}^a\mathcal{O}_j^V | P_1, S_1 \rangle = \overline{U}(P_2, S_2) \left({}^aH_j(\eta, \Delta^2, \mu^2) \gamma_+ + {}^aE_j(\eta, \Delta^2, \mu^2) \frac{i\sigma_{+\nu}\Delta^\nu}{2M} \right) U(P_1, S_1), \quad (31)$$

$$\frac{1}{P_+^j} \langle P_2, S_2 | {}^a\mathcal{O}_j^A | P_1, S_1 \rangle = \overline{U}(P_2, S_2) \left({}^a\tilde{H}_j(\eta, \Delta^2, \mu^2) \gamma_+ \gamma_5 + {}^a\tilde{E}_j(\eta, \Delta^2, \mu^2) \frac{\Delta_+ \gamma_5}{2M} \right) U(P_1, S_1), \quad (32)$$

of these operators are defined in such a way that in the forward limit we encounter the standard Mellin moments of parton densities

$${}^aq_j(\mu^2) = \lim_{\Delta \rightarrow 0} {}^aH_j(\eta, \Delta^2, \mu^2) \quad \text{and} \quad \Delta^a q_j(\mu^2) = \lim_{\Delta \rightarrow 0} {}^a\tilde{H}_j(\eta, \Delta^2, \mu^2). \quad (33)$$

Note that the matrix elements of conformal operators are tensors of rank $j+1$, contracted with the light-like vector n . Hence the reduced ones (31) and (32) are polynomials in η of order $j+1$. In particular, H_j and E_j are of order $j+1$, whereas \tilde{H}_j , \tilde{E}_j and $H_j + E_j$ are of order j , see, e.g., Ref. [116]. Moreover, time reversal invariance and hermiticity ensure that all these polynomials are even under reflection $\eta \rightarrow -\eta$. This then implies that for odd j conformal moments, such as those appearing in the OPE of \mathcal{F}^V form factors, the combination $H_j + E_j$ is actually of order $j-1$.

⁷This can be easily seen from the Taylor expansion of the Wilson coefficients in powers of η/ξ . Taking the spin J as summation label, the entire expansion is given in terms of inverse powers ξ^{-J} . For each given value J there appear $J = \{1, 2, 3, \dots\}$ matrix elements $\eta^n F_{J-n-1}(\eta, \Delta^2, \mu^2)$ with $n = \{0, 1, \dots, J-1\}$.

3.2 Employing the dispersion relation

In this section, we combine the dispersion and the OPE techniques to restore both the imaginary and real part of the CFFs in the physical region. We also give an extended discussion of the subtraction term.

3.2.1 Mellin–Barnes representation for CFFs

We express the Taylor expansion of the CFFs with respect to $\omega = 1/\xi$ in the convenient form analogous to that introduced in Eq. (18)

$${}^a\mathcal{F}(\xi, \vartheta, \Delta^2, Q^2) = \sum_{j=0}^{\infty} [1 \mp (-1)^j] \omega^{j+1} {}^a\mathcal{F}_j(\vartheta, \Delta^2, Q^2) + {}^a\mathcal{C}(\vartheta, \Delta^2, Q^2). \quad (34)$$

Note that the CFFs and so the Taylor coefficients are physical quantities that are independent of the renormalization/factorization scheme that is used for their evaluation.

First, we evaluate the Taylor coefficients ${}^a\mathcal{F}_j$, as defined in Eq. (19), from the conformal OPE (COPE) result (28) taking $\eta/\xi = \eta\omega = \vartheta$ as an independent variable:

$${}^a\mathcal{F}_j \simeq \sum_{\substack{n=0 \\ \text{even}}}^{\infty} {}^aC_{j+n}(\vartheta, Q^2/\mu^2, \alpha_s(\mu)) \vartheta^n {}^aF_{j+n}^{(n)}(\Delta^2, \mu^2), \quad F_j^{(l)} = \frac{1}{l!} \frac{d^l}{d\eta^l} F_j(\eta, \Delta^2, \mu^2) \Big|_{\eta=0}, \quad (35)$$

where j is (even) odd in the (axial-)vector case. Here we used the fact that all considered F_j are even polynomials in η of the order j or $j+1$ and so $F_j^{(l)} = 0$ for $l > j$ or $l > j+1$. Consequently, the sum on the r.h.s. runs only over even n .

Next, we use the analytic properties of the CFFs which ensure that the Taylor coefficients (35) are given by the Mellin moments of the imaginary part. Corresponding to Eq. (19), they then read for general kinematics

$$\int_0^\infty d\xi \xi^j \Im {}^a\mathcal{F}(\xi, \vartheta, \Delta^2, Q^2) = \pi {}^a\mathcal{F}_j(\vartheta, \Delta^2, Q^2). \quad (36)$$

For technical reasons, we extend here and in the following the integration region to infinity using $\Im {}^a\mathcal{F}(\xi, \dots) = 0$ for $\xi > 1$.

Now, we can combine Eqs. (35) and (36). For the DVCS kinematics ($\vartheta = 1$) we have with the notation $\mathcal{F}(\xi, \Delta^2, Q^2) \equiv \mathcal{F}(\xi, \vartheta = 1, \Delta^2, Q^2)$

$$\int_0^\infty d\xi \xi^j \Im {}^a\mathcal{F}(\xi, \Delta^2, Q^2) \simeq \pi \sum_{\substack{n=0 \\ \text{even}}}^{\infty} {}^aC_{j+n}(Q^2/\mu^2, \alpha_s(\mu)) {}^aF_{j+n}^{(n)}(\Delta^2, \mu^2), \quad (37)$$

where we denote the DVCS Wilson coefficients as $C_j(Q^2/\mu^2, \alpha_s(\mu)) \equiv C_j(\vartheta = 1, Q^2/\mu^2, \alpha_s(\mu))$ and make use of the photon virtuality $Q^2 \simeq 2Q^2$. It is worth mentioning that the Mellin moments

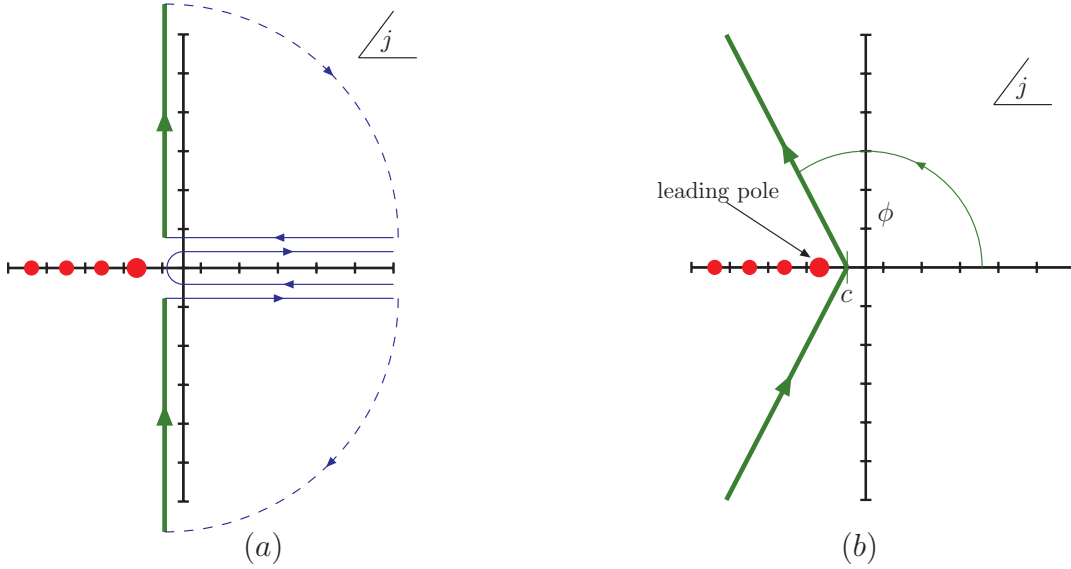


Figure 2: (a) The integration contour in Eq. (38) parallel to the imaginary axis in the complex j -plane. Adding semicircles results in an integration path which encloses the real axis. Contribution of dashed segments vanishes. (b) The integration contour that will be used below in the numerical evaluation of CFFs.

(37) are directly measurable in single spin asymmetries. They contain the sum of all reduced matrix elements built by operators with conformal spin equal or larger than $j + 2$ and so its spin is larger than j .

In the next step we invert the Eq. (37) following the standard mathematical procedure for inverse Mellin transform. To do so we analytically continue the l.h.s. with respect to the conformal spin, which is trivially done by considering j as complex valued. The Mellin moments are holomorphic functions in j , as long as the ξ -integral containing the weight $\xi^j (\ln \xi)^N$ for $N = 0, 1, 2, \dots$ exists, and the condition $\Re j \geq c$, with an appropriate constant c , is satisfied. The choice of c should exclude the singularities in the complex j -plane arising from the endpoint at $\xi = 0$. Notice also that in the limit $\Re j \rightarrow \infty$ the Mellin moments of a regular spectral function vanish, except for a elastic pole contribution, i.e., a $\delta(\xi - 1)$ term. The inverse Mellin transform reads

$$\Im^a \mathcal{F}(\xi, \vartheta, \Delta^2, Q^2) = \frac{1}{2i} \int_{c-i\infty}^{c+i\infty} dj \xi^{-j-1} {}^a \mathcal{F}_j(\vartheta, \Delta^2, Q^2). \quad (38)$$

Here all singularities of the integrand in the complex j -plane lie to the left of integration contour, which is parallel to the imaginary axis, see Fig. 2 (a). The rightmost lying singularity might be related to the leading Regge trajectory, and so we have for $c \equiv \Re j$ the condition⁸ $\alpha(\Delta^2) - 1 < c$.

⁸The leading Regge trajectory corresponds to $\xi^{-\alpha(\Delta^2)}$ behavior of ${}^a \mathcal{F}$, i.e., $\xi^{j-\alpha(\Delta^2)}$ behavior of the integrand in (37), and the pole in $j = \alpha(\Delta^2) - 1$. Note that in perturbation theory the Wilson coefficients and anomalous dimensions possess additional poles at negative integer j . Consequently, if ${}^a \mathcal{F}_j$ is perturbatively expanded we have the condition $\max(\alpha(\Delta^2) - 1, -1) < c$. Moreover, the flavor singlet anomalous dimension matrix in the parity even sector has poles at $j = 0$. These poles could lie right to the pomeron pole $j = \alpha_{\mathbb{P}}(\Delta^2) - 1$, which appear in the nonperturbative ansatz of GPD moments. Hence, we have in this sector the condition $\max(\alpha_{\mathbb{P}}(\Delta^2) - 1, 0) < c$.

There is one comment in order. The analytic continuation of the integrand in Eq. (38), known for non-negative integer j , is not unique. According to Carlson's theorem [117, 118], this ambiguity is resolved by specifying the behavior at $j \rightarrow \infty$. Consequently, the analytic continuation of the Mellin moments must be done in such a way that they vanish (or at least are bounded) in the limit $\Re j \rightarrow \infty$. Especially, one has to avoid an exponential growth, e.g., by a phase factor $e^{ij\pi}$. Obviously, then for $\xi > 1$ the integrand in Eq. (38) does not contribute on the arc with infinite radius that surrounds the first and fourth quadrants. Completing the integration path to a semicircle, Cauchy's theorem states that the imaginary part of the CFFs vanishes for $\xi > 1$ as it should be.

Finally, to restore the real part of the CFFs from the Mellin moments, we plug the imaginary part (38) into the dispersion relation (17), extending the integration interval to $0 \leq \xi' \leq \infty$, and perform the ξ' integration using the principal value prescription. The existence of the integral is ensured by appropriate bounds for $\Re j$. The lower one is $\max(\alpha(\Delta^2) - 1, -1) < c$ or $\max(\alpha_{\mathbb{P}}(\Delta^2) - 1, 0) < c$, see footnote 8, and in addition for the upper one we have $c < 1$ ($c < 0$) in the (axial-)vector case. The integration yields an additional weight factor in the Mellin–Barnes integral (38) which is given by $\tan(\pi j/2)$ and $-\cot(\pi j/2)$ for the vector and axial-vector case, respectively. The whole amplitude for $\xi > 0$ reads

$${}^a\mathcal{F}(\xi, \vartheta, \Delta^2, Q^2) = \frac{1}{2i} \int_{c-i\infty}^{c+i\infty} dj \, \xi^{-j-1} \left[i \pm \left\{ \begin{matrix} \tan \\ \cot \end{matrix} \right\} \left(\frac{\pi j}{2} \right) \right] {}^a\mathcal{F}_j(\vartheta, \Delta^2, Q^2) + {}^a\mathcal{C}(\vartheta, \Delta^2, Q^2). \quad (39)$$

where the Mellin moments are defined by the series (35). The analogous expression for $\xi < 0$ follows from the symmetry relations (15). We stress again that analyticity ties the real and imaginary part in a unique way. This is obvious in the axial-vector case, where the subtraction constant is zero for symmetry reasons. The vector case will be discussed in the next section.

By comparing (39) with (34) one sees that with the help of dispersion relation technique the analytic continuation of the CFFs in the unphysical region, given by the series (39), yields the complex Mellin–Barnes integral (34). The corresponding Mellin moments ${}^a\mathcal{F}_j$ are perturbatively predicted by another series (35), which depends on the GPD moments ${}^aF_{j+n}^n$. This remaining summation we postpone for later.

3.2.2 Discussing the subtraction constant

The evaluation of the subtraction constant \mathcal{C} from the limit $\omega \rightarrow 0$ deserves some additional comments. The definition (20) of this constant suggests that it is entirely determined by short-distance physics. The relevant local operator has dimension two (or spin zero) and simply does

not exist as a gauge invariant one⁹. So on the first sight one would expect that, as in the forward case, the subtraction constant is zero in the (generalized) Bjorken limit. Surprisingly, a more careful look at the OPE result (28) shows that all (gauge invariant local) operators contribute, because the highest possible order in $\eta = \vartheta/\omega$, e.g., $j+1$, of their conformal moments, cancels the suppression factor ω^{j+1} in front of the Wilson coefficients. Hence, the subtraction constant is in fact determined by light-cone physics and resumming all terms proportional to $F_j^{(j+1)}$ leads to:

$${}^a\mathcal{C}(\vartheta, \Delta^2, Q^2) \simeq 2 \sum_{\substack{n=2 \\ \text{even}}}^{\infty} {}^aC_{n-1}(\vartheta, Q^2/\mu^2, \alpha_s(\mu)) \vartheta^n {}^aF_{n-1}^{(n)}(\Delta^2, \mu^2), \quad {}^a\mathcal{C}(\vartheta = 0, \Delta^2, Q^2) \simeq 0. \quad (40)$$

Since $F_j^{(j+1)}$ appears only for $j+1$ even, this constant vanishes for symmetry reasons in the axial-vector case — as it musts — and is absent in the combination $\mathcal{H} + \mathcal{E}$. Moreover, it is predicted to be zero if the virtualities of the photons are equal, i.e., for $\vartheta = 0$. The expression (40) for the subtraction constant has been also derived in the momentum fraction representation at tree level [119], where it was expressed by a so-called D -term [120]. This term entirely lives in the central GPD region and collects the highest possible order terms in η . Hence, its conformal moments provide us $F_j^{(j+1)}$, e.g., for $\eta > 0$,

$$\int_{-\eta}^{\eta} dx \, \eta^j C_j^{3/2} \left(\frac{x}{\eta} \right) D \left(\frac{x}{\eta} \right) = F_j^{(j+1)} \eta^{j+1}. \quad (41)$$

In the following we discuss the subtraction constant for the CFF \mathcal{E} , rather than \mathcal{H} . The reason for doing so is that $E_j^{(j+1)}$ originally arises from a nonperturbatively induced helicity-flip, as we will see in Sect. 5. We note that such nonperturbative effects are absent in linear combination $H_j + E_j$.

A subtraction constant is usually viewed as additional information that cannot be obtained from the imaginary part. However, if $E_j^{(j+1)}$ is the analytic continuation of $E_j^{(n)}$, we should indeed be able to express the subtraction constant by the imaginary part of the CFF \mathcal{E} .

Let us demonstrate such a possible cross talk between subtraction constant and imaginary part in the most obvious manner. To do so we first make the mathematical assumption that ${}^a\mathcal{E}(\xi, \vartheta, \dots)$ vanishes for $\xi \rightarrow 0$. In this case the subtraction in the dispersion relation (17) has been overdone. Taking the $\xi \rightarrow 0$ limit in the dispersion relation indeed leads to the desired relation between subtraction constant and imaginary part:

$${}^a\mathcal{C}(\vartheta, \dots) = \frac{2}{\pi} \int_0^\infty d\xi \, \xi^{-1} \Im {}^a\mathcal{E}(\xi, \vartheta, \dots). \quad (42)$$

⁹Such an operator might be interpreted as the expectation value of a gauge invariant non-local operator that carries spin zero. In the light cone gauge such an operator is for instance given by the local two gluon operator $g^{\mu\nu} B_\mu^a(0) B_\nu^a(0)$. However, in a gauge invariant scheme its Wilson coefficient is zero.

Since the subtraction constant in the equal photon kinematics is vanishing, we derive the sum rule

$${}^a\mathcal{C}(\vartheta = 0, \dots) = \frac{2}{\pi} \int_0^\infty d\xi \xi^{-1} \Im {}^a\mathcal{E}(\xi, \vartheta = 0, \dots) = 0. \quad (43)$$

We remark, however, that this equality is *not* of physical interest, because Regge phenomenology suggests that the small ξ behavior of ${}^a\mathcal{E}$ arises from the pomeron pole and so it will approximately grow with $1/\xi$ in the high-energy asymptotics. Hence, our mathematical assumption was purely academic and the sum rule (43) does not apply.

Let us now consider a realistic behavior of the CFF \mathcal{E} . Comparing the OPE prediction (40) for the subtraction constant with the Mellin moments (35), one realizes that for $j \rightarrow -1$ the only difference is the first term in the series (35). Thus, removing this term and taking the limit leads to a formal definition of the subtraction constant

$${}^a\mathcal{C}(\vartheta, \Delta^2, Q^2) \simeq 2 \lim_{j \rightarrow -1} \left[{}^a\mathcal{E}_j(\vartheta, \Delta^2, Q^2) - {}^aC_j(\vartheta, Q^2/\mu^2, \alpha_s(\mu)) {}^aE_j^{(0)}(\Delta^2, \mu^2) \right]. \quad (44)$$

Here the separate terms on the r.h.s. can be singular and so the analytic continuation plays the role of a regularization. We note that, corresponding to the high-energy ($\xi \rightarrow 0$) behavior, there are also poles and perhaps branch cuts in the complex j -plane, which have to be surrounded first, to arrive at $\Re j = -1$. This is certainly possible if the Mellin moments are meromorphic functions. The situation is more tricky if ${}^a\mathcal{E}_j$ contains singularities at $j = -1$ and the subtraction procedure is maybe not uniquely defined. In particular, the appearance of a fixed singularity at $j = -1$, e.g., a $\delta_{j,-1}$ proportional contribution, might spoil the relation between the subtraction constant and the imaginary part of the corresponding Compton form factor.

Let us explore the consequences in the case that both scheme dependent quantities ${}^aC_{j=-1}$ and ${}^aE_{j=-1}^{(0)}$ can be defined by analytic continuation. The GPD moment, appearing on the r.h.s. of Eq. (44), might be expressed by the kinematical forward quantity

$${}^aE_j^{(0)}(\Delta^2, \mu^2) \simeq \frac{{}^a\mathcal{E}_j(\vartheta = 0, \Delta^2, Q^2)}{{}^aC_j(\vartheta = 0, \Delta^2, Q^2/\mu^2, \alpha_s(\mu))},$$

see Eq. (35) with $\vartheta = 0$. This provides an important relation, which formally reads

$${}^a\mathcal{C}(\vartheta, \Delta^2, Q^2) = 2 \lim_{j \rightarrow -1} \left[{}^a\mathcal{E}_j(\vartheta, \Delta^2, Q^2) - \frac{{}^aC_j(\vartheta, \Delta^2, Q^2/\mu^2, \alpha_s(\mu))}{{}^aC_j(\vartheta = 0, \Delta^2, Q^2/\mu^2, \alpha_s(\mu))} {}^a\mathcal{E}_j(\vartheta = 0, \Delta^2, Q^2) \right]. \quad (45)$$

Remarkably, only the ratio of Wilson coefficients appearing among physical quantities in Eq. (45) is potentially plagued by ambiguities. Hence, we must conclude that in the $j \rightarrow -1$ limit this ratio is scale and scheme independent and has the same value in any order of perturbation theory. This value can thus be read off from the tree level coefficients (29):

$$\lim_{j \rightarrow -1} \frac{{}^aC_j(\vartheta, \Delta^2, Q^2/\mu^2, \alpha_s(\mu))}{{}^aC_j(\vartheta = 0, \Delta^2, Q^2/\mu^2, \alpha_s(\mu))} = 1. \quad (46)$$

This formula has been checked to NLO accuracy. It turns out that radiative α_s corrections blow up in the limit $j \rightarrow -1$; however, the leading singularities in $j - 1$ are ϑ independent.

Relying on the validity of the prescription (45), we can calculate the subtraction constant from the knowledge of the imaginary part. Taking into account Eq. (45), we formally write the desired relation as

$${}^a\mathcal{C}(\vartheta, \dots) = \frac{2}{\pi} \lim_{j \rightarrow -1} \left\{ \int_0^\infty d\xi \xi^j \Im [\mathcal{E}(\xi, \vartheta, \dots) - \mathcal{E}(\xi, \vartheta = 0, \dots)] \right\}_{\text{AC}}, \quad (47)$$

where the integral is analytically regularized. That means that one first has to evaluate the integral for $\max(\alpha(\Delta^2) - 1, -1) < \Re j$ and then perform the analytic continuation to $j = -1$. Certainly, the prescription (47) relies on analyticity. If this property is absent, e.g., because of a fixed pole or singularity at $j = -1$ with a ϑ -dependent residue, the subtraction constant ${}^a\mathcal{C}$ is only partially related to the imaginary part. We remark that in such a case the D -term for GPDs [120], introduced as a separate contribution to cure the spectral representation [24, 88], seems to be justified on the first view. Otherwise the prescription of Ref. [121] for the restoration of the highest possible order in η is more appropriate¹⁰.

Let us remind that the existence of a fixed pole at angular momentum $J = 0$, i.e., $j = -1$ was already argued from Regge phenomenology inspired arguments at the end of the sixties and it was proposed to access it by the uses of finite energy sum rules [123]. The analyses of experimental measurements [124, 125], although not fully conclusive, indicate a fixed pole at $J = 0$. Interestingly, its residue might be related to the Thomson limit of the Compton amplitude [126]. On the theoretical side studies in the partonic [127, 128] or light-cone [129, 130] approach lead to a real term in the transversal part of the (forward) Compton amplitude that in the language of Reggeization was interpreted as a $J = 0$ fixed pole. Nevertheless, via a subtracted sum rule [131, 132, 127, 128] it is related to the imaginary part of the Compton amplitude. This would imply that there is *no* separate D -term contribution in the central GPD region.

3.3 Representation of CFFs in terms of conformal moments

In this section we derive a Mellin–Barnes representation alternative to Eq. (39), which expresses the CFFs in terms of conformal GPD moments rather than the usual Mellin moments. The advantage of such a representation is that the CFFs are expanded in conformal partial waves, which diagonalize the evolution operator to LO and facilitate direct application of conformal

¹⁰The spectral representation is not uniquely defined [122]. Indeed, if one takes into account that both D -term and spectral function are dependent – they arise from different projections of the same spectral function that enters in the improved representation – the choice of a ‘common’ spectral representation [24, 88] plus D -term is equivalent to the improved ones [121].

symmetry beyond LO. In Sect. 3.3.1 we consider the well understood tree-level approximation to spell out the mathematical subtleties that appear in the mapping of conformal moments of GPDs to the Mellin ξ -moments (35) of CFFs. We propose then in Sect. 3.3.2 a Sommerfeld–Watson transformation which allows us to derive the desired Mellin–Barnes representation for CFFs, which has been already derived previously by other methods [98, 101]. Finally, we discuss the Mellin–Barnes representation of conformal GPD moments themselves.

3.3.1 Lessons from a toy example

Let us now have a closer look at the series representation (37) of the Mellin moments ${}^a\mathcal{F}_j$, appearing in the Mellin–Barnes representation (39) for CFFs. To get some insight into its mathematical properties we consider the OPE at tree level. For simplicity, we will discard here the Δ^2 -dependence, which appears only as a dummy variable, as well as the flavor index. The Wilson coefficients of the COPE are given in Eq. (29) and for DVCS kinematics, i.e., $\vartheta = 1$, we immediately have

$$C_j^{\text{tree}}(\vartheta = 1) = {}_2F_1 \left(\begin{matrix} (1+j)/2, (2+j)/2 \\ (5+2j)/2 \end{matrix} \middle| 1 \right) = \frac{2^{j+1}\Gamma(5/2+j)}{\Gamma(3/2)\Gamma(3+j)}. \quad (48)$$

If we form partonic matrix elements of the conformal operators, e.g., for the CFF \mathcal{H} , the conformal moments H_j^{tree} are simply given in terms of Gegenbauer polynomials $\eta^j C_j^{3/2}(1/\eta)$. According to Eq. (35) the corresponding expression of $H_{j+n}^{(n)\text{tree}}$ reads

$$H_j^{\text{tree}}(\eta) = \frac{\Gamma(3/2)\Gamma(1+j)}{2^j\Gamma(3/2+j)} \eta^j C_j^{3/2}\left(\frac{1}{\eta}\right) \Rightarrow H_{j+n}^{(n)\text{tree}} = \frac{(-1)^{n/2}\Gamma(3/2+j+n/2)\Gamma(1+j+n)}{2^n\Gamma(1+j)\Gamma(1+n/2)\Gamma(3/2+j+n)}. \quad (49)$$

Consequently, the Mellin moments (35) are for our toy example given by the following series

$$\mathcal{H}_j^{\text{tree}} = \sum_{\substack{n=0 \\ \text{even}}}^{\infty} \frac{(-1)^{n/2}2^{j+1}(3+2j+2n)\Gamma(3/2+j+n/2)}{(1+j+n)(2+j+n)\Gamma(1/2)\Gamma(1+j)\Gamma(1+n/2)}. \quad (50)$$

As one realizes from the asymptotics of the Γ -functions, for large n with $n \gg j$ the summands behave as $\propto n^{j-1/2}$ and for non-negative integer j this series must be resummed to arrive at a meaningful result, which in our case is simply one. Hence, $\mathcal{H}_j^{\text{tree}} = 1$ and the inverse Mellin transform yields a δ -function. Note that the exponentially growing factor 2^j in the Wilson coefficients (48) is finally cancelled in the conformal Mellin moments (50) by an exponential suppression factor in the conformal GPD moments (49). This cancellation ensures that the imaginary part of the CFF is vanishing for $\eta = \xi > 1$. We conclude that realistic conformal GPD moments for $\eta \geq 1$ are exponentially suppressed by a factor 2^{-j} .

The real part of the CFF can be obtained from the dispersion relation (17), while the subtraction constant follows from (45)

$$\mathcal{C}^{\text{tree}} = \lim_{j \rightarrow -1} 2 \left[\mathcal{H}_j^{\text{tree}} - C_j^{\text{tree}}(1)H_j^{(0)\text{tree}} \right] = 0. \quad (51)$$

This is in agreement with the fact that the highest order terms possible in η are absent for our toy conformal moments, i.e., $H_{n-1}^{(n)\text{tree}} = 0$ for $n > 0$, see Eq. (49). Consequently, the OPE prediction (40) shows that the subtraction constant vanishes, too. Thus, we removed the ambiguity caused by the subtracted dispersion relation, and arrive at the unique result:

$$\int_0^1 d\xi \xi^j \Im \mathcal{H}^{\text{tree}}(\xi) = \pi \quad \Rightarrow \quad \Im \mathcal{H}^{\text{tree}}(\xi) = \pi \delta(1 - \xi), \quad \Re \mathcal{H}^{\text{tree}}(\xi) = -\frac{2}{1 - \xi^2}. \quad (52)$$

Of course, this example is trivial and the findings coincide with the well-known answer,

$$\mathcal{H}^{\text{tree}}(\xi, \vartheta = 1) = \int_{-1}^1 dx \left(\frac{1}{\xi - x - i\epsilon} - \frac{1}{\xi + x - i\epsilon} \right) H(x, \xi), \quad (53)$$

arising from the evaluation of the hand-bag diagram with a partonic GPD $H(x, \eta) = \delta(1 - x)$.

If evolution is included, an explicit resummation of the series for the Mellin moments (37), appearing in the Mellin–Barnes integral (39), cannot be achieved, since each term is labelled by the conformal spin and will evolve differently. There are following possibilities to solve this problem:

- Numerical evaluation of the corresponding series.
- Relying on an approximation of the series.
- Arrangement of the integrand in the Mellin–Barnes integral (39) in such a way that the integration, instead of Mellin moment, runs over the complex conformal spin

The third possibility will be worked out in the next section. In the following we shall study whether an approximation of the series is appropriate. As we just saw, for complex j with $\Re j$ sufficiently small, the ξ independent series (49) converges. If the first few terms are numerically dominating, we might hope that these terms already induce a good approximation of the CFFs. Certainly, if the η dependence in the conformal moments is weak in the vicinity of $\eta = 0$, i.e., if the $F_{j+n}^{(n)}(\Delta^2, \mu^2)$ are numerically small for larger n , the series might be approximated by a finite sum. This should induce a good approximation for the CFFs for smaller values of ξ .

Let us shortly demonstrate how this “expansion” works at tree level. We keep in the conformal moments (49) only the leading term in η^2 for $\eta \rightarrow 0$, i.e., $H_j^{(0)\text{tree}} = 1$ and all terms with $n = 2, 4, \dots$ are neglected. Hence, the Mellin moments (50) read in this approximation

$$\int_0^\infty d\xi \xi^j \Im \mathcal{H}^{\text{tree}}(\xi) \simeq \pi \frac{2^{j+1} \Gamma(5/2 + j)}{\Gamma(3/2) \Gamma(3 + j)}. \quad (54)$$

The inverse Mellin transform and the use of dispersion relation leads then for $\xi \geq 0$ to

$$\Im \mathcal{H}^{\text{tree}}(\xi) \simeq \theta(2 - \xi) \frac{\xi^{\frac{3}{2}}}{\sqrt{2 - \xi}}, \quad \Re \mathcal{H}^{\text{tree}}(\xi) \simeq -2 + \mathcal{O}(\xi^{3/2}). \quad (55)$$

The exponential factor 2^j in the approximated moments (54) induces a wrong support. However, we have still a useful approximation for small values of ξ , where the deviation from the correct result starts at order $\xi^{3/2}$. Naively, one might have expected that the accuracy is of order ξ^2 . We remark, however, that by taking into account the next order in the expansion (49), i.e., $n = 2$ as well, the $\xi^{3/2}$ proportional terms are annulled and the result is then valid up to order $\mathcal{O}(\xi^{5/2})$. That the expansion of the conformal moments with respect to η induces a systematic expansion of the CFFs in powers of ξ is perhaps not true in general.

3.3.2 Complex conformal partial wave expansion

We will now change the integration variable of the Mellin–Barnes integral (39) so that the integration finally runs over the complex conformal spin and the nonperturbative input is given in terms of conformal GPD moments. As mentioned above, in such a basis the evolution operator is diagonal with respect to this quantum number. If this diagonality is not preserved in a given scheme, we can always perform a scheme transformation so that the conformal GPD moments evolve diagonally. Let us start with the Sommerfeld-Watson transformation of the series for the Mellin moments \mathcal{F}_j into a Mellin–Barnes integral. To do this we rewrite the series

$${}^a\mathcal{F}_j(\vartheta = 1, \Delta^2, Q^2) \equiv {}^a\mathcal{F}_j(\Delta^2, Q^2) \simeq \sum_{\substack{n=0 \\ \text{even}}}^{\infty} {}^aC_{j+n}(Q^2/\mu^2, \alpha_s(\mu)) {}^aF_{j+n}^{(n)}(\Delta^2, \mu^2) \quad (56)$$

as an contour integral that includes the real positive axis and add two quarters of an infinite circle, see Fig. 2, and arrive so at the Mellin–Barnes representation:

$${}^a\mathcal{F}_j(\Delta^2, Q^2) \simeq \frac{i}{4} \int_{d-i\infty}^{d+i\infty} dn \frac{1}{\sin(n\pi/2)} {}^aC_{j+n}(Q^2/\mu^2, \alpha_s(\mu)) {}^a\hat{F}_{j+n}^{(n)}(\Delta^2, \mu^2), \quad (57)$$

where ${}^a\hat{F}_{j+n}^{(n)}$ is the analytic continuation of $(-1)^{n/2} {}^aF_{j+n}^{(n)}$ and the integration contour is chosen so that all singularities lie to the left of it. Note that for $j = -1$ the expansion coefficient ${}^a\hat{F}_j^{(j+1)}$ is absent from this formula. Rather, it is contained in the subtraction constant ${}^a\mathcal{C}$. Plugging this representation into Eq. (39), we arrive after the shift of the integration variable $j \rightarrow j - n$ at a Mellin–Barnes representation for the CFFs

$${}^a\mathcal{F}(\xi, \Delta^2, Q^2) \simeq \frac{1}{2i} \int_{c-i\infty}^{c+i\infty} dj \xi^{-j-1} \left[i + \left\{ \begin{matrix} \tan \\ -\cot \end{matrix} \right\} \left(\frac{\pi j}{2} \right) \right] {}^aC_j(Q^2/\mu^2, \alpha_s(\mu)) {}^aF_j(\xi, \Delta^2, \mu^2). \quad (58)$$

Here the conformal moments F_j are now written as a Mellin–Barnes integral

$${}^aF_j(\xi = \eta, \Delta^2, \mu^2) = \frac{i}{4} \int_{d-i\infty}^{d+i\infty} dn \frac{1 \pm e^{ij\pi}}{1 \pm e^{i(j-n)\pi}} (\eta - i\epsilon)^n \frac{{}^a\hat{F}_j^{(n)}(\Delta^2, \mu^2)}{\sin(n\pi/2)}, \quad (59)$$

valid for $0 \leq \eta \leq 1$. The (lower) upper sign corresponds to the (axial-)vector case. We included in this definition a $-i\epsilon$ prescription, which ensures that

$$\frac{1 \pm e^{ij\pi}}{1 \pm e^{i(j-n)\pi}}(\eta - i\epsilon)^n = \frac{1 \pm e^{ij\pi}}{1 \pm e^{i(j-n)\pi}}e^{n(\ln \eta - i\epsilon)} \quad (60)$$

vanishes also for $n \rightarrow -i\infty$ in the complex n -plane rather than generate an exponential j -dependent phase factor. We remark that the exponential suppression in the integral (59), arising from $1/\sin(n\pi/2)$ in the limit $n \rightarrow \pm i\infty$, is in general needed to cancel an exponential growing of ${}_a\hat{F}_j^{(n)}$.

The Mellin–Barnes representation (58) for the CFFs, which we will from now on use in all our numerical analysis, has been already derived in two alternative ways in Refs. [98, 101]. As a gift of the present approach we found for the conformal moments (31) and (32) the Mellin–Barnes integral representation (59), which gives the analytic continuation of the conformal moments. This issue has not been completely resolved before.

We will discuss briefly the representation (59) within our partonic toy GPD to shed light on some tricky points. It can be shown that for the conformal moments of GPD $H(x, \eta) = \delta(1 - x)$ the integral (59) exists for $0 < \eta < 1$, where the integrand can be read off from the second expression in Eq. (49). After completing the integration path, it reduces for complex valued j to the function H_j^{tree} in Eq. (49) and an addenda that arises from the additional phase factors in the definition (59) of conformal moments. For $0 \leq \eta < 1$ we might express our improved findings in terms of hypergeometric functions

$$H_j^{\text{tree}}(\eta) = \frac{\Gamma(3/2)\Gamma(3+j)}{2^{1+j}\Gamma(3/2+j)}\eta^j {}_2F_1\left(\begin{matrix} -j, j+3 \\ 2 \end{matrix} \middle| \frac{\eta-1}{2\eta}\right) - \frac{4^{-j-1}\eta^{3+2j}}{i + \tan(\pi j/2)} \frac{\Gamma(1+j)\Gamma(3+j)}{\Gamma(3/2+j)\Gamma(5/2+j)} {}_2F_1\left(\begin{matrix} 3/2+j/2, 2+j/2 \\ 5/2+j \end{matrix} \middle| \eta^2 - i0\right). \quad (61)$$

Hence for positive odd integer j this formula reduces to the Gegenbauer polynomials (times the conventional normalization factor). The addenda is proportional to $1/(i + \tan(\pi j/2))$, where this factor cancels the corresponding one in the conformal partial wave expansion (58). We can again close the integration path by an infinite arc so that the first and forth quadrant is encircled. It can be shown that the infinite arc does not contribute. Since the integrand stemming from the addenda is a holomorphic function in j , we conclude that the addenda finally vanishes for $0 \leq \eta < 1$. Consequently, we have found that the appropriate analytic continuation of the conformal GPD moments is given by the first term on the r.h.s. of Eq. (61), i.e., the analytic continuation of Gegenbauer polynomials is given by the replacement

$$\frac{\Gamma(3/2)\Gamma(1+j)}{2^j\Gamma(3/2+j)}\eta^j C_j^{3/2}\left(\frac{1}{\eta}\right) \Rightarrow \frac{\Gamma(3/2)\Gamma(3+j)}{2^{1+j}\Gamma(3/2+j)}\eta^j {}_2F_1\left(\begin{matrix} -j, j+3 \\ 2 \end{matrix} \middle| \frac{\eta-1}{2\eta}\right) \quad \text{for } \eta \geq 0. \quad (62)$$

This result allows also for the extension of the η region to $\eta \geq 1$. Of course, symmetry under reflection allows for negative values of η by replacement $\eta \rightarrow -\eta$.

3.3.3 Mellin–Barnes representation of conformal GPD moments

First, notice that ${}^a\hat{F}_j^{(n)}$ from the Mellin–Barnes representation (59) is not an arbitrary function; rather it must be guaranteed that aF_j

- i) is holomorphic in the first and fourth quadrant of the complex j -plane
- ii) reduces for non-negative integers j to a polynomial of order j or $j + 1$
- iii) possesses for $j \rightarrow \infty$ and $\xi \rightarrow 1$ an exponential suppression factor 2^{-j} .

The requirement *i*) is satisfied when it holds for ${}^a\hat{F}_j^{(n)}$. To show that also the second requirement is fulfilled, let us suppose that the analytic continuation of ${}^a\hat{F}_j^{(n)}$ is defined in such a way that it does not grow exponentially for $n \rightarrow \infty$ with $\arg(n) \leq \pi/2$ and fixed j . Moreover, for simplicity let us assume that ${}^a\hat{F}_j^{(n)}$ is a meromorphic function with respect to n . For $0 < \eta < 1$ we can then close the integration contour in Eq. (59) so that the first and forth quadrant are encircled. Cauchy's theorem states that aF_j is given as a sum of the residues in these two quadrants

$${}^aF_j(\eta, \Delta^2, \mu^2) = \frac{\pi}{2} \sum_{\text{poles}} \text{Res} \left[\frac{1 \pm e^{ij\pi}}{1 \pm e^{i(j-n)\pi}} \frac{\eta^n}{\sin(n\pi/2)} {}^a\hat{F}_j^{(n)}(\Delta^2, \mu^2) \right]. \quad (63)$$

This result is in general a series, defining for fixed η a holomorphic function with respect to j . For non-negative integer j , any contribution that does *not* arise from the poles at $n = 0, 2, 4, \dots$ will drop out, due to the factor $1 \pm e^{ij\pi}$. Consequently, in this case only the poles on the real n -axis contribute and with the requirement ${}^aF_j^{(n)} = 0$ for $n \geq j + 2$ we get the polynomial

$${}^aF_j(\eta, \Delta^2, \mu^2) = \sum_{\substack{n=0 \\ \text{even}}}^{j+p} \eta^n {}^aF_j^{(n)}(\Delta^2, \mu^2) \quad \text{for } j = \{1, 3, 5, \dots\} \text{ or } j = \{0, 2, 4, \dots\}, \quad (64)$$

where $p = \{0, 1\}$. Note that for $p = 1$ the highest possible term of order η^{j+1} is now included. Moreover, it is required that for $\eta = \xi > 1$ the following expression, which appears as integrand in the Mellin–Barnes integral (58),

$$\lim_{j \rightarrow \infty} \frac{1}{\sqrt{j}} \left(\frac{\xi}{2} \right)^{-j-1} \left[i + \left\{ \begin{matrix} \tan \\ -\cot \end{matrix} \right\} \left(\frac{\pi j}{2} \right) \right] {}^aF_j(\xi, \Delta^2, \mu^2) \ln^N j, \quad (65)$$

vanishes in the limit $j \rightarrow \infty$ for $\arg(j) \leq \pi/2$. Here we took into account that the Wilson coefficients in fixed order of perturbation theory behave as $\ln^N j / \sqrt{j}$ in the asymptotics we are considering. More precisely, $1/\sqrt{j}$ arises from the factor $\Gamma(j + 5/2)/\Gamma(3 + j)$ in the normalization

of the Wilson coefficients, see Eq. (48), and the logarithmical growing is induced by radiative corrections. The condition (65) is necessary to ensure that the support of the imaginary part of the CFFs is restricted to $|\xi| \leq 1$. Namely, for $\xi > 1$ we can close the integration path to form a contour that encircles the positive real axis. Obviously, the imaginary part drops out and only the poles of the trigonometric functions contribute, yielding the series given by the COPE (28). For $\eta = \xi \rightarrow \infty$ we precisely recover the subtraction constant ${}^a\mathcal{C}$, see Eq. (40), which shows that it is already contained in the final representation (58) of the CFFs in the conformal moments (59).

Moreover, we can easily generalize the formula (59) for the computation of the conformal moments for a given GPD, which has definite symmetry with respect to the momentum fraction x . In this case the analytic continuation of the conformal moments are

$${}^aF_j(\eta, \Delta^2, \mu^2) = \frac{i\Gamma(1+j)}{4\Gamma(3/2+j)} \int_{d-i\infty}^{d+i\infty} dn \frac{1 \pm e^{ij\pi}}{1 \pm e^{i(j-n)\pi}} \frac{(\eta - i\epsilon)^n}{\sin(n\pi/2)} \frac{2^{-n}\Gamma(3/2+j-n/2)}{\Gamma(1+j-n)\Gamma(1+n/2)} \\ \times \text{AC} \left[\int_0^1 dx x^{j-n} {}^aF(x, \eta, \Delta^2, \mu^2) \right]. \quad (66)$$

Here the Mellin moments in the second line appear in the form factor decomposition of the matrix elements of local operators that are built exclusively out of covariant derivatives. Precisely these matrix elements are measured on the lattice [35, 36, 37, 38, 39, 40]. It is understood that $\Re(j-n)$ is restricted to such values that the integral exists. We note that the polynomiality of these moments is ensured by the symmetry we assumed. So for instance for an (anti-)symmetric GPD we have for even (odd) values of n

$$\frac{1}{2} \int_{-1}^1 dx x^n {}^aF(x, \eta, \Delta^2, \mu^2) = \int_0^1 dx x^n {}^aF(x, \eta, \Delta^2, \mu^2) = \sum_{\substack{i=0 \\ \text{even}}}^{n+p} {}^aF_{ni}(\Delta^2, \mu^2) \eta^i, \quad (67)$$

where p takes the values 0 and 1 for even and odd n , respectively. However, irrespective of the symmetry $p=0$ holds true for the combination $H+E$, \tilde{H} , and \tilde{E} .

4 DVCS amplitude up to next-to-next-to-leading order

In Sect. 4.1 we first discuss the predictive power of conformal symmetry in a conformally invariant theory for general kinematics. Here we rely on a special subtraction scheme, the so-called conformal one, in which the renormalized operators are covariant under collinear conformal transformations. This allows us to predict the functional form of the Wilson coefficients up to a normalization factor. This factor is simply the Wilson coefficient that appears in DIS. To reduce the massless QCD to a conformally invariant theory, we intermediately assume that the QCD has a non-trivial fixed-point so that the trace anomaly vanishes. Then we move to the real world and discuss the

inclusion of the running coupling. In Sect. 4.2 we present the results for the DVCS kinematics. The recent progress in the evaluation of radiative corrections in DIS allows us to present the CFFs to NNLO accuracy. However, the trace anomaly induces a mixing of conformal GPD moments due to the evolution. Also note that the forward anomalous dimensions of parity odd conformal GPD moments are mostly unknown beyond NLO. In Sect. 4.3 we present the NLO corrections to the twist-two CFFs in the $\overline{\text{MS}}$ scheme and discuss the inclusion of mixing effects in the Mellin–Barnes representation.

4.1 Conformal OPE prediction and beyond

In the hypothetical conformal limit, i.e., if the β function of QCD has a non-trivial fixed point $\alpha_s^* \neq 0$, the η/ξ dependence of the Wilson coefficients is predicted by conformal symmetry [110, 111, 112, 113]. For all the cases we are considering, Wilson coefficients ${}^a\mathcal{C}^{\text{I}}$, with $a = \{\text{NS}, +, -\}$ and $\text{I} = \{\text{V}, \text{A}\}$, have the same general form. Thus, when there is no possibility of confusion, we will simplify our notation by suppressing both of these superscripts. The COPE prediction for general kinematics reads [114]

$$C_j(\eta/\xi, Q^2/\mu^2, \alpha_s^*) = c_j(\alpha_s^*) {}_2F_1\left(\begin{matrix} (2+2j+\gamma_j(\alpha_s^*))/4, (4+2j+\gamma_j(\alpha_s^*))/4 \\ (5+2j+\gamma_j(\alpha_s^*))/2 \end{matrix} \middle| \frac{\eta^2}{\xi^2}\right) \left(\frac{\mu^2}{Q^2}\right)^{\gamma_j(\alpha_s^*)/2}, \quad (68)$$

where the normalization c_j remains so far unknown. In the kinematical forward limit ($\eta = 0$) the Wilson coefficients coincide with those known from DIS

$$\lim_{\eta \rightarrow 0} C_j(\eta/\xi, Q^2/\mu^2, \alpha_s^*) = c_j(\alpha_s^*) \left(\frac{\mu^2}{Q^2}\right)^{\gamma_j(\alpha_s^*)/2}, \quad (69)$$

see Appendix A. Neither Wilson coefficients (68) nor conformal GPD moments (31), (32) mix under collinear conformal transformations. This implies that they evolve autonomously with respect to a scale change,

$$\mu \frac{d}{d\mu} F_j(\dots, \mu^2) = -\gamma_j(\alpha_s^*) F_j(\dots, \mu^2), \quad (70)$$

$$\mu \frac{d}{d\mu} C_j(\dots, Q^2/\mu^2, \alpha_s^*) = C_j(\dots, Q^2/\mu^2, \alpha_s^*) \gamma_j(\alpha_s^*). \quad (71)$$

Here the anomalous dimensions are the same as in DIS. We also realize that the conformal spin $j+2$ is a good quantum number.

Unfortunately, conformal symmetry is not manifest in a general factorization scheme, and in particular not in the $\overline{\text{MS}}$ scheme. What is required is a special scheme, which ensures that the *renormalized* conformal operators form an irreducible representation of the collinear conformal

group $SO(2,1)$ [114]. The breaking of the covariant behavior with respect to dilatation, e.g., shows up in the mixing of operators' expectation values and of Wilson coefficients under renormalization:

$$\mu \frac{d}{d\mu} F_j(\dots, \mu^2) = - \sum_{k=0}^j \gamma_{jk}(\alpha_s(\mu)) \eta^{j-k} F_k(\dots, \mu^2), \quad (72)$$

$$\mu \frac{d}{d\mu} C_j(\dots, Q^2/\mu^2, \alpha_s(\mu)) = \sum_{k=j}^{\infty} C_k(\dots, Q^2/\mu^2, \alpha_s(\mu)) \gamma_{kj}(\alpha_s(\mu)) \left(\frac{\eta}{\xi}\right)^{k-j}, \quad (73)$$

respectively¹¹. This mixing arises in NLO and is induced by the breaking of special conformal symmetry in LO. The mixing matrix, i.e., γ_{jk} for $j > k$, contains besides a β proportional term also one that does not vanish in the hypothetical conformal limit. Knowing the form of the special conformal symmetry breaking in the \overline{MS} scheme to LO, it was shown that, after rotation, the diagrammatic evaluation of NLO corrections to (flavor nonsinglet) anomalous dimensions [133, 134, 135] and Wilson coefficients [78, 79, 80] in the \overline{MS} scheme coincide, for $\beta = 0$, with the conformal symmetry predictions [136, 114, 77]. A formal proof about the restoration of conformal symmetry, valid to all orders of perturbation theory, has been given in Ref. [114]. Hence, we have no doubt that conformal symmetry can be effectively used for the evaluation of higher order perturbative corrections [137, 101, 102]. The interested reader can find a comprehensive review of the uses of conformal symmetry in QCD in Ref. [115].

Let us suppose that we employ a scheme in which conformal symmetry is manifest in the hypothetical conformal limit. Such a scheme we call a conformal subtraction (CS) scheme. We discuss now the structure of the conformal OPE beyond this limit, i.e., the implementation of the running coupling constant in the Wilson coefficients (68) and the evolution equation. In the simplest case, i.e., forward kinematics, the conformal representation is trivial, as there are only operators without total derivatives left, so we can restore the Wilson coefficients of the full perturbative theory from the result (69) of the conformal limit. Namely, renormalization group invariance of the CFFs allows us to revive the β -proportional term by expanding the exponential¹²

$$c_j(\alpha_s^*) \left(\frac{\mu^2}{Q^2}\right)^{\gamma_j(\alpha_s^*)/2} \Rightarrow c_j(\alpha_s(Q)) \exp \left\{ \int_Q^\mu \frac{d\mu'}{\mu'} \gamma_j(\alpha_s(\mu')) \right\} \quad (74)$$

in terms of $\ln(Q^2/\mu^2)$. Of course, also the evolution of Mellin moments of parton densities is governed by a diagonal evolution equation, i.e., by Eq. (72) with $\eta = 0$. Finally, we are using the

¹¹Both these equations together ensure that the CFF $\mathcal{F}_{j,\xi} \xi^{-j-1} C_j(\dots, Q^2/\mu^2, \alpha_s(\mu)) F_j(\dots, \mu)$ is a renormalization group invariant quantity.

¹²We consider c_j and γ_j as β independent quantities and so their perturbative expansion in the fixed-point and full theory looks the same. Certainly, both of them contain to two-loop accuracy β_0 proportional terms and the anomalous dimensions to three-loop accuracy might be also rewritten in terms of the β function expanded to two-loop accuracy.

normalization condition

$$c_j(\alpha_s) = c_j^{\overline{\text{MS}}}(\alpha_s) \quad (75)$$

and thus we end up with the standard result for the Wilson coefficients of DIS, evaluated in the $\overline{\text{MS}}$ scheme.

For general kinematics the β proportional term is not automatically fixed, so different prescriptions might be used. For a discussion of this issue see Ref. [137]. We will point out here two appealing possibilities.

Let us first assume that the conformal symmetry breaking can be entirely incorporated in the running of the coupling so that the evolution equation for conformal GPD moments is diagonal:

$$\mu \frac{d}{d\mu} F_j(\eta, \Delta^2, \mu^2) = -\gamma_j(\alpha_s(\mu)) F_j(\eta, \Delta^2, \mu^2). \quad (76)$$

Then also the Wilson coefficients in the full theory are simply obtained by replacing the expression for the resummed evolution logs. However, it is likely that the trace anomaly generates a non vanishing β proportional addenda, which will appear at two-loop level. If it does, renormalization group invariance fixes the scale dependence and so the Wilson coefficients in such a scheme read for the full theory

$$C_j^{\text{full}}(\eta/\xi, Q^2/\mu^2, \alpha_s(\mu)) = \left[C_j(\eta/\xi, 1, \alpha_s(Q)) + \frac{\beta}{g}(\alpha_s(Q)) \Delta C_j(\eta/\xi, 1, \alpha_s(Q)) \right] \times \exp \left\{ \int_Q^\mu \frac{d\mu'}{\mu'} \gamma_j(\alpha_s(\mu')) \right\}, \quad (77)$$

where $C_j(\eta/\xi, 1, \alpha_s)$ is the COPE prediction (68). In the forward limit we again require that the Wilson coefficients coincide with the DIS ones, evaluated in the $\overline{\text{MS}}$. Thus, we have the condition that the β proportional addenda vanishes, i.e.,

$$\lim_{\eta \rightarrow 0} \Delta C_j(\eta/\xi, 1, \alpha_s(Q)) = 0. \quad (78)$$

The disadvantage of such a conformal scheme is that a consistent determination of the β proportional addenda ΔC_j requires a diagrammatical evaluation at NNLO, e.g., in the $\overline{\text{MS}}$ scheme. Both the knowledge of the β_0 -proportional terms in the two-loop corrections to the Wilson coefficients and the off-diagonal three-loop corrections to the anomalous dimensions are required. While the former are known in the $\overline{\text{MS}}$ scheme [138, 139], the calculation of the latter, although reducible to a two-loop problem by means of conformal constraints, still requires a great effort. Fortunately, to NNLO only the quark sector suffers from this uncertainty. The best what we can do to NNLO accuracy is to minimize the effects of this lack of knowledge. To do so, we will perform a transformation into a new scheme, called $\overline{\text{CS}}$, where the normalization condition reads

$$\Delta C_j(\eta/\xi, 1, \alpha_s(Q)) = 0, \quad (79)$$

while the mixing term is now shifted to the evolution equation. This mixing term will be suppressed at the input scale by an appropriate initial condition and we might expect that the evolution effects are small, see discussion in Sect. 6.3 below. Hence the Wilson coefficients read now

$$C_j(\eta/\xi, Q^2/\mu^2, \alpha_s(\mu)) = \sum_{k=j}^{\infty} C_k(\eta/\xi, 1, \alpha_s(Q)) \quad (80)$$

$$\times \mathcal{P} \exp \left\{ \int_Q^\mu \frac{d\mu'}{\mu'} \left[\gamma_j(\alpha_s(\mu')) \delta_{kj} + \left(\frac{\eta}{\xi} \right)^{k-j} \frac{\beta}{g} \Delta_{kj}(\alpha_s(\mu')) \right] \right\},$$

where $C_k(\eta/\xi, 1, \alpha_s(Q))$ is given in Eq. (68), Δ_{kj} is determined by the off-diagonal part of the anomalous dimension matrix, and \mathcal{P} denotes the path ordering operation¹³. The renormalization group equation for the conformal moments reads

$$\mu \frac{d}{d\mu} F_j(\cdots, \mu^2) = -\gamma_j(\alpha_s(\mu)) F_j(\cdots, \mu^2) - \frac{\beta(\alpha_s(\mu))}{g(\mu)} \sum_{k=0}^{j-2} \eta^{j-k} \Delta_{jk}(\alpha_s(\mu)) F_k(\cdots, \mu^2). \quad (81)$$

Since this mixing term appears for the first time at NNLO accuracy, and is suppressed at the input scale by the initial condition, we might expect that its effects will be small.

Formulae (80) and (81) are our main result that can be used for the numerical investigation of radiative corrections to DVCS up to NNLO.

4.2 Perturbative expansion of Compton form factors

For DVCS kinematics the general expression for the Wilson coefficients (80) simplifies considerably. Since to twist-two accuracy $\vartheta = \eta/\xi = 1$ is valid, the argument of hypergeometric functions is unity and they simplify to products of Γ functions. Having also in mind that in DVCS the photon virtuality $Q^2 \simeq 2Q^2$ is considered as the relevant scale, the COPE prediction (68) together with Eq. (80) leads to the following expression for the DVCS Wilson coefficients

$$C_j(Q^2/\mu^2, \alpha_s(\mu)) \equiv C_j(\vartheta = 1, Q^2/(2\mu^2), \alpha_s(\mu)) \quad (82)$$

$$= c_j(\alpha_s(Q)) \frac{2^{j+1+\gamma_j(\alpha_s(Q))} \Gamma(\frac{5}{2} + j + \frac{1}{2}\gamma_j(\alpha_s(Q)))}{\Gamma(\frac{3}{2}) \Gamma(3 + j + \frac{1}{2}\gamma_j(\alpha_s(Q)))} \exp \left\{ \int_Q^\mu \frac{d\mu'}{\mu'} \gamma_j(\alpha_s(\mu')) \right\}$$

at the considered NNLO accuracy. Note that the off-diagonal part of the evolution operator does not appear in this approximation, and that we have slightly changed the normalization condition

¹³The path ordering operation defined by

$$\mathcal{P} \exp \left\{ \int_Q^\mu \frac{d\mu'}{\mu'} \gamma_{jk}(\alpha_s(\mu')) \right\} = 1 + \int_Q^\mu \frac{d\mu'}{\mu'} \gamma_{jk}(\alpha_s(\mu')) + \int_Q^\mu \frac{d\mu'}{\mu'} \int_Q^{\mu'} \frac{d\mu''}{\mu''} \sum_{m=k}^j \gamma_{jm}(\alpha_s(\mu')) \gamma_{mk}(\alpha_s(\mu'')) + \dots$$

enables the compact representation of the solution of the non-diagonal renormalization group equations. Obviously, in diagonal case, i.e. for $\gamma_{jk} = \delta_{jk} \gamma_j$, path ordering converts the evolution operator in a simple exponential function.

for $\mu = \mathcal{Q}$. In fact to arrive at the above result, Eq. (80) has to be multiplied by a factor

$$\left(\sqrt{2}\right)^{\gamma_j(\alpha_s(\mathcal{Q}))} \exp\left\{-\int_{\mathcal{Q}/\sqrt{2}}^{\mathcal{Q}} \frac{d\mu'}{\mu'} \gamma_j(\alpha_s(\mu'))\right\} = 1 + \frac{\alpha_s^2(\mathcal{Q})}{(2\pi)^2} \frac{\beta_0}{8} \gamma_j^{(0)} \ln^2(2) + \mathcal{O}(\alpha_s^3), \quad (83)$$

and such terms can be compensated by a change of the normalization condition (79). Here and in the following the first expansion coefficient of $\beta(g)/g = (\alpha_s/4\pi)\beta_0 + \mathcal{O}(\alpha_s^2)$ is $\beta_0 = (2/3)n_f - 11$, where n_f is the number of active quarks.

We now use perturbation theory to determine $C_j(\mathcal{Q}^2/\mu^2, \alpha_s(\mu))$ to NNLO accuracy. In contrast to $F_j(\dots, \mu^2)$, it is customary to express $C_j(\mathcal{Q}^2/\mu^2, \alpha_s(\mu))$ completely expanded in $\alpha_s(\mu)$, i.e., without resummation of leading logs from μ to \mathcal{Q} . This actually corresponds to the result that one would obtain from a diagrammatical calculation, without using the renormalization group equation. Obviously, since the leading logarithms in F_j will be resummed and in C_j not, one will end up with a residual dependence on the factorization scale μ . This scale might also be used as the relevant scale in the running coupling constant. However, for generality, another scale μ_r is better suited for the expansion parameter $\alpha_s(\mu_r)$. The truncation of perturbation theory then implies that our results will depend also on this renormalization scale μ_r .

The perturbative expansion of the DVCS Wilson coefficients (82) in terms of $\alpha_s(\mu_r)$ is done in a straightforward manner by means of

$$\alpha_s(\mu) = \alpha_s(\mu_r) + \beta_0 \frac{\alpha_s^2(\mu_r)}{4\pi} \ln \frac{\mu^2}{\mu_r^2} \quad (84)$$

and consequently we can expand the exponential factor

$$\exp\left\{\int_{\mathcal{Q}}^{\mu} \frac{d\mu'}{\mu'} \gamma_j(\alpha_s(\mu'))\right\} = \left(\frac{\mu^2}{\mathcal{Q}^2}\right)^{\gamma_j(\alpha_s(\mu_r))/2} \left[1 - \frac{\alpha_s^2(\mu_r)}{(2\pi)^2} \frac{\beta_0}{8} \gamma_j^{(0)} \ln \frac{\mathcal{Q}^2}{\mu^2} \ln \frac{\mu^2 \mathcal{Q}^2}{\mu_r^4} + \mathcal{O}(\alpha_s^3)\right]. \quad (85)$$

Furthermore, we use the expansion

$$\frac{2^{j+1+\gamma_j} \Gamma\left(\frac{5}{2} + j + \frac{1}{2}\gamma_j\right)}{\Gamma\left(\frac{3}{2}\right) \Gamma\left(3 + j + \frac{1}{2}\gamma_j\right)} \left(\frac{\mu^2}{\mathcal{Q}^2}\right)^{\gamma_j/2} = \frac{2^{j+1} \Gamma(5/2 + j)}{\Gamma(3/2) \Gamma(3 + j)} \sum_{m=0}^{\infty} \frac{s_j^{(m)}(\mathcal{Q}^2/\mu^2)}{2^m m!} [\gamma_j]^m, \quad (86)$$

where the so-called shift coefficients, which also include the factorization logs, are defined as

$$s_j^{(m)}(\mathcal{Q}^2/\mu^2) = \frac{d^m}{d\rho^m} \left(\frac{\mu^2}{\mathcal{Q}^2}\right)^{\rho} \frac{4^{\rho} \Gamma(3 + j) \Gamma(5/2 + j + \rho)}{\Gamma(5/2 + j) \Gamma(3 + j + \rho)} \Big|_{\rho=0}. \quad (87)$$

The first two shift coefficients read in terms of harmonic sums as

$$s_j^{(1)}(\mathcal{Q}^2/\mu^2) = S_1(j + 3/2) - S_1(j + 2) + 2 \ln(2) - \ln \frac{\mathcal{Q}^2}{\mu^2}, \quad (88a)$$

$$s_j^{(2)}(\mathcal{Q}^2/\mu^2) = \left(s_j^{(1)}(\mathcal{Q}^2/\mu^2)\right)^2 - S_2(j + 3/2) + S_2(j + 2), \quad (88b)$$

where the analytical continuation of these sums are defined by

$$S_1(z) = \frac{d}{dz} \ln \Gamma(z+1) + \gamma_E \quad \text{and} \quad S_2(z) = -\frac{d^2}{dz^2} \ln \Gamma(z+1) + \frac{\pi^2}{6} \quad (89)$$

with $\gamma_E = 0.5772\dots$ being the Euler constant. Taking into account the perturbative expansion of anomalous dimensions and DIS Wilson coefficients, written as

$$\begin{aligned} \gamma_j(\alpha_s) &= \frac{\alpha_s}{2\pi} \gamma_j^{(0)} + \frac{\alpha_s^2}{(2\pi)^2} \gamma_j^{(1)} + \frac{\alpha_s^3}{(2\pi)^3} \gamma_j^{(2)} + \mathcal{O}(\alpha_s^4), \\ c_j(\alpha_s) &= c_j^{(0)} + \frac{\alpha_s}{2\pi} c_j^{(1)} + \frac{\alpha_s^2}{(2\pi)^2} c_j^{(2)} + \mathcal{O}(\alpha_s^3), \end{aligned} \quad (90)$$

the DVCS Wilson coefficients (82) take the form

$$C_j = \frac{2^{j+1}\Gamma(j+5/2)}{\Gamma(3/2)\Gamma(j+3)} \left[c_j^{(0)} + \frac{\alpha_s(\mu_r)}{2\pi} C_j^{(1)}(\mathcal{Q}^2/\mu^2) + \frac{\alpha_s^2(\mu_r)}{(2\pi)^2} C_j^{(2)}(\mathcal{Q}^2/\mu^2, \mathcal{Q}^2/\mu_r^2) + \mathcal{O}(\alpha_s^3) \right], \quad (91a)$$

where

$$C_j^{(1)} = c_j^{(1)} + \frac{s_j^{(1)}(\mathcal{Q}^2/\mu^2)}{2} c_j^{(0)} \gamma_j^{(0)}, \quad (91b)$$

$$\begin{aligned} C_j^{(2)} &= c_j^{(2)} + \frac{s_j^{(1)}(\mathcal{Q}^2/\mu^2)}{2} \left[c_j^{(0)} \gamma_j^{(1)} + c_j^{(1)} \gamma_j^{(0)} \right] + \frac{s_j^{(2)}(\mathcal{Q}^2/\mu^2)}{8} c_j^{(0)} \left(\gamma_j^{(0)} \right)^2 \\ &\quad + \frac{\beta_0}{2} \left(C_j^{(1)}(\mathcal{Q}^2/\mu^2) \ln \frac{\mathcal{Q}^2}{\mu_r^2} + \frac{1}{4} c_j^{(0)} \gamma_j^{(0)} \ln^2 \frac{\mathcal{Q}^2}{\mu^2} \right). \end{aligned} \quad (91c)$$

Notice that the renormalization group logs $\ln(\mathcal{Q}^2/\mu_r^2)$, caused by the running of α_s , and proportional to β_0 , appear for the first time in the NNLO correction $C_j^{(2)}$.

4.2.1 Flavor nonsinglet Wilson coefficients

The flavor nonsinglet Wilson coefficients have the form as indicated in Eqs. (91a)–(91c). We only have to decorate them and the anomalous dimensions with the corresponding superscripts. It has been already taken into account that the DIS Wilson coefficients are normalized as

$${}^{\text{NS}}c_j^{\text{I}(0)} = 1. \quad (92)$$

The radiative corrections to NLO involve the Wilson coefficients of the DIS unpolarized structure function F_1 ,

$${}^{\text{NS}}c_j^{\text{V}(1)} = C_F \left[S_1^2(1+j) + \frac{3}{2} S_1(j+2) - \frac{9}{2} + \frac{5 - 2S_1(j)}{2(j+1)(j+2)} - S_2(j+1) \right], \quad (93)$$

for the vector case and those of the polarized structure function g_1 ,

$${}^{\text{NS}}c_j^{\text{A}(1)} = C_F \left[S_1^2(1+j) + \frac{3}{2} S_1(j+2) - \frac{9}{2} + \frac{3 - 2S_1(j)}{2(j+1)(j+2)} - S_2(j+1) \right], \quad (94)$$

for the axial-vector one. The LO anomalous dimensions read in both cases

$${}^{\text{NS}}\gamma_j^{\text{I}(0)} = -C_F \left(3 + \frac{2}{(j+1)(j+2)} - 4S_1(j+1) \right), \quad (95)$$

where $C_F = (N_c^2 - 1)/(2N_c)$ with N_c being the number of colors.

The expressions for two-loop quantities are lengthy. The nonsinglet anomalous dimensions $\gamma_j^{(1)}$ for the vector and axial-vector case are given, e.g., in Ref. [140], by analytic continuation of j -odd and j -even expressions, respectively. The NNLO Wilson coefficients $c_j^{(2)}$ can be read off for the vector and axial-vector cases from Refs. [141] and [142], respectively. Implementation of evolution to NNLO accuracy requires also the anomalous dimensions to three-loop order [143]. Instead of the exact expressions one might alternatively use an analytic approximation, given for the vector quantities in Refs. [144, 143].

4.2.2 Flavor singlet Wilson coefficients

So far the $\{+, -\}$ basis, which resolves the mixing problem in the flavor singlet sector, has been used for presenting the conformal predictions. However, the Wilson coefficients are in the literature usually given in the $\{Q \equiv \Sigma, G\}$ basis. For convenience, we might express the flavor singlet results in the basis of quark and gluon degrees of freedom. We write the Wilson coefficients as a two-dimensional row vector

$$\mathbf{C}_j^{\text{I}}(\mathcal{Q}^2/\mu^2, \alpha_s(\mu)) = \left({}^\Sigma C_j^{\text{I}}, {}^G C_j^{\text{I}} \right) (\mathcal{Q}^2/\mu^2, \alpha_s(\mu)) \quad \text{for } \text{I} = \{\text{V}, \text{A}\}. \quad (96)$$

In the following we drop the superscript I. The rotation between the two bases is given by the transformation matrix \mathbf{U}_j , defined in Eq. (24). Hence, for the Wilson coefficients we have

$$\mathbf{C}_j(\mathcal{Q}^2/\mu^2, \alpha_s(\mu)) = \left({}^+ C_j, {}^- C_j \right) (\mathcal{Q}^2/\mu^2, \alpha_s(\mu)) \mathbf{U}_j(\mu, \mathcal{Q}), \quad (97)$$

where the $\{+, -\}$ entries are given in Eq. (82). Using the property (B.4) of the transformation matrix within $\mu_0 = \mathcal{Q}$, derived in Appendix B, allows us to perform the transformation at the normalization point $\mu = \mathcal{Q}$ and afterwards restore the scale dependence by an backward evolution:

$$\mathbf{C}_j(\mathcal{Q}^2/\mu^2, \alpha_s(\mu)) = \left({}^+ C_j, {}^- C_j \right) (\mathcal{Q}^2/\mu^2 = 1, \alpha_s(\mathcal{Q})) \mathbf{U}_j(\mathcal{Q}, \mathcal{Q}) \mathcal{E}_j^{-1}(\mu, \mathcal{Q}). \quad (98)$$

Here \mathcal{E}_j^{-1} is the inverse of the evolution operator in the $\{\Sigma, G\}$ basis, defined below in Eq. (120). Since $\mathbf{U}_j(\mathcal{Q}, \mathcal{Q})$ rotates the anomalous dimensions [depending on $\alpha_s(\mathcal{Q})$], we can express for $\mu = \mathcal{Q}$ the flavor singlet contributions in the form

$$\mathbf{C}_j(\mathcal{Q}^2/\mu^2 = 1, \alpha_s(\mathcal{Q})) = \frac{2^{j+1}\Gamma(5/2+j)}{\Gamma(3/2)\Gamma(3+j)} \sum_{m=0}^{\infty} \frac{s_j^{(m)}(\mathcal{Q}^2/\mu^2 = 1)}{2^m m!} \mathbf{c}_j [\gamma_j]^m, \quad \mathbf{c}_j = \left({}^\Sigma c_j, {}^G c_j \right), \quad (99)$$

where the anomalous dimension matrix is defined as

$$\gamma_j = \frac{\alpha_s}{2\pi} \begin{pmatrix} \Sigma\Sigma\gamma_j^{(0)} & \Sigma G\gamma_j^{(0)} \\ G\Sigma\gamma_j^{(0)} & GG\gamma_j^{(0)} \end{pmatrix} + \mathcal{O}(\alpha_s^2). \quad (100)$$

This matrix valued expansion, although resulting from somewhat more involved derivation, is in complete analogy to the flavor nonsinglet result (86).

Acting with the evolution operator $\mathcal{E}_j^{-1}(\mu, \mathcal{Q})$ on Eq. (99) removes the constraint $\mathcal{Q}^2/\mu^2 = 1$ of the shift functions argument. As in the preceding section, we consequently expand with respect to $\alpha_s(\mu_r)$ and finally write the Wilson coefficients (96) in complete analogy to Eq. (91) as

$$C_j = \frac{2^{j+1}\Gamma(j+5/2)}{\Gamma(3/2)\Gamma(j+3)} \left[\mathbf{c}_j^{(0)} + \frac{\alpha_s(\mu_r)}{2\pi} \mathbf{C}_j^{(1)}(\mathcal{Q}^2/\mu^2) + \frac{\alpha_s^2(\mu_r)}{(2\pi)^2} \mathbf{C}_j^{(2)}(\mathcal{Q}^2/\mu^2, \mathcal{Q}^2/\mu_r^2) + \mathcal{O}(\alpha_s^3) \right], \quad (101a)$$

where

$$\mathbf{C}_j^{(1)}(\mathcal{Q}^2/\mu^2) = \mathbf{c}_j^{(1)} + \frac{s_j^{(1)}(\mathcal{Q}^2/\mu^2)}{2} \mathbf{c}_j^{(0)} \gamma_j^{(0)}, \quad (101b)$$

$$\begin{aligned} \mathbf{C}_j^{(2)}(\mathcal{Q}^2/\mu^2) = & \mathbf{c}_j^{(2)} + \frac{s_j^{(1)}(\mathcal{Q}^2/\mu^2)}{2} \left[\mathbf{c}_j^{(0)} \gamma_j^{(1)} + \mathbf{c}_j^{(1)} \gamma_j^{(0)} \right] + \frac{s_j^{(2)}(\mathcal{Q}^2/\mu^2)}{8} \mathbf{c}_j^{(0)} \left(\gamma_j^{(0)} \right)^2 \\ & + \frac{\beta_0}{2} \left[\mathbf{C}_j^{(1)}(\mathcal{Q}^2/\mu^2) \ln \frac{\mathcal{Q}^2}{\mu_r^2} + \frac{1}{4} \mathbf{c}_j^{(0)} \gamma_j^{(0)} \ln^2 \frac{\mathcal{Q}^2}{\mu^2} \right]. \end{aligned} \quad (101c)$$

To LO the DIS Wilson coefficients are normalized as

$$\mathbf{c}_j^{\text{V}(0)} = \mathbf{c}_j^{\text{A}(0)} = (1, 0). \quad (102)$$

In NLO the quark Wilson coefficients correspond to the non-singlet ones given in Eqs. (93) and (94),

$$\Sigma \mathbf{c}_j^{\text{V}(1)} = \text{NS} \mathbf{c}_j^{\text{V}(1)}, \quad (103)$$

$$\Sigma \mathbf{c}_j^{\text{A}(1)} = \text{NS} \mathbf{c}_j^{\text{A}(1)}, \quad (104)$$

while the gluon ones read

$$G \mathbf{c}_j^{\text{V}(1)} = -n_f \frac{(4 + 3j + j^2)S_1(j) + 2 + 3j + j^2}{(1+j)(2+j)(3+j)} \quad (105)$$

$$G \mathbf{c}_j^{\text{A}(1)} = -n_f \frac{j}{(1+j)(2+j)} [1 + S_1(j)]. \quad (106)$$

The entries of the anomalous dimension matrices read to LO in the vector case:

$$\Sigma G \gamma_j^{\text{V}(0)} = -4n_f T_F \frac{4 + 3j + j^2}{(j+1)(j+2)(j+3)}, \quad (107)$$

$$G \Sigma \gamma_j^{\text{V}(0)} = -2C_F \frac{4 + 3j + j^2}{j(j+1)(j+2)}, \quad (108)$$

$$GG \gamma_j^{\text{V}(0)} = -C_A \left(-\frac{4}{(j+1)(j+2)} + \frac{12}{j(j+3)} - 4S_1(j+1) \right) + \beta_0, \quad (109)$$

and in the axial-vector case:

$$\Sigma^G \gamma_j^{A(0)} = -4n_f T_F \frac{j}{(j+1)(j+2)}, \quad (110)$$

$$G^{\Sigma} \gamma_j^{A(0)} = -2C_F \frac{(j+3)}{(j+1)(j+2)}, \quad (111)$$

$$G^G \gamma_j^{A(0)} = -C_A \left(\frac{8}{(j+1)(j+2)} - 4S_1(j+1) \right) + \beta_0, \quad (112)$$

where $C_A = N_c$ and $T_F = 1/2$. At this order the anomalous dimensions in the quark-quark channels are identical to the flavor nonsinglet ones

$$\Sigma \Sigma \gamma_j^{V(0)} = \Sigma \Sigma \gamma_j^{A(0)} = \text{NS} \gamma_j^{(0)}, \quad (113)$$

given in Eq. (95). The NNLO DIS Wilson coefficients for the structure functions F_1 and g_1 are given in Refs. [141, 142]. The NLO singlet anomalous dimensions for the vector and axial-vector cases can be found in Refs. [140, 145] and [146, 147], respectively. To treat the evolution to NNLO approximation we need also the NNLO flavor singlet anomalous dimension matrix. It has been calculated for the vector case in Ref. [148]. We remark that all these quantities are expressed in terms of rational functions and harmonic sums. Several numerical routines for them are available, e.g., in Refs. [149, 150, 151, 152]. Here again one might rely on analytic approximations for the quantities in question, see Refs. [153, 148].

4.2.3 Expansion of the evolution operator

The evolution of the flavor nonsinglet (integer) conformal moments in this $\overline{\text{CS}}$ scheme is governed by

$$\begin{aligned} \mu \frac{d}{d\mu} F_j(\xi, \Delta^2, \mu^2) = & - \left[\frac{\alpha_s(\mu)}{2\pi} \gamma_j^{(0)} + \frac{\alpha_s^2(\mu)}{(2\pi)^2} \gamma_j^{(1)} + \frac{\alpha_s^3(\mu)}{(2\pi)^3} \gamma_j^{(2)} + \mathcal{O}(\alpha_s^4) \right] F_j(\xi, \Delta^2, \mu^2) \\ & - \frac{\beta_0}{2} \frac{\alpha_s^3(\mu)}{(2\pi)^3} \sum_{k=0}^{j-2} \left[\Delta_{jk}^{\overline{\text{CS}}} + \mathcal{O}(\alpha_s) \right] F_k(\xi, \Delta^2, \mu^2). \end{aligned} \quad (114)$$

The solution of the renormalization group equation is given by the path-ordered exponential, appearing in Eq. (80). Unfortunately, the mixing matrix $\Delta_{jk}^{\overline{\text{CS}}}$ is not completely known, and so we can here only deal with the solution for $\Delta_{jk} = 0$:

$$F_j(\xi, \Delta^2, \mu^2) = \mathcal{E}_j(\mu, \mu_0) F_j(\xi, \Delta^2, \mu_0^2), \quad \text{where} \quad \mathcal{E}_j(\mu, \mu_0) = \exp \left\{ - \int_{\mu_0}^{\mu} \frac{d\mu'}{\mu'} \gamma_j(\mu') \right\}. \quad (115)$$

In the numerical analysis we will resum only the leading logarithms and expand the non-leading ones. The result, see Ref. [137], reads

$$\mathcal{E}_j(\mu, \mu_0) = \left[1 + \frac{\alpha_s(\mu)}{2\pi} \mathcal{A}_j^{(1)}(\mu, \mu_0) + \frac{\alpha_s^2(\mu)}{(2\pi)^2} \mathcal{A}_j^{(2)}(\mu, \mu_0) + \mathcal{O}(\alpha_s^3) \right] \left[\frac{\alpha_s(\mu)}{\alpha_s(\mu_0)} \right]^{-\frac{\gamma_j^{(0)}}{\beta_0}}, \quad (116)$$

where

$$\begin{aligned}\mathcal{A}_j^{(1)}(\mu, \mu_0) &= \left[1 - \frac{\alpha_s(\mu_0)}{\alpha_s(\mu)}\right] \left[\frac{\beta_1}{2\beta_0} \frac{\gamma_j^{(0)}}{\beta_0} - \frac{\gamma_j^{(1)}}{\beta_0}\right], \\ \mathcal{A}_j^{(2)}(\mu, \mu_0) &= \frac{1}{2} \left[\mathcal{A}_j^{(1)}(\mu, \mu_0)\right]^2 - \left[1 - \frac{\alpha_s^2(\mu_0)}{\alpha_s^2(\mu)}\right] \left[\frac{\beta_1^2 - \beta_2\beta_0}{8\beta_0^2} \frac{\gamma_j^{(0)}}{\beta_0} - \frac{\beta_1}{4\beta_0} \frac{\gamma_j^{(1)}}{\beta_0} + \frac{\gamma_j^{(2)}}{2\beta_0}\right].\end{aligned}\quad (117)$$

The expansion coefficients of the β function are

$$\begin{aligned}\frac{\beta}{g} &= \frac{\alpha_s(\mu)}{4\pi} \beta_0 + \frac{\alpha_s^2(\mu)}{(4\pi)^2} \beta_1 + \frac{\alpha_s^3(\mu)}{(4\pi)^3} \beta_2 + O(\alpha_s^4), \\ \beta_0 &= \frac{2}{3}n_f - 11, \quad \beta_1 = \frac{38}{3}n_f - 102, \quad \beta_2 = -\frac{325}{54}n_f^2 + \frac{5033}{18}n_f - \frac{2857}{2}.\end{aligned}\quad (118)$$

The flavor singlet case can be treated in the diagonal $\{+, -\}$ basis in the analogous way as the nonsinglet one. Here we present the solution in the $\{Q, G\}$ basis:

$$\begin{pmatrix} \Sigma_{F_j} \\ G_{F_j} \end{pmatrix} (\xi, \Delta^2, \mu^2) = \mathcal{E}_j(\mu, \mu_0) \begin{pmatrix} \Sigma_{F_j} \\ G_{F_j} \end{pmatrix} (\xi, \Delta^2, \mu_0^2). \quad (119)$$

We will expand the evolution operator¹⁴

$$\mathcal{E}_j(\mu, \mu_0) = \mathcal{P} \exp \left\{ - \int_{\mu_0}^{\mu} \frac{d\mu'}{\mu'} \gamma_j(\alpha_s(\mu')) \right\} \quad (120)$$

up to order α_s^2 , and while leading logs remain resummed the non-leading ones are expanded. To have a condensed notation, we perturbatively expand the result in terms of the leading order $\{+, -\}$ modes:

$$\mathcal{E}_j(\mu, \mu_0) = \sum_{a,b=\pm} \left[\delta_{ab} {}^a\mathbf{P}_j + \frac{\alpha_s(\mu)}{2\pi} {}^{ab}\mathcal{A}_j^{(1)}(\mu, \mu_0) + \frac{\alpha_s^2(\mu)}{(2\pi)^2} {}^{ab}\mathcal{A}_j^{(2)}(\mu, \mu_0) + O(\alpha_s^3) \right] \left[\frac{\alpha_s(\mu)}{\alpha_s(\mu_0)} \right]^{-\frac{b\lambda_j}{\beta_0}}, \quad (121)$$

Here the projectors on the $\{+, -\}$ modes are

$${}^{\pm}\mathbf{P}_j = \frac{\pm 1}{{}^+\lambda_j - {}^-\lambda_j} \left(\gamma_j^{(0)} - {}^{\mp}\lambda_j \mathbf{1} \right), \quad (122)$$

where the eigenvalues of the LO anomalous dimension matrix (i.e., ${}^{\pm}\gamma_j^{(0)}$ from Eq. (B.2)) are

$${}^{\pm}\lambda_j = \frac{1}{2} \left(\Sigma\Sigma\gamma_j^{(0)} + {}^G\!G\gamma_j^{(0)} \mp \left(\Sigma\Sigma\gamma_j^{(0)} - {}^G\!G\gamma_j^{(0)} \right) \sqrt{1 + \frac{4 \Sigma G\gamma_j^{(0)} G\Sigma\gamma_j^{(0)}}{\left(\Sigma\Sigma\gamma_j^{(0)} - {}^G\!G\gamma_j^{(0)} \right)^2}} \right), \quad (123)$$

¹⁴Here the path ordering \mathcal{P} is related to the non-diagonality of the anomalous matrix in $\{Q, G\}$ basis.

A straightforward calculation leads to the matrix valued coefficients

$${}^{ab}\mathcal{A}_j^{(1)} = {}^{ab}R_j(\mu, \mu_0|1) {}^a\mathbf{P}_j \left[\frac{\beta_1}{2\beta_0} \gamma_j^{(0)} - \gamma_j^{(1)} \right] {}^b\mathbf{P}_j \quad (124)$$

$$\begin{aligned} {}^{ab}\mathcal{A}_j^{(2)} = & \sum_{c=\pm} \frac{1}{\beta_0 + {}^c\lambda_j - {}^b\lambda_j} \left[{}^{ab}R_j(\mu, \mu_0|2) - {}^{ac}R_j(\mu, \mu_0|1) \left(\frac{\alpha_s(\mu_0)}{\alpha_s(\mu)} \right)^{\frac{\beta_0 + {}^c\lambda_j - {}^b\lambda_j}{\beta_0}} \right] {}^a\mathbf{P}_j \left[\frac{\beta_1}{2\beta_0} \gamma_j^{(0)} - \gamma_j^{(1)} \right] \\ & \times {}^c\mathbf{P}_j \left[\frac{\beta_1}{2\beta_0} \gamma_j^{(0)} - \gamma_j^{(1)} \right] {}^b\mathbf{P}_j - {}^{ab}R_j(\mu, \mu_0|2) {}^a\mathbf{P}_j \left[\frac{\beta_1^2 - \beta_2\beta_0}{4\beta_0^2} \gamma_j^{(0)} - \frac{\beta_1}{2\beta_0} \gamma_j^{(1)} + \gamma_j^{(2)} \right] {}^b\mathbf{P}_j, \end{aligned} \quad (125)$$

where the μ dependence is accumulated in the functions ${}^{ab}R_j(\mu, \mu_0|n) \equiv {}^{ab}R_{jk}(\mu, \mu_0|n)$ defined by

$${}^{ab}R_{jk}(\mu, \mu_0|n) = \frac{1}{n\beta_0 + {}^a\lambda_j - {}^b\lambda_k} \left[1 - \left(\frac{\alpha_s(\mu_0)}{\alpha_s(\mu)} \right)^{\frac{n\beta_0 + {}^a\lambda_j - {}^b\lambda_k}{\beta_0}} \right]. \quad (126)$$

The expansion of the evolution operator (116) or (121) will then be consistently combined with the Wilson coefficients (91) or (101), respectively, see for instance Ref. [137].

4.3 $\overline{\text{MS}}$ results up to NLO order

The DVCS radiative corrections in the $\overline{\text{MS}}$ scheme are known only to NLO. The NLO corrections to the hard-scattering amplitude have been obtained by rotation from the conformal prediction [114, 77] and agree with the diagrammatical evaluation of Refs. [78, 79, 80]. Employing Eq. (C.6), the corresponding Wilson coefficients can be obtained by determining the conformal moments of the hard-scattering amplitude, e.g., summarized in Ref. [154].

The integrals which are needed for the quark part are given in Appendix C of Ref. [137] for integer conformal spin (see also the last paragraph in Appendix C.1). The analytical continuation is straightforward and so in the $\overline{\text{MS}}$ scheme we have

$${}^\Sigma C_j^{\text{V}(1)}(\mathcal{Q}/\mu^2) = C_F \left[2S_1^2(1+j) - \frac{9}{2} + \frac{5 - 4S_1(j+1)}{2(j+1)(j+2)} + \frac{1}{(j+1)^2(j+2)^2} \right] + \frac{{}^\Sigma \gamma_j^{(0)}}{2} \ln \frac{\mu^2}{\mathcal{Q}^2}, \quad (127)$$

$${}^\Sigma C_j^{\text{A}(1)}(\mathcal{Q}/\mu^2) = C_F \left[2S_1^2(1+j) - \frac{9}{2} + \frac{3 - 4S_1(j+1)}{2(j+1)(j+2)} + \frac{1}{(j+1)^2(j+2)^2} \right] + \frac{{}^\Sigma \gamma_j^{(0)}}{2} \ln \frac{\mu^2}{\mathcal{Q}^2}, \quad (128)$$

in vector and axial-vector case, respectively, while ${}^{\text{NS}}C_j^{\text{I}(1)} = {}^\Sigma C_j^{\text{I}(1)}$.

The integral expressions needed for the determination of the singlet gluon contributions we

list in App. C.2. For the gluon conformal moments we obtain

$${}^G C_j^{V(1)}(\mathcal{Q}/\mu^2) = -n_f \frac{(4 + 3j + j^2) [S_1(j) + S_1(j+2)] + 2 + 3j + j^2}{(1+j)(2+j)(3+j)} + \frac{\Sigma^G \gamma_j^{V(0)}}{2} \ln \frac{\mu^2}{\mathcal{Q}^2}, \quad (129)$$

$${}^G C_j^{A(1)}(\mathcal{Q}/\mu^2) = -n_f \frac{j}{(1+j)(2+j)} [1 + S_1(j) + S_1(j+2)] + \frac{\Sigma^G \gamma_j^{A(0)}}{2} \ln \frac{\mu^2}{\mathcal{Q}^2}. \quad (130)$$

The complete anomalous dimension matrix in $\overline{\text{MS}}$ scheme is known to two-loop accuracy [136, 155, 82]. We present here the more involved case of the evolution in singlet sector and will just state the substitutions needed to obtain nonsinglet case results; for the extensive account of the singlet case evolution see also Ref. [100]. Note that our normalization, adopted from DIS, differs from the original one. Anomalous dimensions used in this work are related to those in Ref. [100], denoted as

$$\gamma_{jk} = \mathbf{N}_j \gamma_{jk}|_{[100]} \mathbf{N}_k^{-1}. \quad (131)$$

The transformation matrix is

$$\mathbf{N}_j = N(j) \begin{pmatrix} 1 & 0 \\ 0 & \frac{6}{j} \end{pmatrix}, \quad (132)$$

with the normalization factor

$$N(j) = \frac{\Gamma(3/2)\Gamma(j+1)}{2^j \Gamma(j+3/2)}, \quad (133)$$

originating from the altered definitions (21) and (23) of conformal operators. Explicitly, we have for non-diagonal entries

$$\gamma_{jk} = \frac{2^k \Gamma(j+1) \Gamma(k+3/2)}{2^j \Gamma(k+1) \Gamma(j+3/2)} \begin{pmatrix} {}^{QQ} \gamma_{jk}|_{[100]} & \frac{k}{6} {}^{QG} \gamma_{jk}|_{[100]} \\ \frac{6}{j} {}^{GQ} \gamma_{jk}|_{[100]} & \frac{k}{j} {}^{GG} \gamma_{jk}|_{[100]} \end{pmatrix}, \quad (134)$$

where the diagonal ones,

$$\gamma_j \equiv \gamma_{jj} = \begin{pmatrix} {}^{QQ} \gamma_j|_{[100]} & \frac{j}{6} {}^{QG} \gamma_j|_{[100]} \\ \frac{6}{j} {}^{GQ} \gamma_j|_{[100]} & {}^{GG} \gamma_j|_{[100]} \end{pmatrix}, \quad (135)$$

coincide with the DIS anomalous dimensions.

The evolution operator in the $\overline{\text{MS}}$ -scheme leads already at NLO to a mixing of conformal GPD moments. For integer conformal spin these moments evolve as

$$\mathbf{F}_j(\eta, \Delta^2, \mu) = \sum_{k=0}^j \frac{1 \mp (-1)^k}{2} \boldsymbol{\mathcal{E}}_{jk}(\mu, \mu_0; \eta) \mathbf{F}_k(\eta, \Delta^2, \mu_0). \quad (136)$$

To NLO accuracy the evolution operator is expanded as¹⁵

$$\begin{aligned} \mathcal{E}_{jk}(\mu, \mu_0; \eta) &= \sum_{a,b=\pm} \left[\delta_{ab} {}^a\mathbf{P}_j \delta_{jk} + \frac{\alpha_s(\mu)}{2\pi} \left({}^{ab}\mathcal{A}_j^{(1)}(\mu, \mu_0) \delta_{jk} + {}^{ab}\mathcal{B}_{jk}^{(1)}(\mu, \mu_0) \eta^{j-k} \right) + O(\alpha_s^2) \right] \left[\frac{\alpha_s(\mu)}{\alpha_s(\mu_0)} \right]^{-\frac{b\lambda_k}{\beta_0}}. \end{aligned} \quad (137)$$

The diagonal term $\mathcal{E}_{jj}(\mu, \mu_0; \eta)$ coincides with the evolution operator $\mathcal{E}_j(\mu, \mu_0)$ of the preceding section, where the diagonal anomalous dimensions γ_j are the same in $\overline{\text{MS}}$ and $\overline{\text{CS}}$ scheme. Also the projector ${}^a\mathbf{P}_j$ is the same as before and is defined in Eq. (122). The matrix ${}^{ab}\mathcal{B}_{jk}^{(1)}(\mu, \mu_0)$, defined for $j - k = \{2, 4, \dots\}$ (while 0 otherwise), assumes the form analogous to (124)

$${}^{ab}\mathcal{B}_{jk}^{(1)} = -{}^{ab}R_{jk}(\mu, \mu_0|1) {}^a\mathbf{P}_j \gamma_{jk}^{(1)} {}^b\mathbf{P}_k, \quad \text{for } j - k \text{ even}, \quad (138)$$

while $\gamma_{jk}^{(1)}$ can be expressed as

$$\gamma_{jk}^{(1)} = [\gamma^{(0)}, \mathbf{g} + \mathbf{d}(\beta_0 - \gamma^{(0)})]_{jk}. \quad (139)$$

This equation holds for parity even and odd anomalous dimension matrices, where \mathbf{g}_{jk} and \mathbf{d}_{jk} transform according to Eq. (131). In analogy to Eq. (134), the matrices \mathbf{g}_{jk} and \mathbf{d}_{jk} can be read off from the results given in Ref. [100]. Taking into account the usual properties of projectors, one can conveniently rewrite ${}^{ab}\mathcal{B}_{jk}^{(1)}(\mu, \mu_0)$ as

$${}^{ab}\mathcal{B}_{jk}^{(1)}(\mu, \mu_0) = -{}^{ab}R_{jk}(\mu, \mu_0|1) ({}^a\lambda_j - {}^b\lambda_k) [(\beta_0 - {}^b\lambda_k) {}^a\mathbf{P}_j \mathbf{d}_{jk} {}^b\mathbf{P}_k + {}^a\mathbf{P}_j \mathbf{g}_{jk} {}^b\mathbf{P}_k]. \quad (140)$$

The NLO solution of the evolution operator convoluted with the Wilson coefficients can be more easily treated as the evolution of the conformal GPD moments itself. Namely, the convolution, represented as an infinite series and understood as an analytic function of j , can be expressed in two equivalent forms

$$\begin{aligned} &\sum_{j=0}^{\infty} [1 \mp (-1)^j] \xi^{-j-1} \mathbf{C}_j(\mathcal{Q}^2/\mu^2, \alpha_s(\mu)) \left(\sum_{k=0}^j \frac{1 \mp (-1)^k}{2} \mathcal{E}_{jk}(\mu, \mu_0; \xi) \mathbf{F}_k(\xi, \Delta^2, \mu_0) \right) \\ &= \sum_{j=0}^{\infty} [1 \mp (-1)^j] \xi^{-j-1} \left(\sum_{k=j}^{\infty} \frac{1 \mp (-1)^k}{2} \mathbf{C}_k(\mathcal{Q}^2/\mu^2, \alpha_s(\mu)) \mathcal{E}_{kj}(\mu, \mu_0; 1) \right) \mathbf{F}_j(\xi, \Delta^2, \mu_0). \end{aligned} \quad (141)$$

¹⁵If one would be interested to resum all logs rather than only the leading ones, one certainly has to deal also with the resummation of the non-diagonal entries. This problem has been solved in the flavor nonsinglet sector for $\eta = 1$ in Ref. [156].

The form on the r.h.s. corresponds to “shifting” the evolution to Wilson coefficient which is more convenient for numerical treatment of non-diagonal terms. In this representation it is also obvious that in DVCS kinematics the mixing under evolution is *not* suppressed by powers of ξ^2 . The evolved Wilson coefficients can furthermore be decomposed as

$$\mathbf{C}_j(\mathcal{Q}^2/\mu_0^2, \mu, \mu_0) = \mathbf{C}_j(\mathcal{Q}^2/\mu^2, \alpha_s(\mu)) \boldsymbol{\mathcal{E}}_{jj}(\mu, \mu_0; 1) + \sum_{\substack{k=0 \\ \text{even}}}^{\infty} \mathbf{C}_{j+k+2}(\mathcal{Q}^2/\mu^2, \alpha_s(\mu)) \boldsymbol{\mathcal{E}}_{j+k+2,j}(\mu, \mu_0; 1). \quad (142)$$

Of course, we understand that a consequent expansion in α_s to NLO will be performed. To have a numerically more efficient treatment this sum can be transformed into a Mellin–Barnes integral. Employing the fact that the only residue of $\cot(\pi k/2)$ is $2/\pi$ for even integer values of k , we straightforwardly arrive at

$$\begin{aligned} \mathbf{C}_j(\mathcal{Q}^2/\mu^2, \mu, \mu_0) &= \mathbf{C}_j(\mathcal{Q}^2/\mu^2, \alpha_s(\mu)) \boldsymbol{\mathcal{E}}_{jj}(\mu, \mu_0; 1) \\ &\quad - \frac{1}{4i} \int_{c-i\infty}^{c+i\infty} dk \cot\left(\frac{\pi k}{2}\right) \mathbf{C}_{j+k+2}(\mathcal{Q}^2/\mu^2, \alpha_s(\mu)) \boldsymbol{\mathcal{E}}_{j+k+2,j}(\mu, \mu_0; 1), \end{aligned} \quad (143)$$

where $-2 < c < 0$.

The formulae for the flavor nonsinglet sector (see, for example, Ref. [137]) are simply obtained by reducing the matrix valued quantities to real (or complex) valued ones, by performing the replacements

$$\begin{aligned} \gamma_j &\rightarrow {}^{\text{NS}}\gamma_j, & {}^a\lambda_j &\rightarrow {}^{\text{NS}}\gamma_j^{(0)} = {}^{\Sigma\Sigma}\gamma_j^{(0)}, & {}^a\mathbf{P}_j &\rightarrow 1, \\ \gamma_{jk} &\rightarrow {}^{\text{NS}}\gamma_{jk} = {}^{\Sigma\Sigma}\gamma_{jk}, & \mathbf{g}_{jk} &\rightarrow {}^{\text{NS}}g_{jk} = {}^{\Sigma\Sigma}g_{jk}, & \mathbf{d}_{jk} &\rightarrow {}^{\text{NS}}d_{jk} = {}^{\Sigma\Sigma}d_{jk}. \end{aligned} \quad (144)$$

We recall that in our convention the off-diagonal entries ($j > k$) are dressed with a factor N_j/N_k , e.g., ${}^{\text{NS}}\gamma_{jk} = (N_j/N_k)^{\text{QQ}}\gamma_{jk}|_{[100]}$, and that only to NLO accuracy, considered here, ${}^{\text{NS}}\gamma_{jk}$ coincides with the quark–quark entry ${}^{\Sigma\Sigma}\gamma_{jk}$.

5 Parameterization of GPDs

For the phenomenology of GPDs it is crucial that one has a realistic ansatz at hand. At present, it is popular to use a GPD ansatz [33] that is based on the spectral representation of GPDs [24, 28], for a review on this subject see [157]. We think that our formalism offers the possibility to approach this problem from a new perspective and that it finally leads to a more flexible parameterization. It is also remarkable that the task of modelling the x dependence of GPDs by using the constraints of the lowest moment [158, 159, 160], i.e., $j = 0$ yields elastic form factors, turns in our approach

into the inverse problem. Namely, it is rather the (conformal) spin dependence of the form factors that determines the x dependence, where $j = 0$ serves as an ‘boundary’ condition. Since it is timely to find a parameterization that is the most appropriate for a fitting procedure, we here only briefly outline our considerations.

We recall that the GPD support can be separated into two different momentum fraction regions, both having a dual partonic interpretation, namely, as the exchange of partons in the s -channel and as mesonlike configurations in the t -channel. Moreover, these regions are tied owing to the Poincaré invariance, see, e.g., Ref. [98]. This well-understood support property and its partonic interpretation might be considered a reflection of the conjectured duality between t - and s -channel processes; for a review of its phenomenological application, see Ref. [161]. This point of view opens the door to employ strong interaction phenomenology (combined with some basic principles) in finding a realistic model ansatz for GPDs and partial extraction of its parameters. We believe that it is a promising starting point to think in terms of t -channel exchanges combined with $\text{SO}(3)$ partial wave analysis and Regge phenomenology and then to perform the crossing to the DVCS process. This approach is complementary to those which are based on modelling GPDs in terms of partonic degrees of freedom, see, for instance, [41, 42, 43, 44, 45, 46, 47, 48, 49]. In the next two sections we outline the $\text{SO}(3)$ partial wave analysis of DVCS and, based on an intuitive picture, propose an ansatz for the partial wave amplitudes, appearing in conformal GPD moments. In the third section we try to get insight into the properties of this ansatz, and, finally, in Eq. (165) we present its approximated version convenient for numerical studies and used in subsequent sections. The reader more interested in the applications might just skip to that point.

5.1 $\text{SO}(3)$ partial wave decomposition of conformal GPD moments

It has already been proposed in Ref. [90] to decompose conformal moments of *meson* GPDs into irreducible $\text{SO}(3)$ representations, namely, in terms of Legendre polynomials labelled by the orbital angular momentum quantum number. These functions enter the partial wave decomposition of the t -channel scattering amplitude and depend on the scattering angle $\theta \equiv \theta_{\text{cm}}$, defined in the center-of-mass frame, see Fig. 3(a). After crossing, $\cos \theta$ becomes¹⁶ the inverse of the scaling variable $-\eta$, i.e., $\cos \theta = -1/\eta$ [24, 90]. The basis of Legendre polynomials has later been adopted for the conformal moments of nucleon GPDs, too [91]. Let us here start with the analysis and discussion which basis of polynomials one should employ.

To avoid cumbersome technical details, we restrict ourselves here to massless hadrons, so that the crossing relations between helicity amplitudes become simple: the signs of both four-momenta

¹⁶For the sake of simplicity, here we neglect $\sqrt{1 + M^2/\vec{P}^2}$ proportional corrections and those which die out in the Bjorken limit.

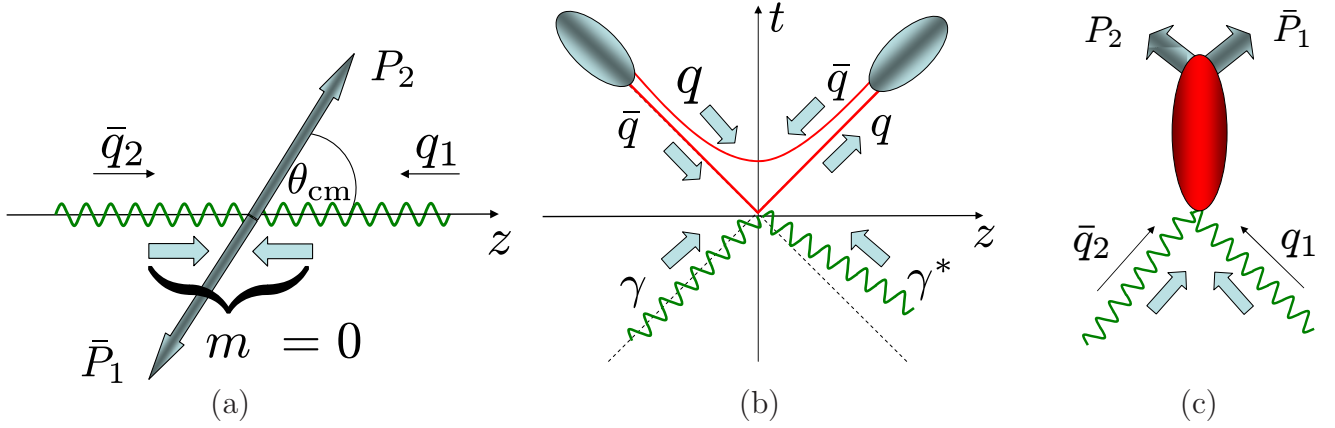


Figure 3: The fusion of two photons into a pair of (massless) mesons in the center-of-mass frame (a), partonic space-time picture (b), and hadronic point of view (c). The thick arrows indicate the spin projection of the particles.

and helicities of the crossed particles are to be changed. However, one has to be careful with the virtual photon¹⁷, which we will not cross, but whose virtuality causes a rotation of helicity amplitudes, i.e., when going from t - to s -channel amplitudes all three helicities of the virtual photon contribute whether it is crossed or not. Interestingly, the dominant contribution for the kinematics we are interested arises if its helicity will flip, too. Hence, either in the s - or in the t -channel one can take that both photons have the *same* helicity in the center-of-mass frame. In the real world, one has to take more care of the rotation of helicity amplitudes, namely, a given s -channel helicity amplitude is expressed as a linear combination of t -channel ones, and for massive and/or virtual particles all helicities contribute.

The partial wave expansion of t -channel helicity amplitudes is given in terms of Wigner d -matrices $d_{\mu,\nu}^J(\theta)$, which are essentially expressed by Jacobi polynomials [162]. Here the quantum number J refers to the total angular momentum, and μ (ν) is given by the helicity difference of initial (final) state particles. In the DVCS process, $\gamma^* h \rightarrow h \bar{\gamma}^{(*)}$, the twist-two CFFs, considered in this paper, appear in the helicity amplitudes in which both photons are transversely polarized and have the same helicity [24, 107]. As discussed above, since one photon is virtual, one can take that the photons in the t -channel process $\gamma^* \gamma^{(*)} \rightarrow h \bar{h}$ also have the same helicities. For the rest of this section, we take them to be -1 , denoted as $\gamma^{*\downarrow} \gamma^\downarrow$ (the amplitude for $\gamma^{*\uparrow} \gamma^\uparrow$ follows from reflection). Hence, for scalar ($h \bar{h}$) and spin-1/2 particles (e.g., $h^\uparrow \bar{h}^\uparrow$) the Wigner d -matrices with $\mu = 0$ (photons) and $\nu = \{+1, 0, -1\}$ appear in the partial wave expansion:

$$\{d_{0,1}^J d_{0,-1}^J\} \quad \text{for} \quad \begin{Bmatrix} h^\uparrow \bar{h}^\downarrow \\ h^\downarrow \bar{h}^\uparrow \end{Bmatrix} \quad \text{and} \quad d_{0,0}^J \quad \text{for} \quad \begin{Bmatrix} h \bar{h} \\ h^\uparrow \bar{h}^\uparrow \end{Bmatrix}. \quad (145)$$

The $\text{SO}(3)$ partial wave expansion of the t -channel helicity amplitudes yields those for the

¹⁷We are indebted to M. Diehl for critique and discussion on this subtle point.

crossed CFFs $\mathcal{H}^{(t)}$ and $\tilde{\mathcal{H}}^{(t)}$, defined via Eqs. (5) and (6) by the replacement $P_1 \rightarrow -\bar{P}_1$ and $q_2 \rightarrow -\bar{q}_2$. The hadronic tensor in the t -channel is obtained by the same substitutions from Eq. (3). The evaluation of the helicity amplitudes in the center-of-mass frame is straightforward. Taking into account the angular dependence arising from the spinor bilinears,

$$\frac{q_1^\alpha - \bar{q}_2^\alpha}{(q_1 - \bar{q}_2) \cdot (P_2 - \bar{P}_1)} \bar{U}(P_2) \gamma_\alpha \frac{1 \mp \gamma_5}{2} V(\bar{P}_1) = \pm \frac{\sqrt{1 - \cos^2 \theta}}{\cos \theta}, \quad (146)$$

we can read off the ‘effective’ partial waves in the $\text{SO}(3)$ expansion of the t -channel CFFs $\mathcal{H}^{(t)}$ and $\tilde{\mathcal{H}}^{(t)}$ for massless hadrons:

$$\mathcal{F}^{(t)}(\cos \theta, \vartheta, s^{(t)}, Q^2) = \sum_{J=1}^{\infty} (2J+1) \frac{1 \pm (-1)^J}{2} f_J(s^{(t)}, \vartheta, Q^2) \frac{\cos \theta}{\sqrt{1 - \cos^2 \theta}} d_{0,1}^J(\theta). \quad (147)$$

Here the upper (lower) sign refers to the parity even (odd) case, in which the total angular momentum is even (odd). The property of the Wigner matrices ensures then that the CFFs as scalar valued functions are invariant under reflection. The lowest partial wave that appears is for a total angular momentum $J = 2(1)$. Up to a phase factor, which is not indicated, the crossing relation for helicity amplitudes simply reads

$$T_{1,\pm 1/2;1,\pm 1/2}(s, t, Q^2) = T_{\mp 1/2,\pm 1/2,-1,-1}^{(t)}(t^{(t)}, s^{(t)}, Q^2), \quad t^{(t)} = s, \quad s^{(t)} = t \quad (148)$$

and leads with $\cos \theta = -1/\eta$ to those for the CFFs:

$$\mathcal{F}(\xi, \vartheta, \Delta^2, Q^2) = \mathcal{F}^{(t)}(\cos \theta = -1/\eta, \vartheta, s^{(t)} = \Delta^2, Q^2) \quad (149)$$

where the photon virtuality asymmetry $\vartheta = \eta/\xi$, cf. Eq. (9), is invariant under crossing. Combining this relation with the general form of the OPE (28), where the Wilson coefficients, as functions of ϑ , are invariant under crossing, we can read off within our conventions the crossing relation for conformal moments [122, 98]

$$F_j(\eta, \Delta^2) = \eta^{j+1} F_j^{(t)}(\cos \theta = -1/\eta, s^{(t)} = \Delta^2). \quad (150)$$

Here $F_j^{(t)}$ are the conformal moments of generalized distribution amplitudes [24, 163]. Finally, a formal comparison of the crossed version of the partial wave expansion (147) with the OPE (28) allows us to identify the partial waves

$$\hat{d}_H^J(\eta) \propto \frac{\eta^J}{\sqrt{\eta^2 - 1}} d_{0,1}^J(\theta)|_{\cos \theta = -1/\eta}, \quad 2 \leq J \leq j+1 \quad \text{for } j = \{1, 3, 5, \dots\}, \quad (151)$$

$$\hat{d}_H^J(\eta) \propto \frac{\eta^J}{\sqrt{\eta^2 - 1}} d_{0,1}^J(\theta)|_{\cos \theta = -1/\eta}, \quad 1 \leq J \leq j+1 \quad \text{for } j = \{0, 2, 4, \dots\}, \quad (152)$$

in the $\text{SO}(3)$ expansion of conformal GPD moments H_j and \tilde{H}_j , where J is an even and odd number, respectively. The symmetry of the Wigner d -matrix ensures that these partial waves are always even polynomials in η of order $J - 2$ or $J - 1$. Consequently, within odd (even) j we see that H_j (\tilde{H}_j) is an even polynomial in η , as it is required from time reversal invariance. The order of these polynomials is $j - 1$ and j for odd and even values of j , respectively. Here we omit further technical details and now discuss the partial wave amplitudes.

5.2 Ansatz for $\text{SO}(3)$ partial wave amplitudes

First, we would like to illustrate with two examples the potential power of crossing, which allows us to consider the t -channel process rather than the s -channel one. For DVCS off a (pseudo)scalar particle, in which the photon helicity is conserved, we have one twist-two CFF \mathcal{H} , which belongs to the parity even sector [121]. The expansion of the corresponding conformal GPD moments is done in terms of the Wigner d -matrix

$$\eta^{j+1} d_{0,0}^J(\theta)|_{\cos\theta=-1/\eta} = \eta^{j+1} P_J(-1/\eta) \quad \text{with} \quad 0 \leq J \leq j+1, \text{ and } J, (j+1) - \text{even}, \quad (153)$$

which is a polynomial in η of order $j+1$ expressed in terms of a Legendre polynomial $P_J(\cos\theta) \equiv d_{0,0}^J(\theta)$. The meaning of the quantum numbers in the crossed channel is obvious: two photons, e.g., travelling oppositely along the z axes, form a two-particle state with zero magnetic quantum number, projected on the z axes, and producing a pair of (pseudo)scalar hadrons, cf. Fig. 3(a). The total angular momentum of the initial state entirely transfer to the orbital angular momentum of the hadrons and so the latter is equal to J . The minimal value of the orbital angular momentum J , determined from the magnetic quantum number of the photons, is zero. Let us have a closer look at the partonic subprocess, which is thought of as the production of a quark-antiquark pair state, labelled by the conformal spin $j+2$, and travelling close to the light cone in different directions. Since at leading twist-two, only chirally even operators appear, helicity conservation holds at short-distances. Namely, the quark and antiquark have *opposite* helicities and, obviously, their spins point in the same direction, see Fig. 3(b). The conformal spin $j+2$ must be larger than $J+1$ and is an odd number in the parity even sector. Hence, all odd conformal partial waves with $J-1 \leq j$ contribute to the $\text{SO}(3)$ partial wave amplitude with the total orbital angular momentum J . However, the quark-antiquark pair is also bound by confinement and so they also represent an intermediate mesonic state with spin J , which consists of $J-1$ units of the orbital angular momentum and one unit of the total angular momentum arising from the aligned spins of the quark and the antiquark. This mesonic resonance then decays into two scalar hadrons. The quark (antiquark) must be combined with an *antiquark* (*quark*), which is picked up from the vacuum. To not alter the quantum numbers of the vacuum, however, a *quark-antiquark* pair must

be picked up with opposite spin (magnetic quantum number), as shown in Fig. 3(b). Suppose that in one hadron the spins of the quark and *antiquark* are opposite, then in the other ones they are aligned. This would be in contradiction with a naive quark model picture and it can be resolved only if one of the produced quarks flips his helicity due to nonperturbative effects.

Let us come back to DVCS off a nucleon, where again s -channel helicity conservation for the photons is required. Then the four CFFs $\mathcal{H}, \dots, \tilde{\mathcal{E}}$ can be expanded with respect to the t -channel partial waves $d_{0,\pm 1}^J$ and $d_{0,0}^J$. However, in our fictional world of massless particles, the helicity nonconserving quantities \mathcal{E} and $\tilde{\mathcal{E}}$ should vanish and so $d_{0,0}^J$ is absent. Hence, we are left only with final states which have opposite helicities, i.e., \mathcal{H} and $\tilde{\mathcal{H}}$, which are expanded with respect to the partial waves (151,152). We can again employ our intuitive picture, and as in the intermediate resonance before, the quark and the antiquark form a spin-one state with the orbital angular momentum $J - 1$. By picking up two quarks and antiquarks from the vacuum the final spin-1/2 nucleon and antinucleon are formed and one would expect that they carry the helicity of the produced quark and antiquark, respectively. The corresponding conformal GPD moment for odd conformal spin $j + 2$ is now a polynomial of order $j - 1$. In the case that the helicity of the produced quark or antiquark is flipped owing to nonperturbative effects, the helicities of the produced nucleons will be the same. The partial wave $d_{0,0}^J$ appears in the conformal GPD moments E_j and also H_j , which are polynomials of order $j + 1$.

Let us emphasise that we have therefore observed a relation between the helicity flip and the order of conformal GPD moments. In general, the conformal GPD moment H_j is an even polynomial in η , which is of order $j + 1$ for odd j . The minimal value of J is now given by the magnetic quantum number of the final state and so it is one. We remind ourselves that in the partial waves (151) a term of the order $j + 1$ in η is absent and so it cannot appear in H_j . However, if we would allow for helicity nonconserved quantities, such a term arises, owing to the partial wave $d_{0,0}^J$, which will then appear in E_j and H_j , see the helicity representation for GPDs in Ref. [106]. We conclude again that the restoration of full polynomiality, namely, up to order $(j + 1)$ for odd j , appears owing to the nonperturbative interaction in which the helicity of the parton is reversed. In other words, the breaking of chirality is encoded in the conformal GPD moments, which for given odd conformal spin $j + 2$ are polynomials of order $j + 1$. Certainly, the highest possible term in η naturally arises as a part of the $\text{SO}(3)$ partial waves. At this stage we see no reason to treat such terms in a special way and to collect them into a separate so-called D -term [120], which was introduced to complete the common spectral representation of GPDs. As mentioned in Sect. 3.2.2, we suggest to cure the spectral representation, e.g., as proposed in Ref. [121], rather than to add a D -term.

The partial wave expansion we wrote down for GPDs was borrowed from the two-photon

fusion into two hadrons. In the case of hard vector meson production, the leading twist-two contributions arise from a longitudinally polarized photon and vector meson. It is easy to name the Wigner matrices, which are the same as for DVCS, namely, we have $d_{0,\pm 1}^J$ and $d_{0,0}^J$ matrices in the $\text{SO}(3)$ expansion of the conformal GPD moments H_j and E_j . The former ones, given by $\sin(\theta)C_{j-1}^{3/2}(\cos\theta)/\sqrt{J(J+1)}$, are expressed by the Gegenbauer polynomials with index $\nu = 3/2$ and the latter ones are the Legendre polynomials, or, if one likes, Gegenbauer polynomials with index $\nu = 1/2$. Again, the helicity nonconserved quantity E_j is formed from $d_{0,0}^J$, while H_j contains $d_{0,1}^J$ and an admixture of the $d_{0,0}^J$ waves. If we now replace the vector meson by a pseudoscalar ones, the same partial waves appear for the parity odd quantities \tilde{H}_j and \tilde{E}_j .

We realize that the $\text{SO}(3)$ partial wave expansions of GPDs are universal, i.e., are the same for the considered processes. Such an expansion has several advantages, e.g., for the analytic continuation of even to odd j values and allows for a simple implementation of the normalization at $j = 0$. It also leads in a natural way to a term of order η^{j+1} in the polynomial E_j for odd values of j . Moreover, it is convenient to have for helicity conserved quantities the same functions that also appear in the conformal $\text{SO}(2,1)$ representation. In a conformally invariant world there would appear only one $\text{SO}(3)$ partial wave with $J = j + 1$.

Inspired by the hadronic view on the t -channel scattering process, see Fig. 3(c), we now propose an ansatz for the partonic partial wave amplitudes that appear in the $\text{SO}(3)$ expansion of the conformal GPD moments. Thereby, we rely on the Regge description of high-energy processes, which states that the high-energy behavior of the s -channel process $\gamma^{(*)}h \rightarrow h\gamma$ is dominated by linear Regge trajectories $\alpha(t)$ of pomeron and meson exchanges in the t -channel. The strength of the photon–photon–to–meson (pomeron) coupling is contained in a vertex factor f_{Jj} that depends on the conformal spin, too. The conformal spin $j + 2$ is considered as a variable conjugated to the partonic momentum fraction x . Thus, as in the case of mesonic distribution amplitudes that are expanded with respect to the Gegenbauer polynomials $C_j^{3/2}(x)$, f_{Jj} can be viewed in the partonic language as a probability amplitude for finding a quark-antiquark pair state with conformal spin $j + 2$ inside of a meson with given spin J . Furthermore, the partial wave amplitudes also contain the propagator $1/(m^2(J) - t) \propto 1/(J - \alpha(t))$ of the exchanged particles, as well as the impact form factor, describing the interaction with the target. These form factors will be modelled by a p -pole ansatz, i.e, monopole ($p = 1$), dipole ($p = 2$), and so on, with a J -dependent cutoff mass squared $M^2(J)$.

All together, we propose the following ansatz for the helicity nonflip conformal GPD moments in terms of partonic partial waves amplitudes, which we write down as a sum over the angular

momentum (we employ the fact that the polynomials are even):

$$\left\{ \begin{matrix} H_j \\ \tilde{H}_j \end{matrix} \right\} (\eta, \Delta^2, \mu_0^2) = \sum_{\substack{J=2, \text{even} \\ 1, \text{odd}}}^{j+1} \frac{f_{JJ}}{J - \alpha(\Delta^2)} \frac{\eta^{j+1-J}}{(1 - \frac{\Delta^2}{M^2(J)})^p} \left\{ \begin{matrix} \hat{d}_{0,1}^J(\eta) \\ \hat{d}_{0,1}^{J+1}(\eta) \end{matrix} \right\} \quad \text{for } j = \begin{cases} \text{odd} \\ \text{even} \end{cases}, \quad (154)$$

where for odd (even) j the sum runs over even (odd) J . Here $\hat{d}_{0,1}^J(\eta) \propto \eta^J d_{0,1}^J(1/\eta)/\sqrt{\eta^2 - 1}$ is the ‘crossed version’ (151,152) of the Wigner matrix, where the rotation matrix of the spinor bilinears is taken off. It is simply our partonic toy model (49), defined for complex valued j in Eq. (62):

$$\hat{d}_{0,1}^{J=j+1}(\eta) = \frac{\Gamma(3/2)\Gamma(3+j)}{2^{1+j}\Gamma(3/2+j)} \eta^j {}_2F_1 \left(\begin{matrix} -j, j+3 \\ 2 \end{matrix} \middle| \frac{\eta-1}{2\eta} \right). \quad (155)$$

For our later convenience, the crossed d -matrices are normalized in the forward limit to one:

$$\lim_{\eta \rightarrow 0} \hat{d}_{\mu,\nu}^J(\eta) = 1. \quad (156)$$

The conformal GPD moments (154) are even polynomials in η of order $j-1$ or j , as required. We also note that they are build from even polynomials $d_{0,1}^{l+1}(\cos \theta) \propto \cos \theta C_l^{3/2}(\cos \theta)$, where $l = \{0, 2, \dots, j-1\}$ or $\{0, 2, \dots, j\}$, with eigenvalue $+1$ under parity transformation. For helicity nonconserved quantities E_j and \tilde{E}_j , analogous ansätze can be written down in terms of Legendre functions. Thereby H_j will get an admixture from $d_{0,0}^J$ partial waves, too.

5.3 Modelling of conformal GPD moments

It is beyond the scope of this paper to present a thorough study of realistic ansätze for GPD moments. We would rather like to convince the reader that the proposed parameterization generically works and then use some simplified version for our numerical studies. One important aspect is the skewness dependence and its approximations. Another, new one, is the implementation of lattice results.

The problem of how different approximations of the skewness dependence will affect the size of the corresponding CFF will be investigated within a toy model. It is similar to Eq. (49), which describes the Compton scattering process at tree level or, in other words, within a noninteracting parton picture. To make it somewhat more realistic, we multiply it with the generically valid Mellin moments of an unpolarized valencelike parton density $35x^{-1/2}(1-x)^3/32$ (here normalized to one):

$$H_j^{\text{toy}}(\xi) = \frac{\Gamma(1/2+j)\Gamma(9/2)}{\Gamma(9/2+j)\Gamma(1/2)} \hat{d}_H^{j+1}(\eta = \xi). \quad (157)$$

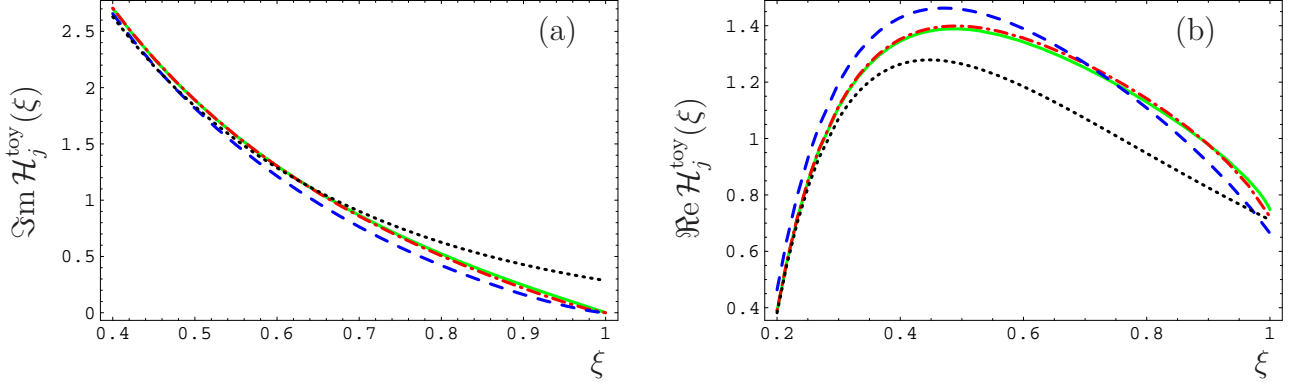


Figure 4: The imaginary (left) and real (right) part of the CFF $\mathcal{H}(\xi, \Delta^2 = 0)$ arising from the toy ansatz (157) for conformal GPD moments within different approximations (159): exact (solid), next-to-leading (dash-dotted), leading (dashed) SO(3) partial waves and $\xi = 0$ (dotted) term.

Here the partial wave $\hat{d}_H^{j+1}(\eta)$, given in Eq. (155), is normalized to one for vanishing skewness η . For the sake of illustration, we now expand $H_j^{\text{toy}}(\xi)$ with respect to Legendre polynomials:

$$\hat{d}_H^{j+1}(\eta) = \hat{d}_{0,0}^j(\eta) + \frac{\eta^2}{4} \sum_{l=0}^{j-2} \frac{1 + (-1)^{j-l}}{2} \left(\frac{\eta}{2}\right)^{j-l-2} \frac{\Gamma(l+3/2)\Gamma(j+1)}{\Gamma(j+3/2)\Gamma(l+1)} \hat{d}_{0,0}^l(\eta), \quad (158)$$

where $\hat{d}_{0,0}^l(\eta) = (\eta/2)^l \sqrt{\pi} \Gamma(l+1) P_l(1/\eta) / \Gamma(l+1/2)$. The first term on the r.h.s. is the leading partial wave, while all other partial waves, contained in the remaining sum, are suppressed by powers of η^2 . We will now study the numerical deviation in the CFF that is induced by an approximation of the partial wave $\hat{d}_H^{j+1}(\eta)$. For this purpose we make three choices: we drop the skewness dependence altogether, take the leading partial wave, and include also the next-to-leading ones:

$$\hat{d}_{H-0}^{j+1} = 1, \quad \hat{d}_{H-\text{LO}}^{j+1} = \hat{d}_{0,0}^j(\eta), \quad \hat{d}_{H-\text{NLO}}^{j+1} = \hat{d}_{0,0}^j(\eta) + \frac{(j-1)j}{(4j^2-1)} \eta^2 \hat{d}_{0,0}^{j-2}(\eta). \quad (159)$$

Note that some care is needed in the truncation of exact partial waves. The approximated partial wave $\hat{d}_{H-\text{NLO}}^{j+1}$ differs for $j=1$ (and also $j=0$) from the exact one by $\eta/27$ ($3/\eta$). This is induced by a pole in $\hat{d}_{0,0}^{-1}(\eta)$ ($\hat{d}_{0,0}^{-2}(\eta)$) that cancels the zero at $j=1$ (or $j=0$) in the expansion coefficient. Finally, this leads to an addenda in the real part of the CFFs that must be subtracted. In our toy example the subtraction term for the next-to-leading approximation reads $-5/27\eta$.

The outcome for the imaginary and real part of the CFF $\mathcal{H}_j^{\text{toy}}(\xi)$ is displayed in the left and right panel of Fig. 4, respectively. In the next-to-leading approximation (dash-dotted) one can hardly see a difference to the exact CFF (solid). If we take only the leading SO(3) partial wave (dashed), we realize that the deviation from the exact CFF (solid) is small over the whole ξ

region, in particular for the imaginary part. Furthermore, making the expansion in powers of ξ^2 and retaining only the leading $\xi = 0$ term (dotted) yields the imaginary part that approaches the exact result already for $\xi \lesssim 0.7$. However, it has an unrealistic feature that it does not vanish in the limit $\xi \rightarrow 1$, as it should. Concerning the real part, both of these approximations start to digress from the exact result for $\xi \gtrsim 0.3$, where the deviation is larger for the expansion in ξ .

To summarize, the expansion with respect to the angular momentum looks promising and works rather well in the case that the leading pole factorizes. We have also found in the expansion with respect to Legendre polynomials, which was used in Ref. [91], that the minimal version of the dual model, i.e., taking leading and next-to-leading partial waves, yields also an astonishing agreement with the exact result. We have also observed that in the experimentally accessible kinematical region the expansion in ξ practically coincides with the exact result, in particular for the imaginary part. Nevertheless, there could be a drawback if the (leading) Regge poles are nonfactorizable as it is the case in our model ansatz (154). The next-to-leading term in the partial wave expansion generates an ‘artificial’ pole, e.g., $1/(j - 1 - \alpha(\Delta^2))$, that is situated on the r.h.s. of the leading Regge pole $1/(j + 1 - \alpha(\Delta^2))$. Such a pole leads to an addendum in the Mellin–Barnes representation for CFFs with the same small ξ -behavior as the leading pole. Thus, we expect that the normalization of the CFFs, e.g., for $\Delta^2 = 0$, is governed by all terms in the partial wave expansion. A closer look at this potential problem should be given somewhere else. For the time being, we rely on the leading term in the expansion with respect to η ,

$$F_j(\eta, \Delta^2, \mu_0^2) = \frac{f_{j+1,j}}{j + 1 - \alpha(\Delta^2)} \frac{1}{(1 - \frac{\Delta^2}{M_j^2})^p} + \mathcal{O}(\eta^2), \quad (160)$$

which we will use in our numerical studies.

Next we fix the normalization of conformal GPD moments at $\Delta = 0$:

$$F_j(\eta = 0, \Delta^2 = 0, \mu_0^2) = \frac{f_{j+1,j}}{1 + j - \alpha(0)}. \quad (161)$$

The conformal moments of helicity nonflip GPDs H_j and \tilde{H}_j are then reduced to the Mellin moments of unpolarized (q) and polarized (Δq) parton densities,

$$\frac{h_{j+1,j}}{1 + j - \alpha(0)} = \int_0^1 dx x^j q(x, \mu_0) \quad \text{and} \quad \frac{\tilde{h}_{j+1,j}}{1 + j - \alpha(0)} = \int_0^1 dx x^j \Delta q(x, \mu_0), \quad (162)$$

respectively. They are parameterized with the guidance of Regge phenomenology, determining its small x behavior to be $x^{-\alpha(0)}$, whereas counting rules suggest their large x behavior, parameterized as $(1 - x)^\beta$ for $x \rightarrow 1$. Corresponding to Eq. (162), the generic ansatz for parton densities in the x space yields the following Mellin moments, e.g.,

$$q(x, \mu_0^2) = N x^{-\alpha_0} (1 - x)^\beta \quad \Rightarrow \quad h_{j+1,j} = N(1 + j - \alpha(0)) B(1 - \alpha_0 + j, \beta + 1), \quad (163)$$

where $B(a, b) = \Gamma(a)\Gamma(b)/\Gamma(a + b)$ is the Euler beta function. Note that the intercept α_0 of the Regge trajectory occurring in our ansatz and that obtained from a given fit of parton densities must agree. Hence, the leading pole in the Mellin moments (163) is cancelled and replaced by the corresponding trajectory¹⁸. Certainly, a more realistic ansatz for parton densities, to be used in global fits, could be obtained by a linear combination of such building blocks. In practice, either one can take the Mellin moments of one of the standard parameterizations of parton densities [3, 4, 5, 6, 7, 8, 9, 10] or, if they are plagued by larger errors or theoretical uncertainties, one can perform a simultaneous fit of exclusive (e.g., DVCS) and inclusive data. Here one has to bear in mind that parton densities are scheme-dependent quantities.

Further constraints for the conformal moments arise at $j = 0$. There they are given by the so-called partonic form factor

$$F_{j=0}(\eta, \Delta^2) = \frac{N_0}{1 - \alpha(\Delta^2)} \frac{1}{(1 - \frac{\Delta^2}{M_0^2})^p}. \quad (164)$$

After adjusting the flavor quantum numbers, the partonic form factors coincide with the measured elastic form factors of the proton. The free parameters left, i.e., the cut-off mass M_0^2 and the power behavior p at large Δ^2 can be taken from a fit to experimental data, where a refinement of our parameterization might be necessary. We note that form factors are scheme independent, except the axial one in the flavor singlet sector. Another advantage of the parameterization (154), which we will not use here, is that the partonic partial wave amplitudes f_{Jj} are related to physical ones, denoted as $f_J(W^2, \vartheta, Q^2)$, in the t -channel. The physical amplitudes f_J are given as a series of partonic ones, where the sum runs over the conformal spin $j+2$. Note that such a relation depends on our scheme conventions, too.

Finally, plugging the normalization (163) into the ansatz (160), we end up with the following simplified GPD parameterization:

$$F_j(\eta, \Delta^2, \mu_0^2) = NB(1 - \alpha(0) + j, \beta + 1) \frac{j + 1 - \alpha(0)}{j + 1 - \alpha(\Delta^2)} \frac{1}{(1 - \frac{t}{M_j^2})^p} + \mathcal{O}(\eta^2). \quad (165)$$

We remark that for large $|\Delta|^2$, the counting rules predict a power-like falloff of form factors as $(1/|\Delta|^2)^{n_s}$, where n_s is the number of spectators, while the large x behavior of parton densities is $(1 - x)^{2n_s - 1}$, i.e.,

$$p = n_s - 1, \quad \beta = 2n_s - 1. \quad (166)$$

An inclusive–exclusive relation between the unpolarized DIS structure function W_2 and the electromagnetic form factor F_2 has also been derived by Drell and Yan within a field–theoretical model

¹⁸Remaining nonleading poles at $j = \{-2 + \alpha_0, -3 + \alpha_0, \dots\}$ are considered an artifact of the parameterization and appear as subleading contributions in the CFFs.

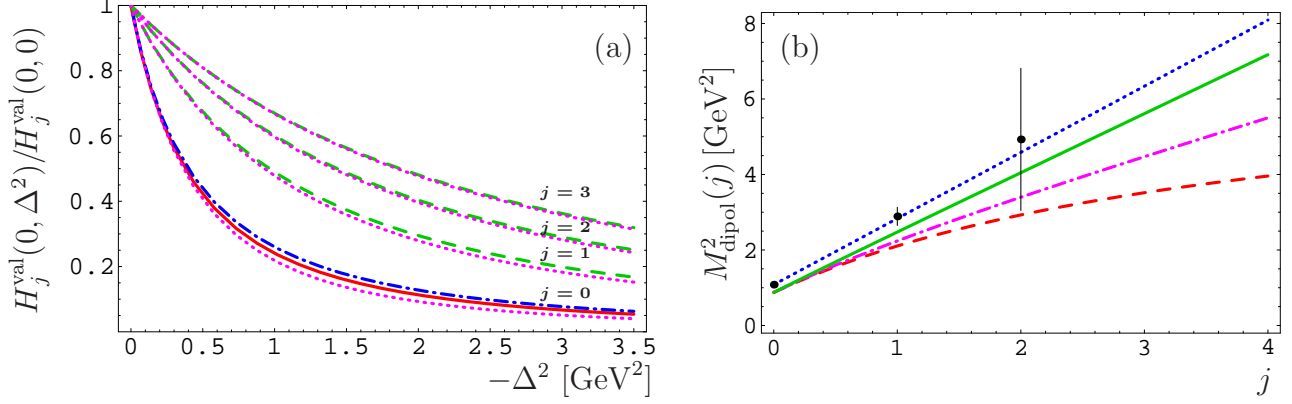


Figure 5: The Δ^2 dependence of the conformal GPD moments (167) for valence quarks (left) and the spin dependence of the effective dipole mass (170) (right). In the left panel the solid line displays the dipole fit (169) to the experimental data and the dash-dotted one is our ansatz (167) with $j = 0$. The dashed and dotted lines show the changes with $j = \{1, 2, 3\}$ for our ansatz and a dipole fit within the dipole masses (170), where $\Delta M^2 = (M_p)^2$. In the right panel we show the effective dipole masses (170) as a function of spin within ΔM^2 : 0 (dashed), M_p^2 (dash-dotted), $(2M_p)^2$ (solid). The dotted line has a slope that arises from $\Delta M^2 = 2(2M_p)^2$ and is compatible with lattice measurements [165] for the flavor nonsinglet combination $u - d$ in the heavy-pion world, which was linearly extrapolated to the physical pion mass.

that accounts for the dynamics of partons [164]. This result coincides with the counting rules for valence quarks. However, one should be aware that for sea-quarks and gluons, these counting rules might be modified; for a discussion see, e.g., Ref. [2]. For simplicity, we will not account for that here.

Finally, we would like to demonstrate that our ansatz (165) can be easily adjusted to the experimental data on electromagnetic form factors and, moreover, that it is well suited to include lattice data. In particular, present lattice measurements [35, 36, 37, 38, 39, 40] give insight into the functional change of the Δ^2 dependence with increasing conformal spin. This dependence arises from two sources: the Regge trajectory and the impact form factor. As an example, we consider the conformal GPD moments of valence quarks, where the Regge trajectory is generically correctly described by $\alpha(t) = \alpha(0) + \alpha' t$ with the intercept $\alpha(0) = 1/2$ and the slope $\alpha' = 1 \text{ GeV}^{-2}$. For two spectators the counting rules state that the impact form factor is a monopole, i.e., $p = 1$. For its cutoff mass we naturally choose two times the proton mass $M_0 \sim 2M_p = 1.88 \text{ GeV}$. Hence, our conformal GPD moments are written as

$$H_j^{\text{val}}(\eta, \Delta^2, \mu_0^2) \propto \frac{1}{1 - \frac{\Delta^2}{m_j^2}} \frac{1}{1 - \frac{\Delta^2}{M_j^2}} + \mathcal{O}(\eta^2). \quad (167)$$

Here we have introduced the monopole mass squared $m_j^2 = (1 - \alpha(0) + j)/\alpha' = (1/2 + j) \text{ GeV}^2$, which arises from the mesonic Regge trajectory. We might also assume that the spin dependence of the monopole mass squared M_j^2 is linear

$$M_j^2 = M_0^2 + \Delta M^2 j. \quad (168)$$

The generic ansatz (167) leads to a satisfying description of the electromagnetic proton form factor. In Fig. 5 (a) we confront this ansatz (dash-dotted) with the dipole fit (solid) of the electromagnetic proton form factor F_1 ,

$$F_1(Q^2 = -\Delta^2) = \frac{1 + Q^2/1.26 \text{ GeV}^2}{\left(1 + \frac{Q^2}{m_{\text{dipol}}^2}\right)^2 \left(1 + \frac{Q^2}{M_p^2}\right)}, \quad m_{\text{dipol}}^2 = 0.71 \text{ GeV}^2, \quad (169)$$

and realize that they fairly agree. We also display the Δ^2 dependence of the conformal moments within the choice $\Delta M^2 = (M_p)^2$. A larger value of ΔM^2 is compatible with the slope measured on lattice in the heavy-pion world, as shown in Fig. 5 (b) (dotted line). However, the intercept differs (in fact, the lowest moment does not describe the $F_1(Q^2)$ data). The masses are extracted from a dipole fit to the lattice data. To compare with our ansatz, we calculated the ‘effective’ masses

$$M_{\text{dipol}}^2 = 2 \left(\frac{\alpha'}{1 + j - \alpha(0)} + \frac{1}{M_0^2 + \Delta M^2 j} \right)^{-1}, \quad (170)$$

appearing in a dipole fit. For $|\Delta^2| < 1 \text{ GeV}^2$ such a ‘refitting procedure’ only weakly modifies the GPD moments, compare dashed and dotted lines in Fig. 5 (a), and so this procedure is justified to some extent.

6 Perturbative corrections of the DVCS cross section

This section is devoted to the numerical analysis of radiative corrections to CFFs. We will concentrate on the CFF \mathcal{H} , since it is the dominant contribution in most of the DVCS observables. The three remaining twist-two CFFs are usually suppressed by kinematical factors [68]. To reveal these CFFs from experimental data, it is therefore crucial to understand the theoretical uncertainties of \mathcal{H} . Our findings can be qualitatively adapted for the helicity nonconserved CFF \mathcal{E} , which enters the parity even sector, too. In this sector we face a peculiarity that is related to the appearance of the pomeron trajectory in high-energy scattering. Technically, it shows up as an essential singularity of the evolution operator at $j = 0$, see anomalous dimensions (108) and (109). Such a singularity is absent from the parity odd sector. Hence, our results in the small ξ

region are not directly applicable to the study of radiative corrections of the two remaining parity odd CFFs $\tilde{\mathcal{H}}$ and $\tilde{\mathcal{E}}$.

Based on our model (154), we introduce in the next section a simplified generic ansatz for conformal GPD moments, which will serve us in our numerical studies of the experimentally accessible kinematical regions. In Sect. 6.2 we shortly discuss the features of flavor singlet and nonsinglet CFFs to LO accuracy. In the following two sections we then elaborately analyze the size of radiative corrections to NLO and, finally, to NNLO accuracy. Thereby, independently of the considered order and scheme, we take the same conformal GPD moments which thus leads to different CFFs. However, note that CFFs are physical observables and do not depend on our conventions. Therefore, conversely, the conformal GPD moments revealed from a measurement of the physical CFFs will depend on both our scheme conventions and the approximation. Nevertheless, the results of our analysis give us a measure for both the reparameterization of the GPD ansatz needed to compensate convention change and for the convergency of the perturbation theory.

6.1 A simplified generic ansatz for conformal GPD moments

The kinematics of interest can be restricted to $\eta = \xi \leq 0.5$, i.e., the Bjorken scaling variable $x_{\text{Bj}} = 2\xi/(1 + \xi)$ is bounded by $2/3$. For simplicity, we do not resum the partial waves and rely on the leading term in the η expansion (165).

Let us specify the other parameters in the ansatz (165) for a valence-like helicity non-flip GPD H . The leading meson Regge trajectory is generically given by $\alpha(t) = \alpha(0) + \alpha't$ with $\alpha(0) = 1/2$ and $\alpha' = 1 \text{ GeV}^{-2}$. For two spectators the counting rules (166) state that $p = 1$ and $\beta = 3$. For the cut-off mass of the impact form factor we choose (168) with $M_0 = 2M_p = 2\Delta M = 1.88 \text{ GeV}$. Hence, we have for our GPD moments:

$$H_j^{\text{val}}(\eta, \Delta^2, \mu_0^2) = \frac{B(1/2 + j, 4)}{B(1/2, 4)} \frac{1}{1 - \frac{2\Delta^2}{(1+2j)\text{GeV}^2}} \frac{1}{1 - \frac{\Delta^2}{M_p^2(4+j)}} + \mathcal{O}(\eta^2), \quad (171)$$

which is normalized to one for $j = 0$ and $\Delta^2 = 0$.

The conformal GPD moments with the flavor nonsinglet combination (A.7) or (A.8), which is also relevant for DVCS, is built from valence and sea quarks. For four active quarks and the SU(2) flavor symmetric sea, the sea quark part arises from the difference of charm and strange (anti-)quarks, cf. Eq. (A.8). Suppose we are at the charm threshold and the charm sea is generated dynamically. Then, essentially, only the (anti-) strange quark counts. We might assume that the $\bar{u}, \bar{d}, \bar{s}$ antiquarks have the same conformal GPD moments and so the breaking of SU(3) flavor symmetry is described by one single parameter $R_{\bar{s}/\bar{u}}$, defined as the ratio of \bar{s} to \bar{u} antiquarks. For the purpose of illustration we consider two alternative cases: one without and one with sea quark

admixture:

$$^{\text{NS}}H_j(\eta, \Delta^2, \mu_0^2) = H_j^{\text{val}}(\eta, \Delta^2, \mu_0^2), \quad (172)$$

$$^{\text{NS}}H_j(\eta, \Delta^2, \mu_0^2) = H_j^{\text{val}}(\eta, \Delta^2, \mu_0^2) - \frac{R_{\bar{s}/\bar{u}}}{2 + R_{\bar{s}/\bar{u}}} H_j^{\text{sea}}(\eta, \Delta^2, \mu_0^2). \quad (173)$$

For the valence quark content we rely on Eq. (171) and the sea quark GPD moments are specified below in the ansatz (175) with $N_{\text{sea}} = 4/15$. For the SU(3) flavor symmetry breaking parameter we choose the often used value $R_{\bar{s}/\bar{u}} = 1/2$.

In the flavor singlet sector we need an ansatz for both quark and gluon conformal GPD moments:

$$\mathbf{H}_j(\eta, \Delta^2, \mu_0^2) = \begin{pmatrix} H_j^\Sigma \\ H_j^G \end{pmatrix}(\eta, \Delta^2, \mu_0^2), \quad H_j^\Sigma = H_j^{\text{sea}} + H_j^{u\text{val}} + H_j^{d\text{val}} = H_j^{\text{sea}} + 3H_j^{\text{val}}. \quad (174)$$

The singlet quark combination consists of sea and valence quarks, cf. (A.7) and (A.8), and we employ isospin symmetry to express the latter within the ansatz (171). Moreover, we rely on the counting rules (166), i.e. $\beta_G = 5, p_G = 2, \beta_{\text{sea}} = 7, p_{\text{sea}} = 3$, and take the same cut-off mass for the impact form factors as for the valence quarks before. Hence, analogously to Eq. (171), the generic ansatz (165) then reads:

$$H_j^{\text{sea}}(\eta, \Delta^2, \mu_0^2) = N_{\text{sea}} \frac{B(1 - \alpha_{\text{sea}}(0) + j, 8)}{B(2 - \alpha_{\text{sea}}(0), 8)} \frac{1}{1 - \frac{\Delta^2}{(m_j^{\text{sea}})^2}} \frac{1}{\left(1 - \frac{\Delta^2}{(M_j^{\text{sea}})^2}\right)^3} + \mathcal{O}(\eta^2), \quad (175)$$

$$H_j^G(\eta, \Delta^2, \mu_0^2) = N_G \frac{B(1 - \alpha_G(0) + j, 6)}{B(2 - \alpha_G(0), 6)} \frac{1}{1 - \frac{\Delta^2}{(m_j^G)^2}} \frac{1}{\left(1 - \frac{\Delta^2}{(M_j^G)^2}\right)^2} + \mathcal{O}(\eta^2), \quad (176)$$

where $M_j^G = M_j^{\text{sea}} = M_p^2(4 + j)$ and $m_j^2 = (1 - \alpha(0) + j)/\alpha'$ is expressed in terms of the intercept and slope of the Regge trajectories, specified below.

The leading trajectory arises now from the ‘pomeron’ exchange. We remind that in deeply inelastic scattering the structure function $F_2 \sim (1/x_{\text{Bj}})^{\lambda(Q^2)}$ grows with increasing Q^2 . Here the exponent is governed by the intercept of the Regge trajectory $\lambda = \alpha(0) - 1$, which is, in the language of Regge phenomenology, that of the soft pomeron (for $Q^2 \rightarrow 0$):

$$\alpha_{\mathbb{P}}(t) = \alpha_{\mathbb{P}}(0) + \alpha'_{\mathbb{P}} t \quad \alpha_{\mathbb{P}}(0) \simeq 1, \quad \alpha'_{\mathbb{P}} = 0.25. \quad (177)$$

However, in hard processes the trajectory will effectively change due to evolution, which differently affects the behavior of quark and gluon parton densities. In particular, the value of $\alpha(0)$ increases, while that of α' decreases with growing resolution scale Q^2 , e.g., see Ref. [166]. In the flavor singlet sector the size of radiative corrections and the strength of evolution crucially depends on the effective pomeron parameters, see for instance the variation of NLO corrections obtained in

[85]. In our numerical studies we shall consider two scenarios in which the radiative corrections to NLO accuracy are respectively small and large. It is known that the corrections to the quark sector are rather stable, while the main uncertainty arises from the gluons, which enter in the perturbative description of CFFs at NLO. Small and large NLO corrections can be obtained by choosing a softer and harder gluon, respectively:

$$\text{“soft” gluon:} \quad N_G = 0.3, \quad \alpha_G(0) = \alpha_{\text{sea}}(0) - 0.2, \quad (178)$$

$$\text{“hard” gluon:} \quad N_G = 0.4, \quad \alpha_G(0) = \alpha_{\text{sea}}(0) + 0.05. \quad (179)$$

Furthermore, we choose a realistic value for $\alpha_{\text{sea}}(0) = 1.1$ and $\alpha'_{\text{sea}} = \alpha'_G = 0.15$, all at the input scale $Q_0^2 = 2.5 \text{ GeV}^2$.

We remark that we normalize the sea quark (175) and gluon (176) moments at $j = 1$, so N_{sea} and N_G give the amount of momentum fraction carried by the considered parton species. Because of the momentum sum rule (A.20), valid in the forward kinematics, we have the constraint

$$N_G + N_{\text{sea}} + \int_0^1 dx \, x [u_v + d_v](x) \equiv 1. \quad (180)$$

Within our toy ansatz for valence quark moments (171) we have for their momentum the generic value $1/3$ and so $N_{\text{sea}} = 2/3 - N_G$. We note, however, that the separate contributions will change during the evolution. In the asymptotic limit $Q \rightarrow \infty$, the evolution equation tells us that $N_G = 4C_F/(4C_F + n_f)$, i.e., that more than 50% of the longitudinal proton momentum is carried by gluons. As it is experimentally verified, at a scale of a few GeV^2 the gluons already carry about 40 % of the momentum.

6.2 Compton form factors to LO accuracy

The CFFs $^S\mathcal{H}$ and $^{NS}\mathcal{H}$ are evaluated from the specified conformal GPD moments by the Mellin–Barnes integral (58). Essentially, we employ here the same technique that is well established in deeply inelastic scattering, only the integrand is now more intricate. The integral does not depend on the integration path, going from $c - i\infty$ to $c + i\infty$, as long as we do not cross any singularities, see Fig. 2 (a). In practice we use this property to get closer to the leading singularity, lying left of the integration path. Since the conformal GPD moments rapidly decrease with growing conformal spin j , we can in practice cut the integration path to a finite length. Moreover, the convergency can be improved by a separate rotation of the integration path in the upper and lower half-plane in such a way that along the path the real part decreases, as shown in Fig. 2 (b). Nevertheless, it is always a good idea to exercise proper care in the choice of the integration path and to check the numerical accuracy. Once this is done for given conformal GPD moments, the numerical

treatment is simple, fast, and stable even in NNLO. We use two different codes for the numerical evaluation, one specifically written in FORTRAN and, alternatively, the integration routine from MATHEMATICA.

For the evaluation of the CFFs to LO accuracy, we use the flavor nonsinglet Wilson coefficients (91a) and (92) as well as the singlet ones (101a) and (102). The \mathcal{Q}^2 evolution is governed by the flavor nonsinglet operator (116) and singlet one (121)–(123), approximated to LO. We equate the factorization scale with the photon virtuality: $\mu^2 = \mathcal{Q}^2$. The various ansätze, given in Eqs. (172), (173), (175), and (176), are taken at the input scale $\mathcal{Q}_0^2 = 2.5 \text{ GeV}^2$. The running coupling in LO approximation is normalized to $\alpha_s(\mathcal{Q}_0^2 = 2.5 \text{ GeV}^2)/\pi = 0.1$, where the number of active quarks is four.

We found it useful to describe the complex valued CFFs in polar coordinates,

$$\mathcal{H}(\xi, \Delta^2, \mathcal{Q}^2) = |\mathcal{H}(\xi, \Delta^2, \mathcal{Q}^2)| \exp \{i\varphi(\xi, \Delta^2, \mathcal{Q}^2)\}, \quad -\pi < \varphi = \arg(\mathcal{H}) \leq \pi, \quad (181)$$

rather than Cartesian ones. This avoids a discussion of radiative corrections in the vicinity of zeros, appearing, e.g., in the real part of certain CFFs. Moreover, the polar coordinates reveal a simple shape of CFFs in their functional dependence on ξ and \mathcal{Q}^2 . This is demonstrated in Fig. 6, where we display the modulus (left) and the phase (right) of the pure valence nonsinglet (up) and the “hard gluon” singlet (down) CFF, respectively. For the former one we choose the kinematical region that covers the phase space of present fixed target experiments, namely $0.05 \lesssim \xi \lesssim 0.5$ [$0.1 \lesssim x_{\text{Bj}} \lesssim 0.65$] and $1 \text{ GeV}^2 \leq \mathcal{Q}^2 \leq 10 \text{ GeV}^2$. For the latter one we also include the phase space that is explored in collider experiments, i.e., $10^{-6} \lesssim \xi \lesssim 0.5$ [$2 \cdot 10^{-6} \lesssim x_{\text{Bj}} \lesssim 0.65$] and $1 \text{ GeV}^2 \leq \mathcal{Q}^2 \leq 100 \text{ GeV}^2$. The simple shape of both the modulus and the phase is perhaps a more general feature of CFFs and should not be considered as an artifact of our approximation [85]. It is for $1 \text{ GeV}^2 \leq \mathcal{Q}^2 \leq 10 \text{ GeV}^2$ almost independent on the photon virtuality. In Sect. 6.3.1 we will have a closer look to the evolution. Here we remark only that both the moduli and phases of CFFs are rather “planar” in fixed target kinematics. With increasing $1/\xi$ the evolution starts strongly to affect the modulus in the singlet sector. It grows with increasing scale \mathcal{Q}^2 , namely, in such a way that the resumed logarithmical scaling violations lead to a power like change of its $1/\xi$ -dependence. This feature is well known from unpolarized DIS and in agreement with experimental DVCS results [65, 66, 67]. The phase is much less affected by evolution and in the small ξ region it is nearly independent of ξ . It monotonously decreases from its input value to be changed by less than 25% at $\mathcal{Q}^2 = 100 \text{ GeV}^2$.

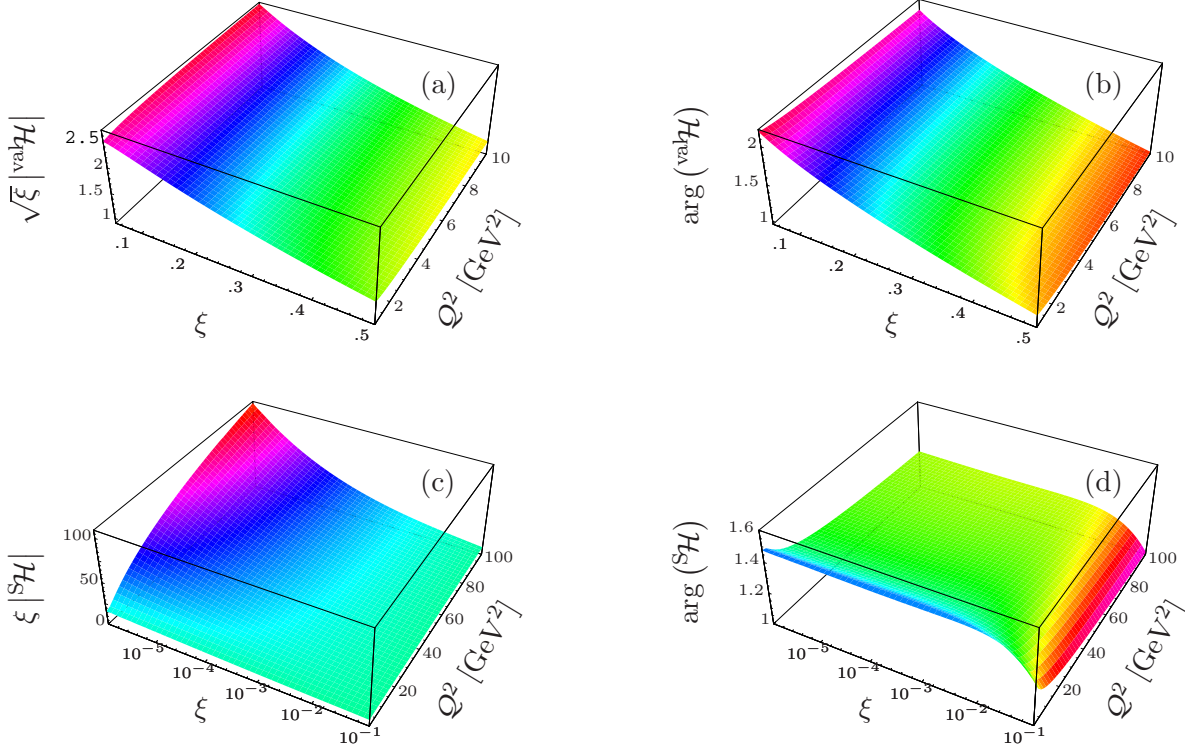


Figure 6: The scaled moduli (a,c) and phases (b,d) of the flavor nonsinglet (up) and singlet (down) CFF \mathcal{H} are displayed to LO accuracy versus Q^2 and ξ for fixed $\Delta^2 = -0.25 \text{ GeV}^2$. At the input scale $Q_0^2 = 2.5 \text{ GeV}^2$ we use the ansätze (172) and (179) for conformal GPD moments. The running coupling is normalized to $\alpha_s(Q_0^2)/\pi = 0.1$, where the number of active quarks is set to four.

6.3 Size of NLO radiative corrections: $\overline{\text{CS}}$ versus $\overline{\text{MS}}$ scheme

Now we explore the radiative corrections to NLO accuracy and in particular the differences between the $\overline{\text{CS}}$ and $\overline{\text{MS}}$ schemes, separately for the flavor nonsinglet and singlet sector. Before we do so let us explain the relation between these schemes and define the quantities that serve us as measure for the size of perturbative corrections.

The perturbative expansion of a CFF in the $\overline{\text{CS}}$ scheme, e.g., for the flavor nonsinglet case, might be structurally written to NLO as

$$\mathcal{F} = \left[C^{(0)} + \frac{\alpha_s}{2\pi} (C^{(1)\overline{\text{CS}}} + C^{(0)} \mathcal{A}^{(1)}) \right] \mathcal{E}^{(0)} \otimes F^{\overline{\text{CS}}} + \mathcal{O}(\alpha_s^2). \quad (182)$$

Here $\mathcal{E}^{(0)}$ denotes the evolution operator (116) in LO approximation and $\mathcal{A}^{(1)}$ is the NLO correction. The convolution symbol \otimes indicates the integration over the complex valued conformal spin j , which is for shortness not particularized, where the measure includes the appropriate normalization and ξ dependence, see (58) and (91a). By construction, in the forward kinematics

this scheme is *identical* with the $\overline{\text{MS}}$ one, see normalization condition (75). However, for DVCS kinematics the form of Wilson coefficients and evolution operator in the $\overline{\text{MS}}$ scheme are already at NLO modified by off-diagonal, i.e., η proportional, terms, see Eqs. (72) and (73). Because of the particularity of the DVCS process, where $\eta = \xi$, both Wilson coefficients and evolution operator are finally modified by an infinite sum of terms, which appears then in front of the conformal GPD moments, cf. Eq. (141):

$$\mathcal{F} = \left[C^{(0)} + \frac{\alpha_s}{2\pi} (C^{(1)\overline{\text{MS}}} + C^{(0)} \mathcal{A}^{(1)} + C^{(0)} \oplus \mathcal{B}^{(1)}) \right] \mathcal{E}^{(0)} \otimes F^{\overline{\text{MS}}} + \mathcal{O}(\alpha_s^2). \quad (183)$$

Here $C^{(0)} \oplus \mathcal{B}^{(1)}$ contains off-diagonal part of the evolution operator, where \oplus symbolizes the summation over the conformal spin, cf. Eq. (142). Since the physical observable \mathcal{F} is independent of our conventions, the conformal moments in both schemes are related to each other by a scheme transformation. At the input scale $\mathcal{Q}^2 = \mathcal{Q}_0^2$, where $\mathcal{E}^{(0)} = 1$, $\mathcal{A}^{(1)} = 0$, and $\mathcal{B}^{(1)} = 0$, we might express this transformation by a finite factorization (or renormalization) constant $z^{(1)}$:

$$F^{\overline{\text{MS}}} = F^{\overline{\text{CS}}} + \frac{\alpha_s}{2\pi} z^{(1)}(\eta) \oplus F^{\overline{\text{CS}}}, \quad C^{(1)\overline{\text{CS}}} = C^{(1)\overline{\text{MS}}} + C^{(0)} \oplus z^{(1)}. \quad (184)$$

For (positive) integer conformal spin the triangular matrix $z_{jk}^{(1)}(\eta) = \eta^{j-k} z_{jk}^{(1)}$ contains *only* off-diagonal entries, i.e., $j \geq k + 2$. Note that the change of Wilson coefficients is of course η -independent, while the skewness dependence of the conformal GPD moments is altered, which is at least suppressed by a factor η^2 . In particular, the two lowest GPD moments are untouched by the scheme transformation, while the (positive non-vanishing integer) moments are modified by α_s and η^2 suppressed contributions:

$$F_0^{\overline{\text{MS}}} = F_0^{\overline{\text{CS}}}, \quad F_1^{\overline{\text{MS}}} = F_1^{\overline{\text{CS}}}, \quad \text{and} \quad F_j^{\overline{\text{MS}}} = F_j^{\overline{\text{CS}}} + \frac{\alpha_s}{2\pi} \mathcal{O}(\eta^2) \quad \text{for} \quad j = 3, 4, \dots. \quad (185)$$

Strictly spoken, the truncation of the perturbative expansion also induces a discrepancy in the CFFs between these two schemes, which is beyond the approximation we are dealing with, i.e., of order α_s^2 . However, the conformal GPD moments revealed from a given data set will differ to order α_s . In the following we study the NLO corrections in both schemes within the same ansatz. The resulting deviation in the CFFs can be viewed as a measure for the needed reparameterization of conformal GPD moments by altering their η dependencies.

We introduce now the quantities that we utilize as a measures of the scheme dependence and, foremostly, as indicators of the convergency of the perturbation series. It is natural to employ for this purpose the ratio of the CFF at order N^PLO to the one at order N^{P-1}LO , where $P = \{0, 1, 2\}$ stands for LO, NLO, and NNLO order, respectively:

$$\frac{\mathcal{H}^P}{\mathcal{H}^{P-1}}(\xi, \Delta^2, \mathcal{Q}^2 | \mathcal{Q}_0^2) \equiv K^P(\xi, \Delta^2, \mathcal{Q}^2 | \mathcal{Q}_0^2) \exp\{i\delta^P \varphi(\xi, \Delta^2, \mathcal{Q}^2 | \mathcal{Q}_0^2)\}. \quad (186)$$

The phase difference

$$\delta^P \varphi = \arg \left(\frac{\mathcal{H}^{\text{N}^P \text{LO}}}{\mathcal{H}^{\text{N}^{P-1} \text{LO}}} \right) \sim \mathcal{O}(\alpha_s^P) \quad (187)$$

is formally of order $(\alpha_s/2\pi)^P$. If convergency holds, it diminishes in higher orders. Under this circumstance the ratio of moduli

$$K^P = \frac{|\mathcal{H}^{\text{N}^P \text{LO}}|}{|\mathcal{H}^{\text{N}^{P-1} \text{LO}}|} \quad (188)$$

approaches one, i.e., its deviation from one vanishes, too:

$$\delta^P K = K^P - 1 \sim \mathcal{O}(\alpha_s^P) . \quad (189)$$

If we suppose that the perturbative expansion is not ill-behaved, then the radiative corrections should not overshoot the size itself of the CFF in a given order, i.e.,

$$\left| \mathcal{H}^{\text{N}^P \text{LO}} - \mathcal{H}^{\text{N}^{P-1} \text{LO}} \right| = r \left| \mathcal{H}^{\text{N}^{P-1} \text{LO}} \right| \quad \text{with} \quad r < 1 . \quad (190)$$

If this inequality holds true, the phase difference (187) is geometrically constrained by the value of r , otherwise it is independent. More precisely, we have the upper bound

$$|\sin \delta^P \varphi| \leq r \quad \Rightarrow \quad |\delta^P \varphi| \leq \frac{\pi}{2} r \quad \text{for} \quad r \leq 1 . \quad (191)$$

Moreover, the triangle inequality, applied to Eq. (190), constrains the variation of the modulus, namely, $r \geq |\delta^P K|$. Employing the cos-theorem, we can appraise the radiative corrections (190), quantified by the ratio r , from the variation of the phase and modulus. It will turn out that in our analysis the phase difference $|\delta^P \varphi|$ is always small, i.e., $|\delta^P \varphi| \ll \pi/2$. Hence, we can rely on the expanded version of this theorem,

$$r^2 \approx (\delta^P K)^2 + (1 + \delta^P K)(\delta^P \varphi)^2 , \quad (192)$$

which gives us a simple form of the constraint among the variations of the modulus and phase as well as the size of radiative corrections. Note that in the case of a (very) small phase change the variation of the modulus is roughly estimated to be $|\delta^P K| \sim r$.

6.3.1 Flavor nonsinglet sector

The flavor nonsinglet CFF $^{\text{NS}}\mathcal{H}$ is straightforwardly evaluated from the two ansätze (172) and (173) by means of the Mellin–Barnes integral (58). The Wilson coefficients, needed for our NLO ($P = 1$) analysis, are listed for the $\overline{\text{CS}}$ and $\overline{\text{MS}}$ scheme in Sect. 4.2.1 and 4.3, respectively, while

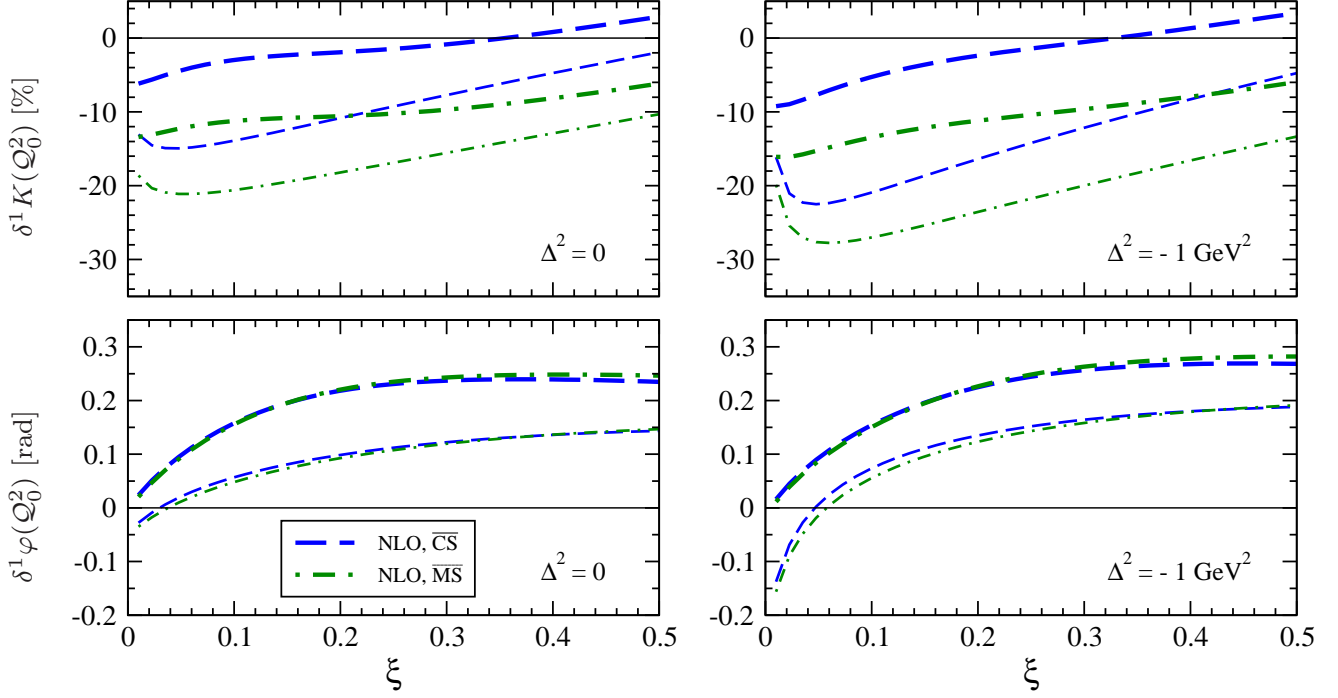


Figure 7: The relative NLO radiative corrections (189) and (187) to $^{\text{NS}}\mathcal{H}$ for $\Delta^2 = 0$ (left) and $\Delta^2 = -1 \text{ GeV}^2$ (right) are plotted versus ξ for the moduli (up) and phases (down) within the $\overline{\text{CS}}$ (dashed) and $\overline{\text{MS}}$ (dash-dotted) scheme. Thin and thick lines refer to a valence-like ansatz (172) and one with a sea-quark admixture (173), given at the input scale $Q_0^2 = 2.5 \text{ GeV}^2$. We equated the scales $\mu_f = \mu_r = Q$ and take the normalization condition $\alpha_s(Q_0^2)/\pi = 0.1$.

the relevant expansion of the evolution operator can be read off from Sects. 4.2.3 and 4.3. As said above, we combine the perturbative expansion of the Wilson coefficients with that of the evolution operator in a consistent manner, where the leading logs are resummed, cf. Eqs. (182) and (183). As long as it is not stated otherwise we equate the factorization $\mu_f \equiv \mu$ and renormalization μ_r scales with the photon virtuality Q . As input scale for the conformal GPD moments we use as before $Q_0^2 = 2.5 \text{ GeV}^2$. This input scale serves us also to normalize the coupling constant $\alpha_s(Q_0^2)/\pi = 0.1$, where its running is described by the *exact* numerical solution of the NLO renormalization group equation.

In Fig. 7 we display the relative NLO corrections (189) and (187) in the $\overline{\text{CS}}$ (dashed) and $\overline{\text{MS}}$ (dash-dotted) scheme to the moduli (up) and phases (down) for the phase space of present fixed target experiments. Thereby, we employ the pure valence-like ansatz (thin lines), i.e., Eq. (172), and the one with a sea quark admixture (thick lines), given in Eq. (173). For the mo-

momentum transfer squared we take two extreme values, namely, $\Delta^2 = 0$ (left) and $\Delta^2 = -1 \text{ GeV}^2$ (right). Comparing the resulting radiative corrections for both choices, one realizes that the Δ^2 -dependencies only slightly influence their size.

Due to the radiative corrections the phases (lower panels) increase by a small amount, except for the valence-like ansatz (thin lines) where we observe a decrease for smaller values of ξ . In any case, the absolute value of the phase differences $|\delta^P \varphi|$ does not exceed 0.1π rad. The influence of the NLO corrections on the moduli (upper panels) is more pronounced. Generally, they *moderately* reduce the moduli, however, for the sea quark admixture ansatz in the $\overline{\text{CS}}$ (thick dashed) there is a small increase at larger values of ξ . The modulus is more affected for the valence-like ansatz (thin) than for the one with a sea quark admixture (thick), while in the case of the phase difference the situation is reversed.

Comparing the corrections in the $\overline{\text{CS}}$ (dashed) and $\overline{\text{MS}}$ (dash-dotted) scheme, one realizes that in the former scheme they are smaller for the moduli, while the phase differences are almost independent of the specific choice. This is in agreement with the findings of Ref. [101], where a slightly different ansatz has been chosen. As explained above, the difference between the two schemes originates from the skewness dependence. For positive integer conformal spin, we would count them in the conformal GPD moments as η^2 effects, suppressed by $\alpha_s/2\pi$. However, as we also spelled out, in DVCS kinematics we should not use $\eta = \xi$ as an expansion parameter, since the change of Wilson coefficients is η -independent. Indeed, roughly spoken, the moduli differences in both schemes are of the same order as the radiative corrections themselves and nearly ξ independent. This observation should be understood as a warning that η^2 suppressed terms in conformal GPD moments perhaps cannot be simply neglected by formal η^2 counting.

We consider now the evolution to LO and NLO accuracy, where we compare the modulus and phase at a given scale with those at the input scale, quantified by the ratios:

$$\Delta K(Q^2, Q_0^2) = \frac{|\mathcal{H}(Q^2)|}{|\mathcal{H}(Q_0^2)|} - 1 \quad \Delta \varphi(Q^2, Q_0^2) = \arg \left(\frac{\mathcal{H}(Q^2)}{\mathcal{H}(Q_0^2)} \right). \quad (193)$$

Note that in contrast to the definitions (187) and (189), in which the variation is denoted by δ , here we do not compare the CFFs in different order, but rather measure the strength of the evolution within a given order. The evolution in the $\overline{\text{MS}}$ scheme is consistently treated, i.e., the mixing of conformal GPD moments is taken into account. We remark, however, that this effect is tiny and can be safely neglected. For instance, for the quantity

$$\frac{|\text{NS}\mathcal{H}(Q^2)| - |\text{NS}\mathcal{H}^{\text{dia}}(Q^2)|}{|\text{NS}\mathcal{H}(Q^2)|},$$

where the superscript ‘dia’ stands for neglecting the non-diagonal parts in the anomalous dimension

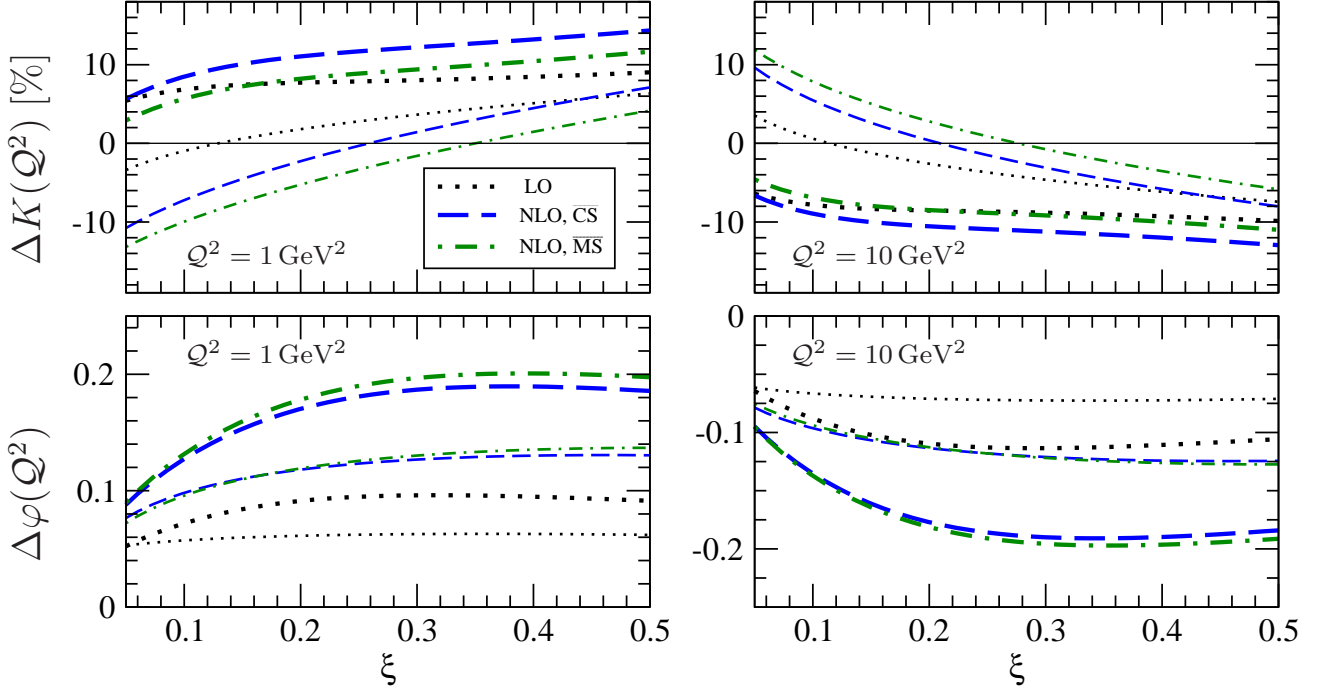


Figure 8: The modulus (up) and phase (down) changes of the evolved CFFs $^{\text{NS}}\mathcal{H}$ are plotted for fixed $Q^2 = 1 \text{ GeV}^2$ (left), $Q^2 = 10 \text{ GeV}^2$ (right), and $\Delta^2 = -0.25 \text{ GeV}^2$ versus ξ in LO (dotted) and NLO: $\overline{\text{CS}}$ (dashed) and $\overline{\text{MS}}$ (dash-dotted) scheme. The ansätze and scale setting prescriptions are the same as in Fig. 7.

$^{\text{NS}}\gamma_{jk}$, we find in a broad range of ξ and Q a value on the level of few per mil. The phase differences are negligible, too.

In Fig. 8 we show the evolution effects for the same ansätze as before, in LO (dotted) and NLO for both the $\overline{\text{CS}}$ (dashed) and $\overline{\text{MS}}$ (dash-dotted) schemes. In the left and right panels we plot the quantities (193) at a scale $Q^2 = 1 \text{ GeV}^2$ and $Q^2 = 10 \text{ GeV}^2$, respectively. For simplicity, we do not perform any matching at the charm threshold. As already observed for the radiative corrections at the input scale, see lower panels in Fig. 7, the phase differences in right [left] panels in Fig. 8 are again rather small and lie for forward [backward] evolution in the interval $-0.06\pi \cdots -0.02\pi$ $[0.02\pi \cdots 0.06\pi]$ rad. The signs tell us that the phases decrease during the evolution to a larger scale. Radiative corrections amplify this effect, where the differences between both schemes are again tiny. Comparing the upper left and right panels, we see that for the valence-like ansatz in LO (thin dotted line) the evolution mildly affects the moduli, i.e., of the order of about $\pm 5\%$ at

the edges of the phase space¹⁹ explored in the present fixed target experiments.

Furthermore, the modulus crosses for low and high values of Q^2 (upper left and right panels) the zero line at almost the same point $\xi \simeq 0.12$ to LO accuracy (thin dotted). This means that the CFF in the vicinity of this point is nearly scale independent. As in DIS, the evolution predicts a decreasing modulus for $\xi > \xi_0$ and increasing one for $\xi < \xi_0$ with growing Q^2 . The value of ξ_0 is a function of Δ^2 and depends on the input. In our example it is shifted by radiative corrections to the right (thin dashed and dash-dotted lines). This balance effect arises from the fact that forward evolution suppresses (enhances) the large (small) momentum fraction region.

The radiative corrections lead to an amplification of the evolution effects. Note that the Wilson coefficients now also depend on Q^2 and the perturbative corrections are getting smaller with increasing Q^2 . Now the variation of the CFF modulus reaches for the valence-like ansatz (thin lines) the $\mp 10\%$ [$\mp 15\%$] (for small ξ) to $\pm 8\%$ [$\pm 6\%$] (for large ξ) level in the $\overline{\text{CS}}$ (dashed) [$\overline{\text{MS}}$ (dash-dotted)] scheme. For the ansatz with sea quark admixture (thick lines) there is no crossing point with the zero line anymore and so the ‘balance-point’ is shifted outside of the discussed kinematical region. Also here the strength of evolution grows by radiative corrections and varies in the range from $\pm 6\%$ (small ξ) to $\pm 15\%$ (large ξ).

As we realized, in both ansätze the NLO corrections within the $\overline{\text{MS}}$ (dash-dotted lines) and the $\overline{\text{CS}}$ (dashed lines) change the LO prediction (dotted line). The differences, caused by the scheme dependence, mainly arises from the different Wilson coefficients to NLO, which are multiplied with the LO evolution operator. The contribution of the diagonal part of the NLO anomalous dimensions is small, i.e., about one percent. As we spelled out above, the influence of the non-diagonal part, appearing in the $\overline{\text{MS}}$ scheme in the anomalous dimensions, is negligible.

We would like to briefly confront evolution effects with experimental measurements from the Hall A experiment at Jefferson LAB [75], where scaling was reported. Within the lever arm $1.5 \text{ GeV}^2 \leq Q^2 \leq 2.5 \text{ GeV}^2$, we find for the valence-like ansatz that the scaling violation due to the LO evolution is small, namely, the modulus of the CFF varies by about 1.2% for $x_{\text{Bj}} = 0.36$ (i.e., $\xi = 0.22$) and $\Delta^2 = -0.25 \text{ GeV}^2$, while a sea quark admixture can lead to a change of up to 4%. In NLO the variation for the former ansatz is -0.5% [-2%] for the $\overline{\text{CS}}$ [$\overline{\text{MS}}$] scheme, while for the later one we find 5.7% [4.3%]. If one naturally assumes that for $x_{\text{Bj}} = 0.36$ the valence components dominate, one might conclude that the observed scaling in Ref. [75] indicates the smallness of higher twist contributions. However, in modelling of GPDs one usually realizes that the role of sea quarks in the CFFs is more pronounced than in DIS structure functions.

¹⁹For $-\Delta^2 \sim 1 \text{ GeV}^2$ this evolution effect might increase to become of the order of $\pm 10\%$ for smaller values of ξ . This is caused by the shift of the leading meson Regge pole to the left, approaching the $j = -1$ pole of the anomalous dimension, see Eq. (95).

variation, order/ ξ	0.05	0.1	0.25	0.5
μ_f , LO	3.7 [-6.9]	0.7 [-8.5]	-3.8 [-9.5]	-8.0 [-10.9]
μ_f , NLO ($\overline{\text{CS}}$)	0.5 [-0.8]	0.7 [-0.7]	0.8 [-0.3]	-0.1 [-0.8]
μ_f , NLO ($\overline{\text{MS}}$)	0.3 [-0.6]	0.7 [-0.3]	1.0 [0.3]	0.4 [0.2]
μ_r , NLO ($\overline{\text{CS}}$)	5.5 [1.3]	4.9 [0.6]	2.9 [-0.4]	0.3 [-1.6]
μ_r , NLO ($\overline{\text{MS}}$)	7.9 [3.9]	7.6 [3.2]	5.7 [2.2]	2.9 [0.8]

Table 1: Variation (194) in percent of the nonsinglet CFFs $^{\text{NS}}\mathcal{H}$ induced by separate factorization and renormalization scale changes from $\mathcal{Q}^2/2 \cdots 2\mathcal{Q}^2$. Here we used the valence-like [with sea quark admixture] conformal GPD moments (172) [(173)] and set $\mathcal{Q}^2 = 4 \text{ GeV}^2$ and $\Delta^2 = -0.25 \text{ GeV}^2$.

Interestingly, it has been argued that indeed the leading Regge trajectory essentially contributes to DVCS even in the valence region, in contrast to DIS [167]. We only like to point out here that even for fixed target kinematics a detailed view on scaling breaking effects for the net contribution to CFFs is *necessary* and that it might be used to constrain the GPD ansatz.

So far we have considered only the scale setting prescription $\mu_f = \mu_r = \mathcal{Q}$. Change obtained by choosing another prescription within the same input scale \mathcal{Q}_0 is often considered as an estimate for the possible size of higher order corrections. Let us have a closer look at this point of view. A change of μ_r modifies the size of the Wilson coefficients by formally inducing a β_0 proportional contribution $\alpha_s^2/(2\pi)^2$ that is multiplied with the NLO correction to the Wilson coefficients themselves, see Eq. (91c). A modification of μ_f essentially corresponds to the difference between the expanded and non-expanded version of the evolution operator which is formally also of higher order in α_s . However, besides non-leading log terms, it contains also leading ones, e.g., proportional to $\alpha_s^2/(2\pi)^2 \ln^2(\mu_f/\mathcal{Q}_0)$. Certainly, whenever a new entry appears in the next order that is completely independent of these quantities then the rough higher order estimate can fail.

Let us explore these estimates in more detail by employing the definitions

$$\delta_i = \frac{|\mathcal{H}(\mathcal{Q}^2|\mu_i^2 = 2\mathcal{Q}^2)| - |\mathcal{H}(\mathcal{Q}^2|\mu_i^2 = \mathcal{Q}^2/2)|}{|\mathcal{H}(\mathcal{Q}^2|\mu_i^2 = \mathcal{Q}^2)|}, \quad (194)$$

where μ_i is the factorization ($i = f$) [renormalization ($i = r$)] scale and the renormalization [factorization] scale is fixed to be \mathcal{Q}^2 . At LO we can only change the prescription for the ambiguous factorization scale setting. As one can read off from Tab. 1, the scale uncertainty to LO goes from about 4% [−7%] to −8% [−11%] with increasing ξ for the valence-like [with sea quark admixture] ansatz. Comparing with the upper right panel in Fig. 8, we realize that this uncertainty reflects nothing else but the LO evolution itself. As we have expected, these numbers are not correlated to the perturbative corrections. At NLO the factorization scale dependence is drastically reduced

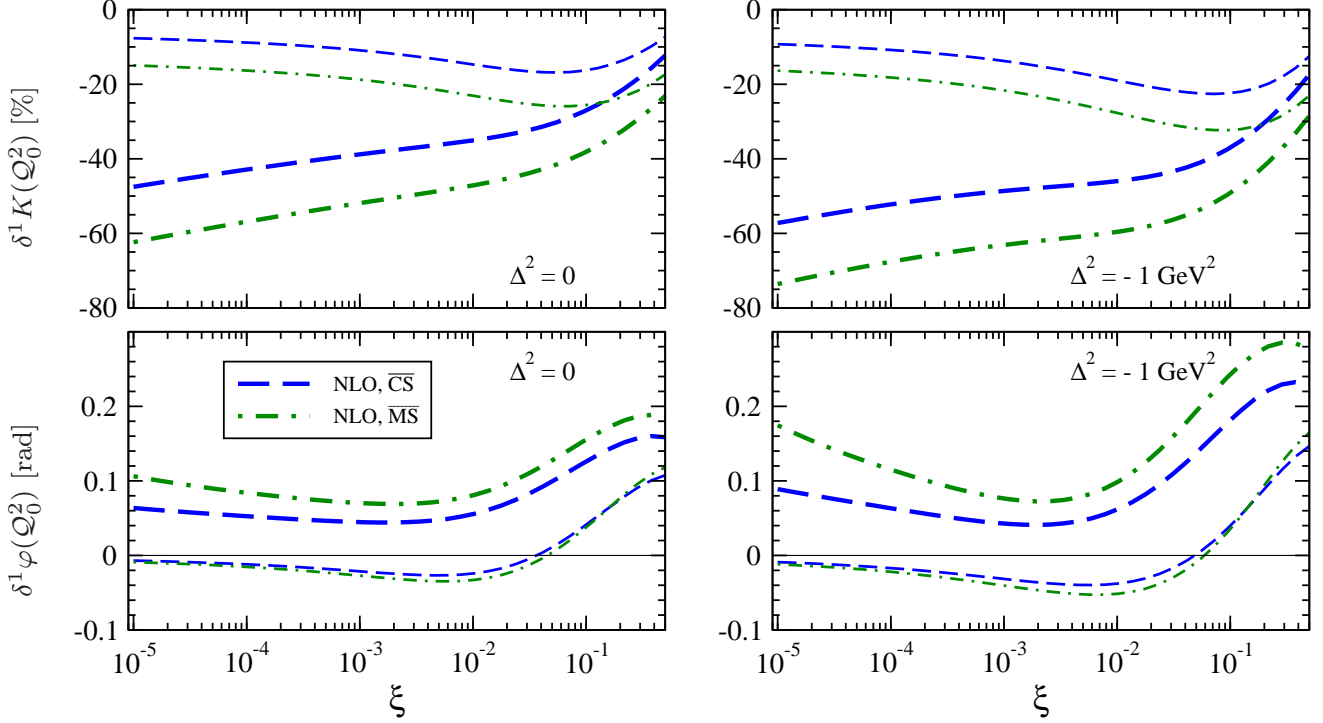


Figure 9: The relative NLO radiative corrections (187) and (189) are plotted versus ξ for the modulus (up) and phase (down) of $^S\mathcal{H}$ for $\Delta^2 = 0$ (left) and $\Delta^2 = -1 \text{ GeV}^2$ (right): $\overline{\text{CS}}$ (dashed) and $\overline{\text{MS}}$ (dash-dotted) scheme. Thick (thin) lines refer to the “hard” (“soft”) gluon parameterization, where the scale setting prescriptions are the same as in Fig. 7.

and is now only about $\pm 1\%$ or even smaller in both schemes. At this order, the renormalization scale dependence arises and the modulus of the CFF can vary of up to 6% [8%] by changing the scale in the $\overline{\text{CS}}$ [$\overline{\text{MS}}$] scheme. We will come back to these numbers and compare them with the actual NNLO corrections in the $\overline{\text{CS}}$ scheme, evaluated in Sect. 6.4. We should stress here that the uncertainties with respect to the factorization scale setting are ‘maximized’ at LO. Or, in other words, revealing GPDs from experimental data in this approximation means that one does not know at which resolution scale μ_f^2 this information was extracted. Was it Q^2 , $Q^2/2$, or ...?

6.3.2 Flavor singlet sector

For the numerical studies in the flavor singlet sector we use the same scale prescriptions and normalization conditions as in the preceding section. As input we alternatively take the ‘soft’ and ‘hard’ gluonic ansätze (178) and (179), respectively. The Wilson coefficients for the $\overline{\text{CS}}$ are listed in Eqs. (101a) and (101b) and the evolution operator can be read off from Eq. (121). The results for the $\overline{\text{MS}}$ scheme are collected in Sect. 4.3.

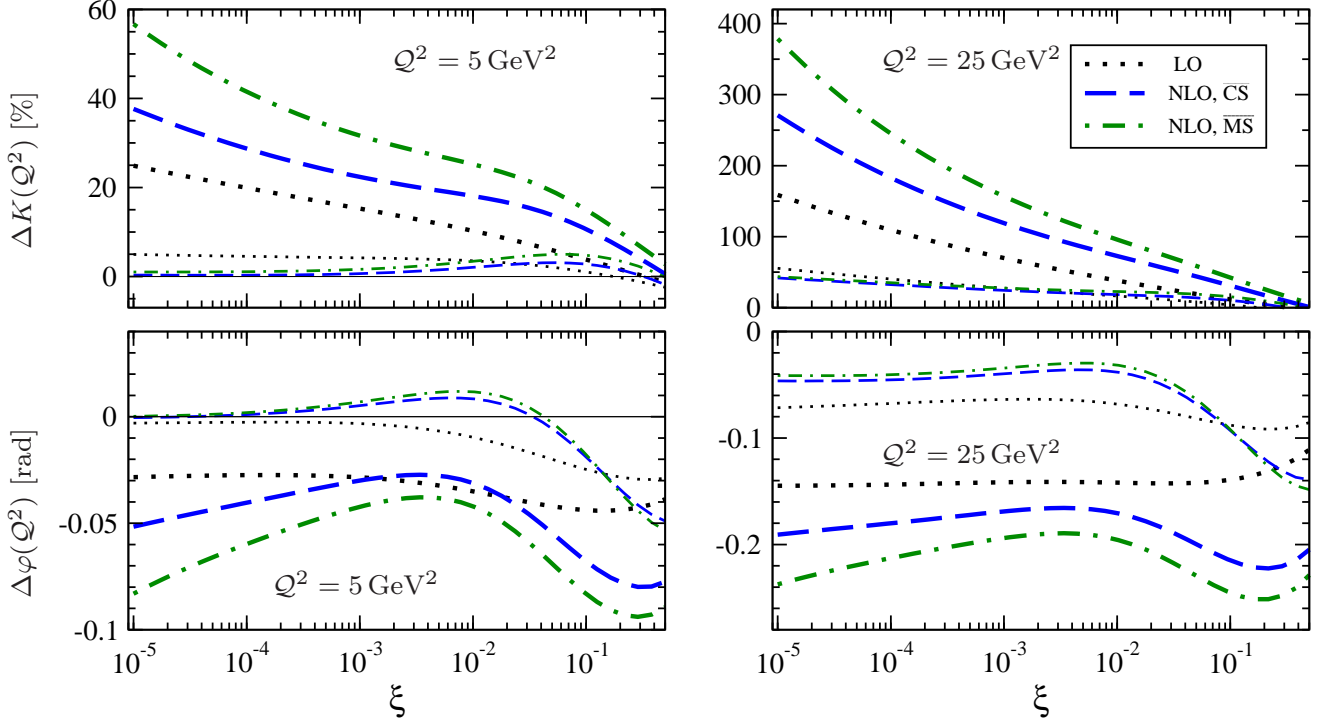


Figure 10: Evolution of the flavor singlet CFFs ${}^S\mathcal{H}$. The moduli (up) and phases (down) are plotted for fixed $Q^2 = 5 \text{ GeV}^2$ (left), $Q^2 = 25 \text{ GeV}^2$ (right), and $\Delta^2 = -0.25 \text{ GeV}^2$ versus ξ in LO (dotted) and NLO for the $\overline{\text{CS}}$ (dashed) and $\overline{\text{MS}}$ (dash-dotted) scheme. The ansätze and scale setting prescriptions are the same as in Fig. 9.

In Fig. 9 we plot the relative NLO corrections (187) and (189) for the moduli (up) and phase differences (down) at the input scale $Q_0^2 = 2.5 \text{ GeV}^2$, again for the two extreme values of the momentum transfer squared: $\Delta^2 = 0$ (left) and $\Delta^2 = -1 \text{ GeV}^2$ (right). As in the nonsinglet case, the variation of the phase differences from LO to NLO is not large and does not exceed 0.09π rad for $\Delta^2 = -1 \text{ GeV}^2$ and is even smaller for $\Delta^2 = 0$. However, the NLO corrections to the moduli have now a wider variety. This is related to the fact that at NLO the gluons enter the hard scattering part of the DVCS amplitude the first time. For the ‘soft’ gluon ansatz (thin lines) they lead to a small decrease of the CFF of about 10 – 20% and 15 – 30% for the $\overline{\text{CS}}$ and $\overline{\text{MS}}$ scheme, respectively. In contrast, if the gluon is ‘hard’ (thick lines) it cancels partly the sea quark dominated LO contribution and reduces so drastically the modulus of the CFF. Since in this scenario the gluonic part grows with decreasing ξ faster than the sea quark one, the modulus of the CFF monotonously decreases, too. For our ansatz the reduction reaches 80% at very small ξ and large Δ^2 . As in the nonsinglet case, we observe again that the radiative corrections are a

bit smaller at $\Delta^2 = 0$. Another similarity is that in the $\overline{\text{CS}}$ scheme they are up to 5 – 20% smaller than in the $\overline{\text{MS}}$ one. Although the size of perturbative corrections can be very large, the phase differences are still small. This is caused by the fact that the phase is dominated by the leading pole of the ansatz. Let us stress that the rather large corrections to the hard scattering part, induced by gluons, should not be considered an argument against the applicability of perturbation theory.

We study now the evolution effects to LO and NLO approximation. The ratios (193) are plotted in Fig. 10 versus ξ for two fixed values $Q^2 = 5 \text{ GeV}^2$ and $Q^2 = 25 \text{ GeV}^2$, where $\Delta^2 = -0.25 \text{ GeV}^2$. The moduli (up) in the ‘soft’ gluon scenario (thin lines) are relatively mildly affected by evolution and they grow with decreasing ξ . Both the modification of the LO (dotted) prediction and the difference between the $\overline{\text{CS}}$ (dashed) and $\overline{\text{MS}}$ (dash-dotted) schemes are rather small. However, we remark that the NLO contributions to the anomalous dimensions are getting large in the small ξ region, e.g., about 100%, which is eventually compensated by the evolved NLO Wilson coefficients. We also found that the off-diagonal entries in the anomalous dimensions cannot be neglected anymore. Their contribution to the net result can grow from a few percent in the large ξ region to over 25% in the small one. This is related to the fact that the off-diagonal entries (139) contain now $j = 0$ poles, which arise from the LO anomalous dimensions (108) and (109). In the “hard” gluon scenario the evolution effects, the NLO corrections and the scheme dependence are quite large. The NLO corrections to the evolution are dominated by those to the anomalous dimensions. We again observe that the NLO corrections are smaller in the $\overline{\text{CS}}$ scheme. The scheme dependence partly arises from the NLO Wilson coefficients, yielding in the former scheme smaller corrections, which evolve with the LO evolution operator, however, also due to the off-diagonal part in the anomalous dimensions. Corresponding to the evolution effects that appear in the moduli, the phase differences in the “soft” scenario are much smaller than in the “hard” one. However, also in the latter case they cannot be considered large. Again, we see that at least within our ansätze the phase is protected from radiative corrections, since their leading pole is in the vicinity of $j = 0$.

Table 2 lists the changes of the CFF that come from the variation of the factorization and renormalization scales, see Eq. (194). The first row demonstrates that the factorization scale variation in LO is correlated with the evolution, compare with dotted lines in Fig. (10). In the fixed target region the evolution and the associated variation is weak. However, approaching the small ξ region, its strength is growing, in particular for the ‘hard’ gluon ansatz. One would normally expect that the scale variation is getting smaller at NLO. But this is not the case for the small ξ region, rather the sign is reversed and its magnitude increases. This behavior completely differs from the one in the fixed target kinematics and it tells us that the factorization logs in the small ξ region are enhanced. Hence, already from these NLO findings one might wonder

variation, order/ ξ	10^{-5}	10^{-3}	10^{-1}	0.25	0.5
μ_f , LO	13.2 [49.5]	9.4 [29.4]	2.1 [7.3]	-1.5 [1.7]	-4.8 [-2.6]
μ_f , NLO ($\overline{\text{CS}}$)	-26.8[-67.6]	-15.8 [-30.1]	-2.8 [0.4]	-0.5 [2.2]	-0.3 [1.4]
μ_f , NLO ($\overline{\text{MS}}$)	-32.0[-48.8]	-19.1 [-40.5]	-3.6 [0.2]	-0.6 [2.6]	0.0 [2.0]
μ_r , NLO ($\overline{\text{CS}}$)	9.3 [46.8]	7.8 [26.8]	6.5 [11.1]	4.6 [7.0]	2.4 [3.8]
μ_r , NLO ($\overline{\text{MS}}$)	13.8 [76.5]	12.1 [42.3]	10.9 [17.7]	8.7 [12.2]	6.1 [8.0]

Table 2: Relative changes (194) in percent of the singlet CFFs \mathcal{H} within the separate variation of the factorization and renormalization scale from $Q^2/2 \dots 2Q^2$. Here we used the soft [hard] conformal GPD moments (178) [(179)] and set $Q^2 = 4 \text{ GeV}^2$ and $\Delta^2 = -0.25 \text{ GeV}^2$.

whether a perturbative treatment of the evolution in the usual manner is justified. The change of the renormalization scale yields variations of the few to ten percent in the ‘soft’ gluon scenario, and, with decreasing ξ , to much larger ones in the ‘hard’ gluon scenario. These numbers reflect simply the size of the NLO corrections for the former and latter scenario, respectively, and do not necessarily indicate that the perturbative expansion of the Wilson coefficients is ill-defined. Whether this is the case or not can be only clarified by a NNLO evaluation.

6.4 Radiative corrections beyond NLO

To investigate the radiative corrections in NNLO, we use the $\overline{\text{CS}}$ scheme within the Wilson coefficients (91a)–(91c) and (101a)–(101c), as well as the evolution operators (116) and (121). We stress again that the perturbative expansion is consistently done as a power series in $\alpha_s/2\pi$ to the order N^2LO , where the running of the coupling is described to the same order. We again calculate CFF \mathcal{H} , where the model ansatz for conformal GPD moments, scale setting, and normalization of the running coupling are spelled out above. We remind that the mixing term, appearing at three-loop level in the anomalous dimensions is unknown. Fortunately, we found that at NLO the mixing term in the $\overline{\text{MS}}$ scheme is small (tiny) for flavor (non-)singlet CFFs in the fixed target kinematics. Therefore, we expect that it is justified to neglect a NNLO mixing term for these quantities in the $\overline{\text{CS}}$ scheme. Unfortunately, this is not true for the singlet part at smaller values of ξ , where we observed at NLO about 30% effect at $\xi = 10^{-5}$ and $Q^2 = 100 \text{ GeV}^2$. Roughly speaking, we would presume that the mixing at NNLO is given by the contribution of the diagonal NLO anomalous dimensions times $(-\beta_0)\alpha_s/2\pi \sim 0.4$, which is additionally suppressed by the initial condition. All together, we expect that for small ξ the neglected mixing contributes to the net result at the 10% level.

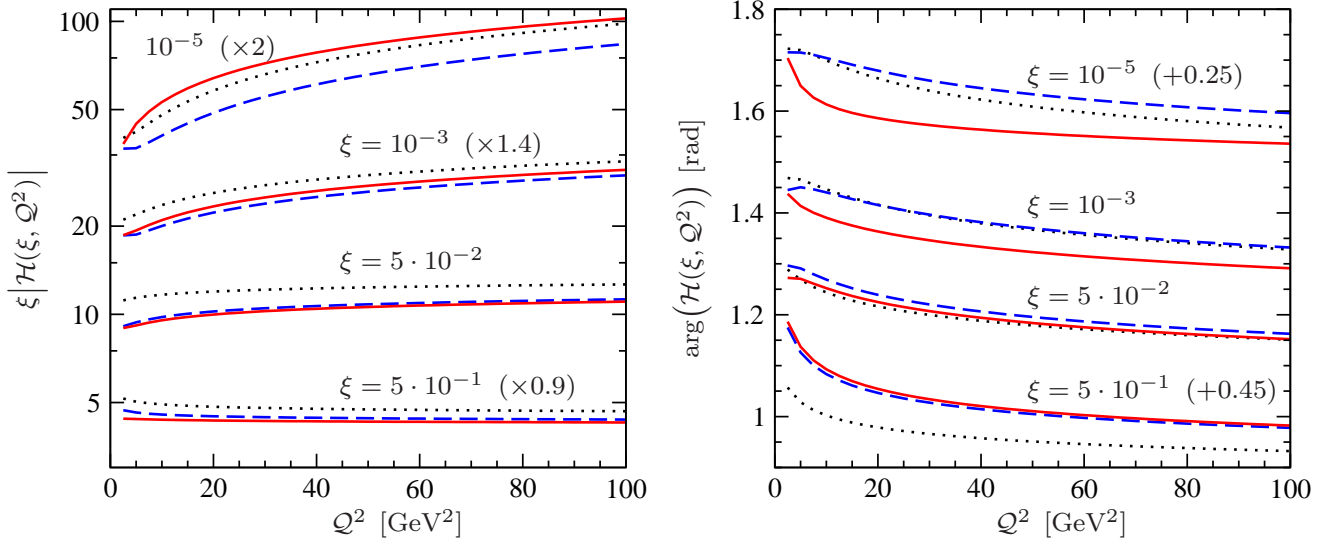


Figure 11: The modulus (left) and the phase (right) of the rescaled singlet CFF $\xi^S \mathcal{H}(\xi, Q^2)$ versus Q^2 . Here the ‘soft’ gluon ansatz is used within $\Delta^2 = -0.25 \text{ GeV}^2$ to LO (dotted), NLO (dash-dotted), and NNLO (solid).

In Fig. 11 we visualize the general features of the radiative corrections for fixed target and collider experiments up to NNLO in the parity even sector. Thereby, we employ the flavor singlet CFF $^S \mathcal{H}$ within the ‘soft’ gluon ansatz (178) at $\Delta^2 = -0.25 \text{ GeV}^2$. As pointed out in the preceding section, in this ansatz both the modulus, scaled with ξ , (left panel) and the phase (right panel) are mildly affected by NLO corrections (dashed). As it can be seen, the NNLO corrections (solid) are insignificant for both of them at the input scale $Q^2 = 2.5 \text{ GeV}^2$ over the whole ξ region. As long as we stay away from the very small ξ region, the perturbative prediction for the evolution is stable, starting at NLO, too. But approaching the small ξ region, NNLO corrections are growing in size, which already shows up in a splitting of the $\xi = 10^{-3}$ NNLO and NLO trajectories, smaller for the modulus and larger one for the phase. The $\xi = 10^{-5}$ NNLO trajectory, compared to the NLO one, is affected by rather large corrections, which are of the same size as the NLO ones, but with a competing overall sign. With increasing Q^2 the NNLO trajectory approaches the LO one. Such an ill behavior reflects the competition of the Bjorken limit, i.e., $Q^2 \rightarrow \infty$, and the high energy limit, i.e., $1/\xi \rightarrow \infty$. Indeed, the expansion parameter is rather $\ln(1/\xi)\alpha_s(Q)/2\pi$. Since the slopes of the NLO and NNLO trajectories are getting closer at large values of Q^2 , one can easily imagine that using a larger input scale would alleviate this problem. Indeed, it entirely originates from the resummed poles in the anomalous dimensions at $j = 0$ and so it is universal (process independent) and the same one that appears for parton densities. Below we will come back to this issue. The changes of the phases with respect to Q^2 is for any given ξ smaller than

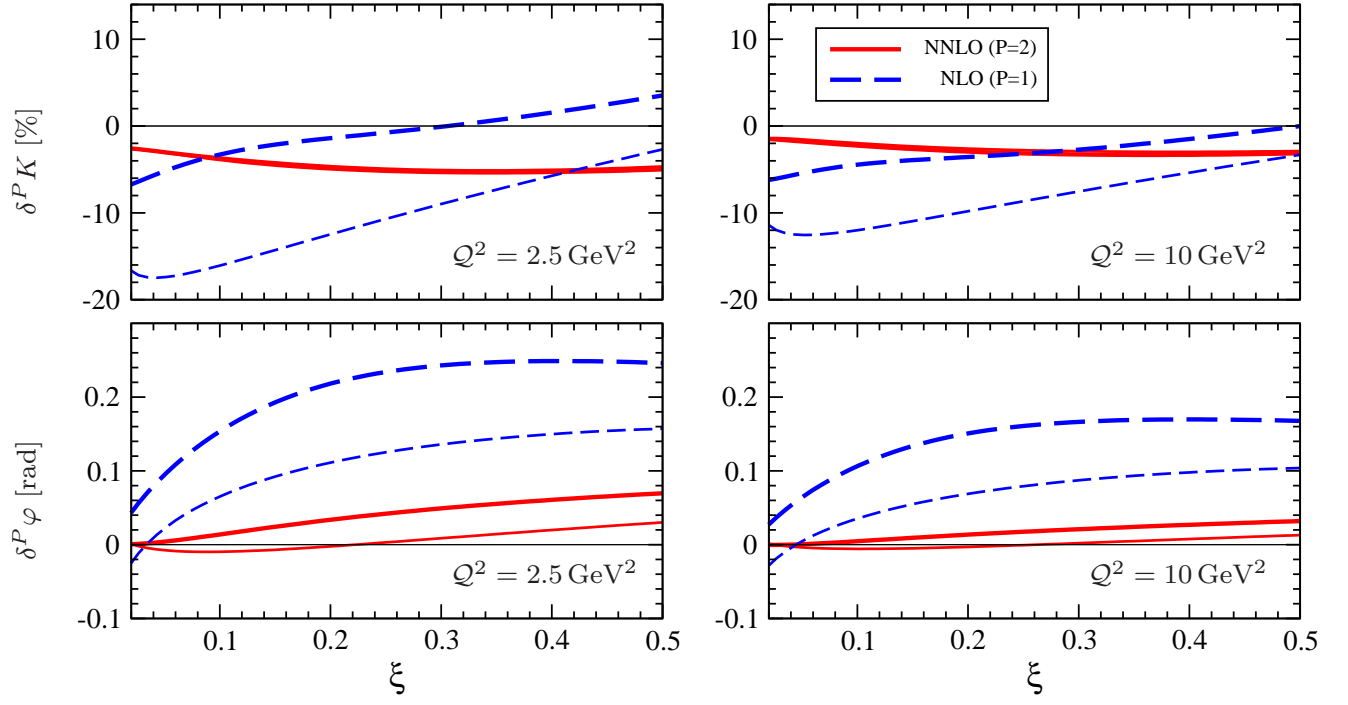


Figure 12: The relative NLO (dashed) and NNLO (solid) radiative corrections to the flavor nonsinglet CFF $^{\text{NS}}\mathcal{H}$ in the $\overline{\text{CS}}$ scheme at the input scale $Q_0^2 = 2.5 \text{ GeV}^2$ (left) and $Q^2 = 10 \text{ GeV}^2$ (right) and $\Delta^2 = -0.25$. The moduli (189) and phase differences (187) are shown in the upper and lower panels, respectively. The results without and with sea quarks are shown as thin and thick lines, respectively, which are indistinguishable for NNLO moduli.

0.03π rad and according to Eq. (191) they are bound by the ratio of moduli. In the small ξ region the phase approaches the value $\pi/2$ and so the CFF is dominated by the imaginary part. This value is driven by both the pole, which is in our ansatz (174) in the vicinity of $j = 0$, and the essential singularity of the evolution operator at $j = 0$, resulting from poles in the anomalous dimensions (108) and (109).

In Fig. 12 we present a more detailed view on the radiative corrections in the flavor nonsinglet sector for the moduli (up) and the phase differences (down). The left panels show the radiative corrections at the input scale $Q_0^2 = 2.5 \text{ GeV}^2$, while in the right panels we evolve the input to the scale $Q^2 = 10 \text{ GeV}^2$. This gives a measure of the radiative corrections arising from the evolution operator. Let us first discuss those for the moduli that arise at the input scale, i.e., the left upper panel. The NLO corrections for both a valence-like ansatz (thin) and one with a sea quark admixture (thick) have for the relevant fixed target kinematics a variance of about 20%. In NNLO this is reduced to the 5% level. More precisely, the radiative corrections reduce the CFF both without and with sea quark ansatz by about 2 – 5%. If we evolve them to 10 GeV^2 then the NNLO radiative corrections further reduce by 1 – 2%, while at NLO the variance of them is of

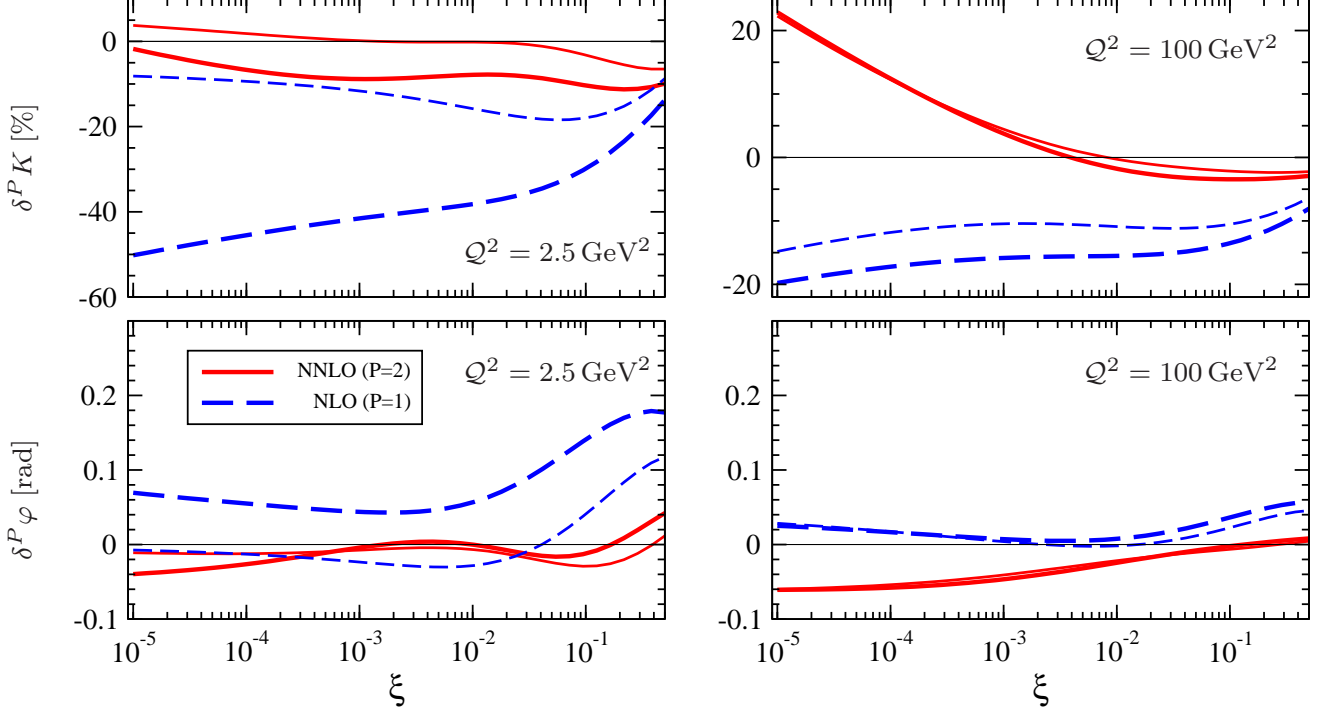


Figure 13: The relative NLO (dashed) and NNLO (solid) radiative corrections in the $\overline{\text{CS}}$ scheme are plotted versus ξ for the modulus (up) and phase (down) of singlet $^S\mathcal{H}$ for $\Delta^2 = -0.25$ at the input scale $Q_0^2 = 2.5 \text{ GeV}^2$ (left) and $Q^2 = 100 \text{ GeV}^2$ (right). The results for the “soft” and “hard” gluon ansatz are shown as thin and thick lines, respectively.

about 13%, cf. right upper panel. The radiative corrections to the phases are already dictated by those to the moduli. Already to NLO, they are smaller than 0.05π [0.08π] rad for the ansatz without [with] sea quarks and shrink further with evolution. They become tiny at NNLO, see lower panels. Obviously, there is an improvement in the perturbative expansion, which is roughly of the same order we estimated from the variation of the scales, see Tab. 1. However, a closer look to the separate contributions, arising from different color factors, shows that there is a cancellation between the C_F^2 and the β_0 proportional terms [101]. The latter is negative and about two times larger than the former, positive one, Hence both of them partly compensate each other. Without this delicate cancellation the NNLO corrections would be almost on the 10% level. Let us mention that the scale dependencies are now almost ξ independent and are of the order of -1.5% and 3% for the factorization and renormalization scale, respectively.

In Fig. 13 we display the relative radiative corrections for the flavor singlet CFF in a manner analogous to Fig. 12. However, we evolve the quantities in questions to a scale of 100 GeV^2 , shown in the right panels. From the left panel, where corrections are given at the input scale, we certainly realize that the large negative NLO corrections (thick dashed) to the modulus in the ‘hard’ gluon

order/ ξ	10^{-5}	10^{-4}	10^{-3}	10^{-2}	10^{-1}	0.25	0.5
NLO	2.4 [24.9]	2.8 [21.0]	3.5 [18.1]	5.0 [15.8]	5.8 [10.9]	4.4 [7.1]	2.4 [3.9]
NNLO	-1.6 [3.4]	-0.6 [5.6]	0.3 [6.5]	0.6 [5.7]	2.2 [6.7]	3.5 [6.9]	3.7 [5.9]

Table 3: Variation (194) of $^s\mathcal{H}$ in percent within the change of renormalization scale from $\mathcal{Q}^2/2$ to $2\mathcal{Q}^2$. Here we used the soft [hard] conformal moments (178) [(179)] and set $\mathcal{Q}_0^2 = \mathcal{Q}^2 = 4 \text{ GeV}^2$ and $\Delta^2 = -0.25 \text{ GeV}^2$.

scenario are shrunk to less than 10% (thick solid), in particular in the small ξ region. For the ‘soft’ gluon case the NNLO corrections (thin solid) are reduced to $\pm 5\%$. However, for $\xi \sim 0.5$, the corrections are reduced only unessentially and are still around 5% and 10% at NNLO level. The phase differences (lower panel) are becoming tiny at NNLO. If evolution is now switched on, our findings drastically change. For $\xi \gtrsim 5 \cdot 10^{-2}$ they are stabilized for the moduli on the level of about 3% at $\mathcal{Q}^2 = 100 \text{ GeV}^2$. However, they start to grow with decreasing ξ and reach at $\xi \approx 10^{-5}$ the 20% level. It is remarkable that the relative sign of the NLO and NNLO corrections change and that they are becoming independent of the input. This behavior is also reflected in the phase differences, which decrease to -0.02π rad. As already explained above, this breakdown of perturbation theory stems only from the anomalous dimensions and is thus universal, i.e., process independent.

Finally, we comment on the scale dependencies. As it has been already seen in Tab. 2, the variation within the factorization scale increases in the small ξ region with the perturbative order. To NNLO, we find for instance at $\xi = 10^{-5}$ a variation of 44% [105%] for the ‘soft’ [‘hard’] gluon ansatz. This is about two [1.5] times larger than that observed at NLO, where the sign is alternating. This simply reflects the breakdown of perturbative expansion of the evolution operator, as we have already seen. The NLO estimates of the higher order corrections, obtained by the variation of the renormalization scale, were for the ‘soft’ gluon scenario comparable to the actual NNLO result at the input scale. However, the corresponding estimates for the ‘hard’ gluon ansatz in the small ξ region were too pessimistic, substantially overestimating the calculated NNLO corrections. Since our input scale $\mathcal{Q}_0^2 = 2.5 \text{ GeV}^2$ in Tab. 2 was lower than the average scale $\mathcal{Q}^2 = 4 \text{ GeV}^2$ it might be that these large estimates are partly contaminated by the factorization logs. In Tab. 3 we show the renormalization scale dependence, but now for the input scale $\mathcal{Q}_0^2 = 4 \text{ GeV}^2$. Compared to Tab. 2 the modifications in NLO are not large. We also realize that the renormalization scale independency is improved at NNLO level.

To summarize our findings, we saw that NLO radiative corrections are moderate in the nonsinglet case but can be rather large in the singlet sector for a ‘hard’ gluon ansatz. The factorization

scale dependence, substantial at LO, becomes for kinematics of fixed target experiments small already at NLO. However, it is getting worse in the small ξ region. Interestingly, we also observe a scheme dependence at NLO of the order of 10% to 20%, which entirely arises due to skewness effects, where the radiative corrections are more pronounced in the $\overline{\text{MS}}$ scheme than in the $\overline{\text{CS}}$ one. At NNLO we have found that the perturbative corrections are getting reasonably small at the input scale and for the evolution in the fixed target kinematics. Both the factorization and renormalization scale dependencies are reduced to the level of a few percent. So far these findings suggest that the perturbative expansion is a reliable tool. However, we saw that the perturbative expansion of the evolution breaks down in the small ξ region. Fortunately, this breakdown is universal, and as long as one precisely defines the scheme and the approximation, perturbation theory can be used as a tool to relate different processes. We will demonstrate this in the next section.

7 Fitting procedure of experimental data

The DVCS data measured in fixed target [63, 64] and collider [65, 66, 67] experiments have been confronted in the literature with theoretical predictions, e.g., color dipole model [168], collinear factorization approach within an aligned jet model inspired GPD ansatz [169] and the minimal dual GPD parameterization [91], see also Ref. [68] for a first analysis within the double distribution ansatz. Certainly, confronting model ansätze with DVCS data is a too rigid approach and should be considered only as a first step towards extracting GPD parameters within a given ansatz. A fitting procedure for DVCS data in the small ξ and large Q^2 region has been proposed within the double log approximation of the deeply virtual Compton scattering amplitude to LO accuracy [166]. There a pomeron inspired GPD model was employed²⁰, where the singlet quarks were dynamically generated. Thus, the number of fitting parameters could be reduced to three, namely, normalization, slope-parameter, and input scale.

We will now demonstrate that the Mellin–Barnes representation of the CFFs is appropriate for a more general GPD fitting procedure. Technically, we use the standard fitting routine MINUIT [171]. This routine calls a FORTRAN code that evaluates the CFFs from conformal GPD moments, depending on a few fitting parameters.

²⁰A Regge pole model for the virtual Compton scattering amplitude was also used for a fitting procedure in Ref. [170].

7.1 Setting the scene

The DVCS amplitude interferes with the Bethe–Heitler bremsstrahlung one and so we have a rich selection of observables, mainly in the interference term. The decomposition in terms of CFFs is generally challenging. We will deal here with the easiest case, namely, the fitting of small $x_{\text{Bj}} \cong 2\xi$ data for the DVCS cross section. In this kinematics the interference term, integrated over the azimuthal angle, can be neglected and the DVCS cross section can be extracted from the photon leptonproduction one by subtracting the Bethe–Heitler bremsstrahlung cross-section. In the DVCS cross section we can safely neglect terms that are kinematically suppressed by ξ^2 :

$$\frac{d\sigma}{d\Delta^2}(W, \Delta^2, Q^2) \approx \frac{4\pi\alpha^2}{Q^4} \frac{W^2\xi^2}{W^2 + Q^2} \left[|\mathcal{H}|^2 - \frac{\Delta^2}{4M_p^2} |\mathcal{E}|^2 + \left| \tilde{\mathcal{H}} \right|^2 \right] (\xi, \Delta^2, Q^2) \Big|_{\xi = \frac{Q^2}{2W^2 + Q^2}}. \quad (195)$$

Here we have expressed the scaling variable ξ in terms of the photon virtuality Q^2 and the photon–proton center–of–mass energy W , defined by $W^2 = (P_1 + q_1)^2$. The leading Regge trajectory, appearing in $\tilde{\mathcal{H}}$, arises from mesons with generic intercept $\alpha(0) \approx 1/2$, which is less than the intercept $\alpha_{\mathbb{P}}(0) \approx 1$ of the pomeron dominated CFFs \mathcal{H} and \mathcal{E} . Thus, the squared CFF $\left| \tilde{\mathcal{H}} \right|^2$ can be neglected, too, since it is approximately suppressed by one power of ξ . More care has to be taken about the remaining combination of \mathcal{H} and \mathcal{E} CFFs. Taking the mean value of $\ll \Delta^2 \gg = -0.17 \text{ GeV}^2$, which has been measured by the H1 collaboration [67] for $|\Delta^2| < 1 \text{ GeV}^2$, we find that the helicity flip contribution is in the Δ^2 integrated cross section kinematically suppressed as

$$- \frac{\ll \Delta^2 \gg}{4M_p^2} \sim 5 \cdot 10^{-2}. \quad (196)$$

Hence, in this kinematical region, it might be justified to neglect the squared CFF $|\mathcal{E}|^2$. But in the differential cross section at larger values of $-\Delta^2$, $|\mathcal{E}|^2$ might contribute to some larger extent. Since it is not possible to separate by the present data set the \mathcal{H} and \mathcal{E} contributions, we simplify our analysis by neglecting the latter one. All together, the DVCS cross section reduces in the small ξ -region to:

$$\frac{d\sigma}{d\Delta^2}(W, \Delta^2, Q^2) \approx \frac{4\pi\alpha^2}{(2W^2 + Q^2)^2} \frac{W^2}{W^2 + Q^2} |\mathcal{H}|^2 \left(\xi = \frac{Q^2}{2W^2 + Q^2}, \Delta^2, Q^2 \right). \quad (197)$$

As we have clearly pointed out in the preceding section, the perturbative expansion of the evolution operator is ill-defined in the small $x_{\text{Bj}} \cong 2\xi$ region for the (singlet) parity even sector. Nevertheless, we have argued that this should not affect the task of relating different processes within perturbative QCD. One can ask the question: How to resum this alternating series of $\ln(1/\xi)\alpha_s/2\pi$ terms? An answer is certainly needed for the analysis of a large amount of high precision data, as it is the case in DIS. Here, indeed, some progress has been recently reported,

see, e.g., Ref. [172]. Concerning the situation in DVCS, the solution of the problem would certainly improve our partonic interpretation of the nucleon content, however, is rather irrelevant for the analysis of present experimental measurements, as we will see. This problem will also affect the forward limit of conformal GPD moments, which provide the Mellin moments of parton densities. Since for fitting parton densities to experimental data it is also necessary to precisely specify the procedure, e.g., definition of perturbative expansion of evolution operator, flavor scheme, and running of the coupling, we do not rely on any of the standard parameterizations. Rather, we fit the data ourselves, within our specifications, and then compare results with a specific choice of parton density parameterization from literature. The perturbative expansion of the DIS structure function F_2 reads:

$$F_2(x_{\text{Bj}}, Q^2) = \frac{1}{2i\pi} \int_{c-i\infty}^{c+i\infty} dj \, x_{\text{Bj}}^{-j} \left[Q_S^2 \mathbf{c}_j(\alpha_s(Q^2)) \mathbf{q}_j(Q^2) + Q_{\text{NS}}^2 {}^{\text{NS}}\mathbf{c}_j(\alpha_s(Q^2)) {}^{\text{NS}}\mathbf{q}_j(Q^2) \right], \quad (198)$$

where $\mathbf{c}_j = (\Sigma_{c_j}, \text{G}_{c_j})$ and ${}^{\text{NS}}\mathbf{c}_j$ are the DIS Wilson coefficients corresponding to the structure function F_2 . They can be found in Ref. [141], where we set the spin label $n = j + 1$. Again, we equate the factorization and renormalization scales with the photon virtuality Q^2 and consistently combine the perturbative expansion of the Wilson coefficients with the one of the evolution operator. The evolution of the parton density moments is governed by the evolution equations (115) and (119). These moments are related to the conformal GPD ones in the forward kinematics (161), e.g., cf. (A.16),

$$\mathbf{q}_j(\mu_0^2) = \begin{pmatrix} \Sigma_{H_j} \\ \text{G}_{H_j} \end{pmatrix} (\eta = 0, \Delta^2 = 0, \mu_0^2). \quad (199)$$

We will employ in this kinematics our ansatz (175) and (176), see also Ref. [173], where we neglect for simplicity the flavor nonsinglet contribution. Moreover, instead of decomposing the singlet quark contributions in valence and sea quarks, we use the effective parameterization

$$H_j^\Sigma(\eta, \Delta^2, \mu_0^2) = N_\Sigma \frac{B(1 - \alpha_\Sigma(0) + j, 8)}{B(2 - \alpha_\Sigma(0), 8)} \frac{1}{1 - \frac{\Delta^2}{(m_j^\Sigma)^2}} \frac{1}{\left(1 - \frac{\Delta^2}{(M_j^\Sigma)^2}\right)^3} + \mathcal{O}(\eta^2). \quad (200)$$

From the inspection of the standard parameterizations of parton densities, we found that the contributions from the flavor nonsinglet sector generally don't exceed the 10% level. Here it is effectively included in the parameterization of the singlet quark contribution. Pre-fitting the data we found that the fits are almost insensitive to the parameters α'_Σ , α'_G and that $\Delta M_\Sigma = \Delta M_\text{G} \approx 0$ is the preferred value. According to the common fits to vector-meson electroproduction data in the small ξ region, we set $\alpha'_\Sigma = \alpha'_\text{G} = 0.15 \text{ GeV}^{-2}$. Moreover, we neglect the j -dependence in the cut-off masses M_j^Σ and M_j^G , i.e., put $\Delta M_\Sigma = \Delta M_\text{G} = 0$. As relevant fitting parameters we thus choose

$$N_\Sigma, \alpha_\Sigma(0), M_0^\Sigma, \quad N_\text{G}, \alpha_\text{G}(0), M_0^\text{G}. \quad (201)$$

Obviously, in fits of the DIS structure function F_2 we have only four parameters, where $\alpha_\Sigma(0)$ and $\alpha_G(0)$ actually determine the powers of x_{Bj} and N_Σ and N_G the normalization. Note that although in our ansätze the conformal GPD moments are normalized to $H_{j=1}^\Sigma(\eta, \Delta^2 = 0, \mu_0^2) = N_\Sigma$ and $H_{j=1}^G(\eta, \Delta^2 = 0, \mu_0^2) = N_G$, we do not impose the momentum sum rule $N_\Sigma + N_G = 1$ here²¹. This minimal parameterization is not so well suited to provide a high quality fit to the DIS data. This is not our goal here; rather we would like to relate the DIS data with the DVCS data, which have much larger error bars. The Δ^2 slope of the DVCS amplitude is controlled by the cut-off masses M_0^Σ and M_0^G . The normalization and the ξ -dependence of this amplitude at $\Delta^2 = 0$ is as in DIS fixed by the remaining parameters $N_\Sigma, \alpha_\Sigma(0), N_G, \alpha_G(0)$. Within the assumption that the skewness parameter is negligible in the conformal GPD moments, we also loose the possibility to control the normalization of the DVCS amplitude by the skewness dependence. As demonstrated above by inspection of radiative corrections in different schemes, compare dashed and dash-dotted lines in Fig. 9, the differences in normalization, caused by the ξ -dependence, is almost skewness independent. Within our ansatz we found a 10% – 20% effect for the modulus of the amplitude, which means that the cross section would differ of about 20% – 40%. The inclusion of skewness dependence, controlled by a corresponding parameter, will be considered somewhere else. In our simplified model ansatz we do not explicitly adjust the normalization of the DVCS amplitude relative to DIS one. However, for given mean value $\ll \Delta^2 \gg$ the normalization of the DVCS amplitude, integrated over Δ^2 , is controlled also by the parameters M_0^Σ and M_0^G , which determine the Δ^2 -slope.

7.2 Lessons from fits

In Fig. 14 we confront the outcome of a simultaneous χ^2 -fit to the DVCS (39 data points) and DIS (85 data points) data in the $\overline{\text{CS}}$ scheme to NNLO accuracy. We equated the factorization and renormalization scale with the photon virtuality, used the conformal GPD moment ansätze at the input scale $\mu_0^2 = 4 \text{ GeV}^2$, fixed the number of flavors to $n_f = 4$, and used for $\alpha_s(2.5 \text{ GeV}^2)/\pi = 0.0976$ ²². In the upper left panel we display the fit to the H1 [67] and ZEUS [66] DVCS data versus $-\Delta^2$ for fixed Q^2 and W , while the upper right and lower left ones show the DVCS cross section, integrated over $|\Delta^2| < 1 \text{ GeV}^2$, versus Q^2 and W dependence, where the remaining variable W or Q^2 is fixed. The fit to the DIS H1 data [174] is plotted in the lower right panel, where for

²¹ Note that the whole momentum fraction region, i.e., $0 \leq x \leq 1$, contributes to this rule, however, our fits constrain only the small x_{Bj} region, where $x_{Bj} \leq x \leq 1$. For technical reasons, however, we assume a certain large x or j behavior. A modification of this behavior, which is only weakly constrained in our fits, might be used to restore the momentum sum rule. An improved treatment will be given somewhere else.

²²Employing the standard procedure for the NNLO running of coupling, we find that this value corresponds to $\alpha_s(M_Z^2) = 0.114$, at the standard reference scale $M_Z = 91.18 \text{ GeV}$.

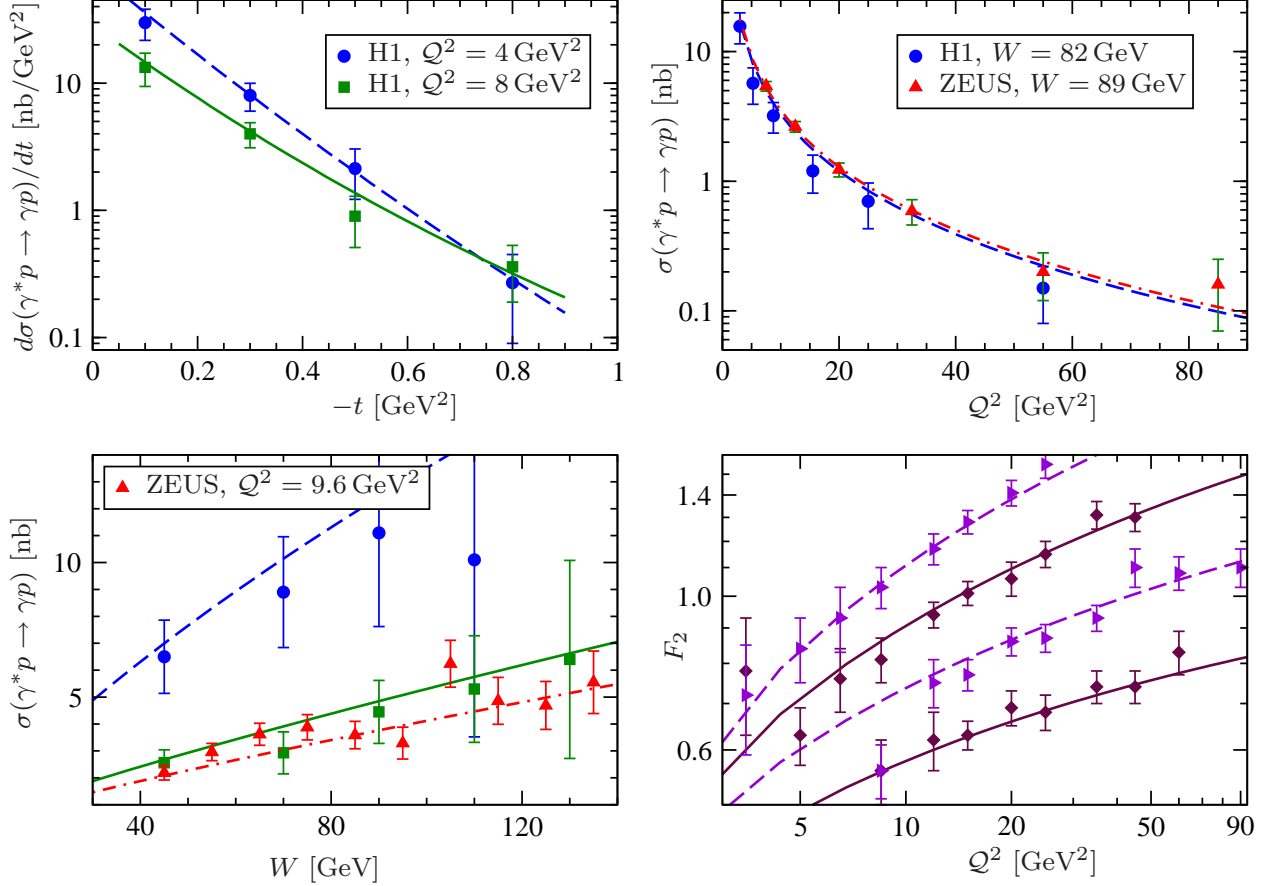


Figure 14: Simultaneous fit to the DVCS and DIS data in the $\overline{\text{CS}}$ scheme to NNLO. Upper left panel DVCS cross section for $Q^2 = 4 \text{ GeV}^2$ and $W = 71 \text{ GeV}$ (circles, dashed) as well as $Q^2 = 8 \text{ GeV}^2$ and $W = 82 \text{ GeV}$ (squares, solid) [67]. Upper right panel DVCS cross section ($|\Delta^2| < 1 \text{ GeV}^2$) versus Q^2 for $W = 82 \text{ GeV}$ (H1, circles, dashed) and $W = 89 \text{ GeV}$ (ZEUS, triangles, dash-dotted) [66]. Lower left panel DVCS cross section versus W $Q^2 = 4 \text{ GeV}^2$ (H1, circles, dashed), $Q^2 = 8 \text{ GeV}^2$ (H1, squares, solid), and $Q^2 = 9.6 \text{ GeV}^2$ (ZEUS, triangles, dash-dotted). Lower right panel shows $F_2(x_{Bj}, Q^2)$ versus Q^2 for $x_{Bj} = \{8 \cdot 10^{-3}, 3.2 \cdot 10^{-3}, 1.3 \cdot 10^{-3}, 5 \cdot 10^{-4}\}$ [174].

order (scheme)	$\alpha_s(M_Z)$	N_Σ	$\alpha_\Sigma(0)$	M_Σ^2	N_G	$\alpha_G(0)$	M_G^2	χ^2	$\chi^2/\text{d.o.f.}$	$\chi_{\Delta^2}^2$
LO	0.130	0.157	1.17	0.228	0.527	1.25	0.263	100	0.85	38.5
NLO ($\overline{\text{MS}}$)	0.116	0.172	1.14	1.93	0.472	1.08	4.45	109	0.92	4.2
NLO ($\overline{\text{CS}}$)	0.116	0.167	1.14	1.34	0.535	1.09	1.59	95	0.80	2.2
NNLO ($\overline{\text{CS}}$)	0.114	0.167	1.14	1.17	0.571	1.07	1.39	91	0.77	2.2

Table 4: Parameters extracted from a simultaneous fit to the DVCS cross section and DIS structure function F_2 , where $\alpha_s(M_Z)$, $\alpha'_\Sigma = \alpha'_G = 0.15 \text{ GeV}^{-2}$, and $\Delta M_\Sigma = \Delta M_G = 0$ are fixed and $\mu_0^2 = 4 \text{ GeV}^2$.

clarity not all points are displayed²³. As one realizes by eye inspection, the normalization, scale- and Δ^2 -dependency are separately well described.

From Table 4 one can see that the quality of these simultaneous fits for the 124 data points is satisfying. For instance, for the NLO fit in $\overline{\text{CS}}$ scheme, where now $\alpha_s(2.5 \text{ GeV}^2)/\pi = 0.1036$, we get $\chi^2 = 95$, i.e., $\chi^2/\text{d.o.f.} = 0.8$. Taking into account the NNLO order corrections, the quality of the fit slightly improves, i.e., $\chi^2/\text{d.o.f.} = 0.77$. As one can realize by comparison of the last two rows in Tab. 4, the resulting parameters remain stable. The largest modification appears in the cut-off masses, which reduce from NLO to NNLO by about 13%. Thereby, contribution to χ^2 coming from the eight data points of the differential cross section (upper left panel in Fig. 14), denoted $\chi_{\Delta^2}^2 = 2.2$ (last column in Tab. 4), indicates an equally good fit to the Δ^2 -slope in NLO and NNLO.

To understand better the double role of the cut-off masses in the fitting procedure, let us compare the LO parameters with the NLO ones, where their changes are much more pronounced. Although in LO the fit to all data yields seemingly reasonable $\chi^2/\text{d.o.f.} = 0.85$, the Δ^2 -slope (determined by the small squared cut-off masses $M_\Sigma^2 \sim M_G^2 \sim 0.25 \text{ GeV}^2$) turns out to be $\sim 30 \text{ GeV}^{-2}$, which is incompatible with $\sim 6 \text{ GeV}^{-2}$ indicated by the data [67]. Or, in other words, to leading order accuracy $\chi_{\Delta^2}^2 = 38.5$ is unacceptably large. Therefore, we conclude that the relative normalization between the DIS structure function and the integrated DVCS cross section is correctly reproduced in the fits by reducing the latter one by forcing the steeper Δ^2 -dependence. This also implies that at $\Delta_{\min}^2 \approx 0$ the normalization of the differential DVCS cross section and the structure function F_2 cannot be simultaneously described within our ansatz. A separate fit to the DVCS data yields a slope that is getting compatible with the measured one; however, the overall normalization is now deteriorated and so the quality of the fit is worse, namely, $\chi^2/\text{d.o.f.} = 4.8$. Certainly, this is related to the fact that we have no control over the skewness dependence of the

²³Not shown, but used in fits, are H1 F_2 data for $x_{\text{Bj}} = \{1.3 \cdot 10^{-2}, 5 \cdot 10^{-3}, 2 \cdot 10^{-3}, 8 \cdot 10^{-4}, 3.2 \cdot 10^{-4}, 2 \cdot 10^{-4}, 1.3 \cdot 10^{-4}, 8 \cdot 10^{-5}\}$.

conformal GPD moments²⁴. Therefore, non-trivial skewness dependence should be introduced in such a way to make $|\mathcal{H}|$, and consequently the normalization of the DVCS cross section, smaller. We remind, however, that the inclusion of the skewness dependence within the spectral representation of GPDs is usually done in such a way that the skewness effect leads to an *increase* of $|\mathcal{H}|$.

Let us finally compare the NLO fits in the $\overline{\text{CS}}$ and $\overline{\text{MS}}$ schemes. The fit in the latter scheme is compared to the former one a bit off. We find $\chi^2/\text{d.o.f.} = 0.92$, while in the $\overline{\text{CS}}$ scheme $\chi^2/\text{d.o.f.} = 0.8$. Also here the largest changes appear in the cut-off masses, in particular the gluon one. However, the quality of the Δ^2 -fit to the differential cross section is acceptable, namely, $\chi^2_{\Delta^2} = 4.2$, compared to $\chi^2_{\Delta^2} = 2.2$ in the $\overline{\text{CS}}$ scheme. As discussed in Sect. 6.3 above, these schemes differ only in the skewness dependence of the conformal GPD moments. Instead of adjusting the normalization by changing the skewness dependence, it is done within our ansatz by increasing the slope. Hence, we must conclude that a more precise extraction of GPD parameters requires the inclusion of the skewness effect for $\Delta^2 = 0$.

7.3 Comparison and partonic interpretation of the results

We would like now to confront our findings with the parton densities, as obtained from global DIS fits. In Fig. 15, we plot the singlet quark and gluon distributions

$$x \begin{pmatrix} \Sigma q \\ G q \end{pmatrix} (x, \mu_0^2) = \frac{1}{2i\pi} \int_{c-i\infty}^{c+i\infty} dj \, x^{-j} \begin{pmatrix} \Sigma H_j \\ G H_j \end{pmatrix} (\eta = 0, \Delta^2 = 0, \mu_0^2), \quad (202)$$

respectively, to LO (dotted), NLO for the $\overline{\text{MS}}$ (dash-dotted) and $\overline{\text{CS}}$ (dashed) as well as to NNLO (solid) at the input scale $\mu_0^2 = 4 \text{ GeV}^2$. Note that the difference between the two schemes arises purely due to the skewness dependence, which affects only the DVCS fit. As argued above, we do not expect the outcome of, e.g., our simultaneous DVCS and DIS NLO fit, to coincide with any of the standard parameterizations for parton densities. Indeed, we explicitly saw this for the parton density fits of the H1 and ZEUS collaborations. However, it turns out that the flavor singlet quark parton density agrees very well with the parameterization of Alekhin [175], which is plotted with error bands. Here the difference between the both schemes and NNLO order corrections are rather small. As is well known, the gluon distribution is much less constrained by a pure DIS fit. Here our central values lie outside the error band of the Alekhin parameterization. However, our error band of the NLO fit in the $\overline{\text{CS}}$ scheme would overlap with Alekhin's one. Note that we have

²⁴ As a side effect, arising from this ill-defined fitting task, we observed that the central value of the resulting parameters, in particular of the cut-off masses, are getting sensitive to the accuracy of numerics and they can vary inside the error bands. In NLO and NNLO fits, by increasing the numerical accuracy, we observed a variation of the central values only on the per mil level.

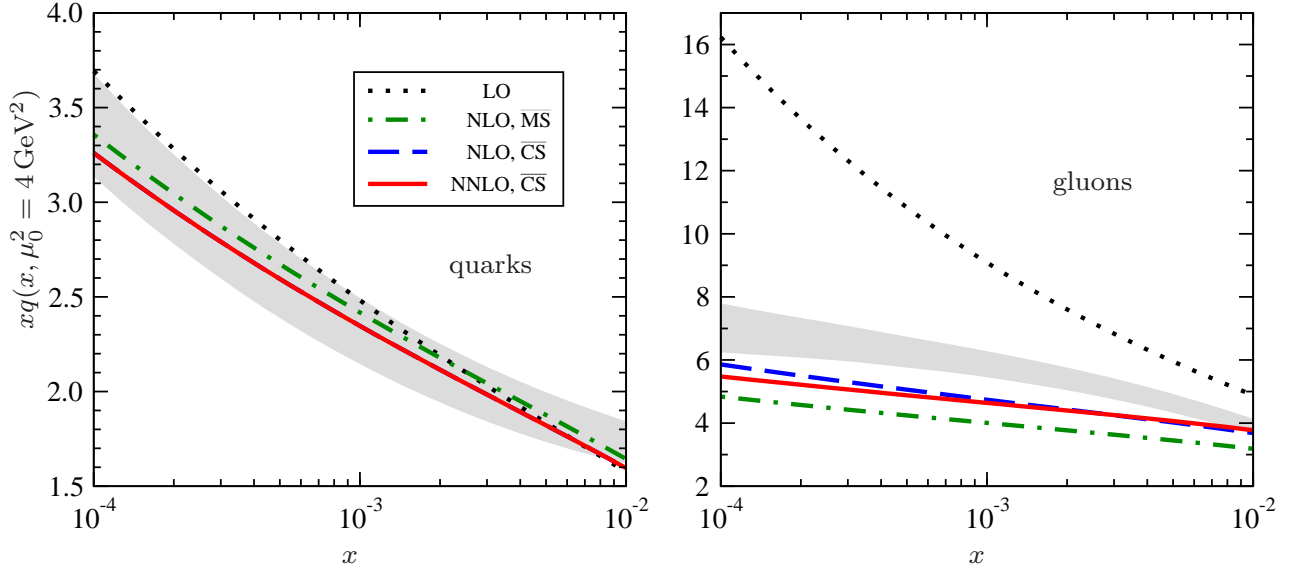


Figure 15: The parton densities are shown for quarks (left) and gluons (right) at the input scale $\mu_0^2 = 4 \text{ GeV}^2$. The meaning of the lines are the same as before: LO (dotted), NLO for $\overline{\text{MS}}$ (dash-dotted) and $\overline{\text{CS}}$ (dashed), as well as NNLO (solid), the last two being indistinguishable in the quark case. The bands show Alekhin's NLO parameterization with errors [175].

used the same settings for α_s as Alekhin, however, the procedures for the fits is slightly different. As said above, we have neglected the flavor nonsinglet contribution, took a fixed $n_f = 4$ scheme for both the evolution of the running coupling and the conformal GPD moments, and assumed a generic j -dependence of the conformal GPD moments at the input scale. However, as we realize a posteriori, these simplifications are justified within the error bands.

Although GPDs are amplitudes, it was shown that for $\eta = 0$ they have a probabilistic interpretation in the infinite momentum frame within the parton picture [53, 54, 55, 56]. More precisely, their Fourier transform with respect to the transversal degrees of freedom

$$H(x, \vec{b}) = \int \frac{d^2 \vec{\Delta}}{(2\pi)^2} e^{-i\vec{b} \cdot \vec{\Delta}} H(x, \eta = 0, \Delta^2 = -\vec{\Delta}^2), \quad (203)$$

can be interpreted as parton densities that besides the longitudinal momentum fraction depend also on the impact parameter \vec{b} . The averaged squared distance of a parton from the center of the nucleon might be expressed by the slope of the corresponding GPD

$$\langle \vec{b}^2 \rangle(x, Q^2) = \frac{\int d\vec{b} \vec{b}^2 H(x, \vec{b}, Q^2)}{\int d\vec{b} H(x, \vec{b}, Q^2)} = 4B(x, Q^2), \quad (204)$$

where the slope is defined as

$$B(x, Q^2) = \frac{d}{d\Delta^2} \ln H(x, \eta = 0, \Delta^2, Q^2) \Big|_{\Delta^2=0}. \quad (205)$$

In Fig. 16 we display the resulting slope for the flavor singlet quark combination (left) and gluon (right) GPD, respectively. Here we exclude the LO result, which within our ansatz fails to describe

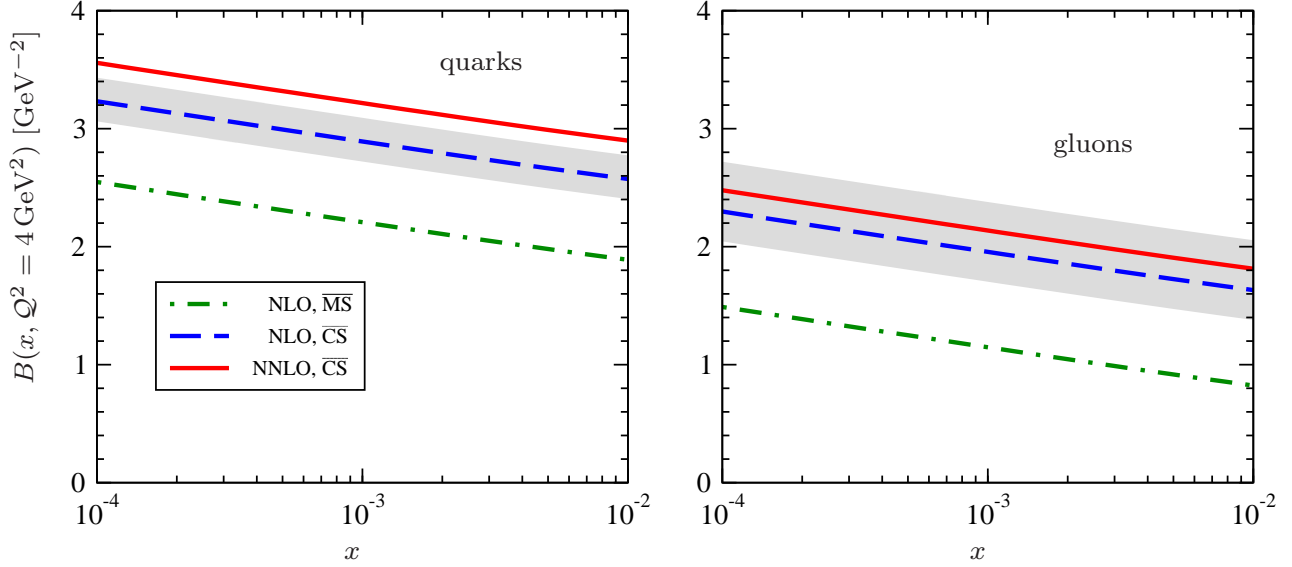


Figure 16: The GPD slope, defined in Eq. (205), is shown for quarks (left) and gluons (right) at the input scale $Q^2 = 4 \text{ GeV}^2$. The meaning of the lines are the same as in Fig. 15 and the band shows the errors for the NLO fit in the $\overline{\text{CS}}$ scheme.

the Δ^2 dependence of the differentiated DVCS cross section. As observed before [166], within the pomeron inspired ansatz, the slope parameter slightly increases with decreasing x and is smaller for gluons than for quarks. As explained above, the difference between the $\overline{\text{CS}}$ (dashed) and $\overline{\text{MS}}$ (dash-dotted) scheme is in fact induced by our ansatz being rigid with respect to skewness. We would also expect that a more flexible ansatz would reduce the differences between NLO (dashed) and NNLO (solid) results. Compared to the LO analysis of Ref. [166], we find, e.g., for $x = 10^{-3}$ and $Q^2 = 4 \text{ GeV}^2$, that the central value of the slope to NLO accuracy in the $\overline{\text{CS}}$ scheme is for quarks (gluons) about 35% (55%) smaller. In particular, for gluons is our NLO analysis now compatible with the slope extracted from J/ψ photo- or electroproduction, see, e.g., Refs. [176, 177, 30]. This process is dominated by the two gluon exchange and its measured Δ^2 slope of the differential cross section, which is nearly Q^2 independent, is about 5 GeV^{-2} . This is consistent with two times the value we extracted from our DVCS analysis in the $\overline{\text{CS}}$ scheme, see right panel in Fig. 16. This slope yields the spatial averaged size squared for gluons of

$$\langle \vec{b}^2 \rangle_{\text{gluon}}(x = 10^{-3}, Q^2 = 4 \text{ GeV}^2) = 0.30_{-0.04}^{+0.07} \text{ fm}^2 \quad (0.33_{-0.04}^{+0.08} \text{ fm}^2) \quad (206)$$

to NLO (NNLO) accuracy. The central value is about 20% (10%) smaller than the one of Refs. [178, 179], however, still compatible within errors. We consider this a further wink that in the GPD phenomenology perturbative corrections should be taken into account.

8 Conclusions

In this article we have derived the leading twist-two Compton form factors represented as Mellin–Barnes integrals in terms of conformal GPD moments with their evolution included. Thereby, we have used the standard framework, known from DIS, which is based on the local operator product expansion and dispersion relation techniques and we have confirmed known results, derived using other methods. For instance, this representation can be obtained in a straightforward way from the momentum fraction representation, which also allows other GPD related processes, e.g., the hard electroproduction of mesons, to be represented by a Mellin–Barnes integral. Although the original motivation for this representation, the solution of the LO evolution equation, is tied to conformal symmetry, we explicitly showed here that there is no problem in using this Mellin–Barnes integral representation beyond LO within the standard $\overline{\text{MS}}$ scheme, in which conformal symmetry is not explicitly manifested. This opens a new road for the ‘global’ analysis of experimental data within the perturbative GPD formalism to NLO accuracy.

We have combined the Mellin–Barnes representation with conformal symmetry predictions, which would hold true if there existed a nontrivial fixed-point in QCD. Formally, in the perturbative sector one sets the β function to zero. Unfortunately, the return to the real $\beta \neq 0$ world is plagued by an ambiguity, which we have shifted to the evolution equation where, consequently, it induces at NNLO a mixing of conformal GPD moments. We have argued that this mixing can be safely neglected in the fixed target kinematics, but will, however, influence the radiative corrections for small values of Bjorken-like scaling parameter ξ .

The outcome of our numerical analysis can be summarized as follows. To leading-order accuracy, the scale setting prescription is most problematic, and this ambiguity directly translates into the ignorance of the scale that enters the (moments of) GPD. For fixed target kinematics, this problem diminishes already in NLO. There radiative corrections are moderate in the flavor nonsinglet sector, whereas can be larger in the singlet one, due to the appearance of gluons. With increasing experimental precision, one might also employ evolution to constrain the conformal GPD ansätze. To test the reliability of perturbation theory, we have studied NNLO corrections and found that they are indeed small, 5% or even less.

In contrast to fixed target kinematics, in the small x_{Bj} region our studies have clarified the situation with perturbative expansion of the evolution operator being ill-defined in the kinematics of interest, whereas the perturbative expansion of Wilson coefficients presents no difficulties. As in DIS, this bad behavior arises from $\ln(1/\xi)\alpha_s$ terms, induced by the $j = 0$ poles of the anomalous dimensions in the parity even sector, where $j+2$ is the conformal spin. Nevertheless, these poles are universal and, as we have demonstrated, the large fluctuation of the scaling prediction within the considered order does not influence the quality of fits, and, in particular, the possibility of relating

DVCS and DIS data. Hence, the problem of treatment or resummation of these large corrections is relevant primarily to our partonic interpretation of the nucleon content. As long as we precisely define the treatment of the evolution operator, perturbative QCD can be employed as a tool for analyzing data in the small x_{Bj} region. According to this, the reported large-scale dependence in the hard vector-meson electroproduction might not necessarily lead to the conclusion that this process cannot be analyzed within the GPD formalism. We also note that progress in the resummation of $\ln(1/x_{\text{Bj}})\alpha_s$ corrections in DIS has recently been achieved by two groups, see, e.g., Ref. [172].

Although we have studied only the parity even sector, one can imagine what happens in the parity odd one. The analytic properties of Wilson coefficients in both sectors are similar and the parity odd anomalous dimensions do not suffer from poles at $j = 0$. Hence we expect that the radiative corrections have similar features in the fixed target kinematics as in the parity even case and do not grow large in the small x_{Bj} region, which anyway can hardly be accessed in experiments.

So far in the literature experimental data have been analyzed by comparing one or another ansatz with measurements. In particular, in the small x_{Bj} region, where the Bjorken and the high-energy limit are competitors, the success of such an approach is based on trial and error. Indeed, as in the unpolarized DIS case, data can only be successfully fitted by a kind of fine tuning procedure of the relevant parameters within a clearly defined, however, ambiguous scheme. The most important advantage of the Mellin–Barnes representation, as demonstrated in this paper up to NNLO, is that it is adequate for building the fitting procedure of hard photon and meson electroproduction data. Certainly, a great deal of work, e.g., resummation of $\text{SO}(3)$ partial waves, study of skewness dependence, and choosing an appropriate set of parameters, must be done to release the full power of this framework.

To conclude, we would suggest the analysis of experimental data to NLO accuracy within the standard $\overline{\text{MS}}$ scheme. This drastically reduces the theoretical uncertainties, present in the LO approximation, particularly in relating different processes, e.g., hard photon and meson electroproduction. The Mellin–Barnes representation allows us to write flexible fitting routines, which are fast enough and numerically stable, and thus it provides a reliable and systematic procedure to for analyzing experimental data. This we consider the main step towards a global analysis of experimental data, related to GPDs.

Note added

After the manuscript was submitted to hep-ph, the evaluation of the subtraction constant has been also given in Eq. (22) of Ref. [180]. Our formula (47), approximated to LO, expressed in momentum fraction space, and written down for CFF \mathcal{H} , yields the aforementioned result

and contains a prescription for treating the appearing divergencies. Related work has been also presented in Refs. [181, 182].

Acknowledgements

This project has been supported by the German Research Foundation (DFG), Croatian Ministry of Science, Education and Sport under the contracts no. 119-0982930-1016 and 098-0982930-2864, U.S. National Science Foundation under grant no. PHY-0456520, and EU project Joint Research Activity 5: GPDs. The authors would like to thank the theory group at the University of Regensburg for its warm hospitality. D.M. is grateful for invitations at the Thomas Jefferson National Accelerator Facility and Service de Physique Nucléaire (Saclay). For both clarifying and inspiring discussions we are indebted to I. Anikin, H. Avakian, M. Diehl, M. Garçon, V. Guzey, D. Ivanov, M. Kirch, A. Manashov, B. Pire, A. Schäfer, L. Schoeffel, P. Schweigert, L. Szymanowski, O.V. Teryaev, S. Wallon, and C. Weiss.

A Normalization of Wilson coefficients and anomalous dimensions

Here we establish the normalization of the Wilson coefficients of the OPE (28) in the forward kinematics

$${}^a C_j^I(\vartheta = 0, Q^2/\mu^2 = 1, \alpha_s) = {}^a c_j^I(\alpha_s), \quad (\text{A.1})$$

where ${}^a c_j^V(\alpha_s)$ and ${}^a c_j^A(\alpha_s)$ are the Wilson coefficients that appear in the perturbative description of the DIS unpolarized and polarized structure function F_1 and g_1 , respectively, for $\mu = Q$.

The hadronic DIS tensor is related to the Compton scattering tensor (1) by the optical theorem

$$W_{\mu\nu} = \frac{1}{2\pi} \Im T_{\mu\nu}(q, P = 2p, \Delta = 0), \quad (\text{A.2})$$

where $p = P_1 = P_2$. We recall that the DIS hadronic tensor for a longitudinally polarized target might be written in terms of the structure functions $F_1(x_{\text{Bj}}, Q^2)$, $F_L(x_{\text{Bj}}, Q^2)$, and $g_1(x_{\text{Bj}}, Q^2)$:

$$W_{\mu\nu} = -\tilde{g}_{\mu\nu}^T F_1(x_{\text{Bj}}, Q^2) + \frac{\tilde{p}_\mu \tilde{p}_\nu}{p \cdot q} F_L(x_{\text{Bj}}, Q^2) - i\Lambda \epsilon_{\mu\nu qp} \frac{1}{p \cdot q} g_1(x_{\text{Bj}}, Q^2), \quad (\text{A.3})$$

where $x_{\text{Bj}} = \xi = Q^2/2\nu M$ and $\Lambda = 1$ is the polarization of the target with respect to the \vec{p} direction. Both F_1 and g_1 structure functions are expressed to leading power accuracy as

$$\left\{ \begin{matrix} F_1 \\ g_1 \end{matrix} \right\}(x, Q^2) = \frac{1}{2} \sum_{a=u, \bar{u}, \dots, G} Q_a^2 \int_x^1 \frac{dy}{y} \left\{ \begin{matrix} {}^a c \\ \Delta {}^a c \end{matrix} \right\} \left(\frac{x}{y}, \frac{Q^2}{\mu^2}, \alpha_s(\mu) \right) \left\{ \begin{matrix} {}^a q \\ \Delta {}^a q \end{matrix} \right\}(y, \mu^2), \quad (\text{A.4})$$

where the flavor sum runs over quarks, antiquarks, and gluons. Here $(\Delta)c_a$ are the partonic cross sections, depending on the factorization scale μ . The polarized and unpolarized (anti-)parton distributions are denoted as q_a and Δq_a [$(\Delta)\bar{q}_a = (\Delta)q_{\bar{a}}$], respectively, and Q_a are the fractional electrical charges

$$Q_u = Q_c = \frac{2}{3}, \quad Q_d = Q_s = \frac{1}{3}, \quad Q_G^2 = \frac{1}{n_f} \sum_{a=u,d,\dots} Q_a^2 \quad \text{for gluons,} \quad (\text{A.5})$$

while the coefficient functions are normalized as follows

$$(\Delta)^a c = \delta(1-x) + \mathcal{O}(\alpha_s) \quad \text{for } a = \{u, \bar{u}, d, \dots\} \quad \text{and} \quad (\Delta)^G c = \mathcal{O}(\alpha_s). \quad (\text{A.6})$$

Since the evolution will yield a mixing of the quark singlet and gluon parton densities, it is appropriate to introduce a group theoretical decomposition in flavor nonsinglet and singlet densities. For three active light quarks these combinations are

$$\begin{aligned} (\Delta)^{\text{NS}} q &= 2(\Delta)^u q + 2(\Delta)^{\bar{u}} \bar{q} - (\Delta)^d q - (\Delta)^{\bar{d}} \bar{q} - (\Delta)^s q - (\Delta)^{\bar{s}} \bar{q} \\ (\Delta)^{\Sigma} q &= (\Delta)^u q + (\Delta)^{\bar{u}} \bar{q} + (\Delta)^d q + (\Delta)^{\bar{d}} \bar{q} + (\Delta)^s q + (\Delta)^{\bar{s}} \bar{q}, \end{aligned} \quad (\text{A.7})$$

while for four active quarks they read:

$$\begin{aligned} (\Delta)^{\text{NS}} q &= (\Delta)^u q + (\Delta)^{\bar{u}} \bar{q} - (\Delta)^d q - (\Delta)^{\bar{d}} \bar{q} - (\Delta)^s q - (\Delta)^{\bar{s}} \bar{q} + (\Delta)^c q + (\Delta)^{\bar{c}} \bar{q} \\ (\Delta)^{\Sigma} q &= (\Delta)^u q + (\Delta)^{\bar{u}} \bar{q} + (\Delta)^d q + (\Delta)^{\bar{d}} \bar{q} + (\Delta)^s q + (\Delta)^{\bar{s}} \bar{q} + (\Delta)^c q + (\Delta)^{\bar{c}} \bar{q}, \end{aligned} \quad (\text{A.8})$$

The corresponding squared charge factors are defined in Eq. (27). In the singlet case the parton densities with $a = \{+, -\}$ are eigenvectors of the evolution equation, i.e., all distributions satisfy the evolution equation

$$\mu^2 \frac{d}{d\mu^2} (\Delta)^a q(x, \mu^2) = \int_x^1 \frac{dy}{y} (\Delta)^a P\left(\frac{x}{y}, \alpha_s(\mu)\right) (\Delta)^a q(y, \mu^2) \quad \text{for } a = \{\text{NS}, +, -\} \quad (\text{A.9})$$

where $(\Delta)^a P$ are the splitting kernels. The rotation to this basis results into the replacement of the flavor sum in (A.4).

$$\sum_{a=u,\bar{u},\dots,G} \Rightarrow \sum_{a=\text{NS},+,-} . \quad (\text{A.10})$$

Using the optical theorem (A.2) and the parameterization of the Compton tensor (3) and the DIS hadronic tensor (A.3) we find that the structure functions are related to the CFFs by

$$\left\{ \begin{matrix} F_1 \\ g_1 \end{matrix} \right\} (x_{\text{Bj}}, Q^2) = \frac{1}{2\pi} \Im \left\{ \frac{\mathcal{H}}{\tilde{\mathcal{H}}} \right\} (\xi = x_{\text{Bj}} - i0, \dots) \Big|_{\Delta=0}. \quad (\text{A.11})$$

Forming Mellin moments, we find by means of Eq. (36)

$$\int_0^1 dx x^j \left\{ \begin{matrix} F_1 \\ g_1 \end{matrix} \right\} (x, Q^2) = \frac{1}{2} \sum_{a=\text{NS}, \pm} Q_a^2 \left\{ \begin{matrix} {}^a c^V \\ {}^a c^A \end{matrix} \right\}_j (\alpha_s(Q)) \left\{ \begin{matrix} {}^a H \\ {}^a \tilde{H} \end{matrix} \right\}_j (\eta = 0, \Delta^2 = 0, Q^2), \quad (\text{A.12})$$

and, on the other hand, in terms the parton densities and coefficient moments of Eq. (A.4)

$$\int_0^1 dx x^j \left\{ \begin{matrix} F_1 \\ g_1 \end{matrix} \right\} (x, Q^2) = \frac{1}{2} \sum_{a=\text{NS}, \pm} Q_a^2 \left\{ \begin{matrix} {}^a c \\ \Delta^a c \end{matrix} \right\}_j (\alpha_s(Q)) \left\{ \begin{matrix} {}^a q \\ \Delta^a q \end{matrix} \right\}_j (Q^2), \quad (\text{A.13})$$

with definitions

$$(\Delta)^a q_j(Q^2) = \int_0^1 dx x^j (\Delta)^a q(x, Q^2), \quad (\Delta)^a c_j(\alpha_s) = \int_0^1 dx x^j (\Delta)^a c(x, 1, \alpha_s). \quad (\text{A.14})$$

From this we obtain the equalities

$$\begin{aligned} {}^a c_j(\alpha_s) {}^a q_j(Q^2) &= {}^a c_j^V(\alpha_s) {}^a H_j(\eta = 0, \Delta^2 = 0, Q^2), \\ \Delta^a c_j(\alpha_s) \Delta^a q_j(Q^2) &= {}^a c_j^A(\alpha_s) {}^a \tilde{H}_j(\eta = 0, \Delta^2 = 0, Q^2). \end{aligned} \quad (\text{A.15})$$

The normalization of the conformal operators (21) and (23) is chosen so that their reduced matrix elements in the forward kinematics reduce to those used in DIS. Taking into account that Eqs. (31) and (32) relate the forward matrix elements to the conformal moments H_j and \tilde{H}_j , we find, for instance, in the unpolarized case for odd j

$$\begin{aligned} {}^a H_j \Big|_{\Delta=0} &= \frac{1}{P_+^{j+1}} \langle p | {}^a \mathcal{O}_j^V | p \rangle = \frac{1}{2p_+^{j+1}} \langle p | \bar{\psi}_a(0) \gamma_+ \left(i \vec{D}_+ \right)^j \psi_a(0) | p \rangle = {}^a q_j + {}^a \bar{q}_j \quad \text{for } a = \{u, d, s\}, \\ {}^a H_j \Big|_{\Delta=0} &= \frac{1}{P_+^{j+1}} \langle p | {}^a \mathcal{O}_j^V | p \rangle = \frac{1}{2p_+^{j+1}} \langle p | \bar{\psi}(0) \lambda^a \gamma_+ \left(i \vec{D}_+ \right)^j \psi(0) | p \rangle = {}^a q_j \quad \text{for } a = \{\text{NS}, \Sigma\}, \\ {}^G H_j \Big|_{\Delta=0} &= \frac{1}{P_+^{j+1}} \langle p | {}^G \mathcal{O}_j^V | p \rangle = \frac{1}{2p_+^{j+1}} \langle p | G_+^\mu(0) \left(i \vec{D}_+ \right)^{j-1} G_{\mu+}(0) | p \rangle = {}^G q_j. \end{aligned} \quad (\text{A.16})$$

Hence, from the identity (A.15) we find the desired normalization for the Wilson coefficients

$${}^a c_j^V(\alpha_s) = {}^a c_j(\alpha_s) \quad \text{and} \quad {}^a c_j^A(\alpha_s) = \Delta^a c_j(\alpha_s).$$

Taking the forward limit in the evolution equation (81) and comparing it with the moments of Eq. (A.9), we also establish from the identities (A.16) the definition of the anomalous dimensions in terms of moments of the splitting kernel

$$\int_0^1 dx x^j {}^a P(x, \alpha_s) = -\frac{1}{2} {}^a \gamma_j^V(\alpha_s), \quad \int_0^1 dx x^j \Delta^a P(x, \alpha_s) = -\frac{1}{2} {}^a \gamma_j^A(\alpha_s). \quad (\text{A.17})$$

Note that within our definitions, the momentum sum rule for $j = 1$ is established by

$$\frac{1}{P_+^2} \langle P_2, S_2 | {}^\Sigma \mathcal{O}_1^V | P_1, S_1 \rangle + \frac{1}{P_+^2} \langle P_2, S_2 | {}^G \mathcal{O}_1^V | P_1, S_1 \rangle = \frac{2}{P_+^2} \langle P_2, S_2 | \Theta_{++} | P_1, S_1 \rangle, \quad (\text{A.18})$$

which results in the scale independent expectation value of the energy-momentum tensor

$$\Theta_{++} = \frac{i}{2} \bar{\psi} \gamma_+ \overleftrightarrow{D}_+ \psi + G_+^{a\mu} G_{\mu+}^a, \quad (\text{A.19})$$

projected on the plus light-cone components. In the forward case the sum rule (A.18) reduces to

$$\Sigma q_1(\mu) + G q_1(\mu) = \frac{1}{2(p_+)^2} \langle p | \Theta_{++} | p \rangle \equiv 1. \quad (\text{A.20})$$

As a consequence of the scale independence the anomalous dimensions satisfy the relation:

$$\Sigma \Sigma \gamma_1^V(\alpha_s) + G \Sigma \gamma_1^V(\alpha_s) = G G \gamma_1^V(\alpha_s) + \Sigma G \gamma_1^V(\alpha_s) = 0. \quad (\text{A.21})$$

B Bases in the flavor singlet sector

The transformation of the gluon and quark singlet conformal operators to the basis of the \pm ones is defined in Eq. (24). In the following we drop the superscript $I \in \{V, A\}$. By making use of the evolution equation it can be easily shown that the two dimensional anomalous dimension matrix is diagonalized by the rotation

$$\begin{pmatrix} +\gamma_j & 0 \\ 0 & -\gamma_j \end{pmatrix} = \mathbf{U}_j \begin{pmatrix} \Sigma \Sigma \gamma_j & \Sigma G \gamma_j \\ G \Sigma \gamma_j & G G \gamma_j \end{pmatrix} (\mathbf{U}_j)^{-1} - \left(\mu \frac{d}{d\mu} \mathbf{U}_j \right) (\mathbf{U}_j)^{-1}. \quad (\text{B.1})$$

Let us suppose that for a given scale μ_0 the inhomogeneous term vanishes, i.e., $\mu \frac{d}{d\mu} \mathbf{U}|_{\mu=\mu_0} = 0$. At this reference point the eigenvalues of the anomalous dimension matrix are

$$\pm \gamma_j = \frac{1}{2} \left(\Sigma \Sigma \gamma_j + G G \gamma_j \pm \sqrt{(\Sigma \Sigma \gamma_j - G G \gamma_j)^2 + 4 \Sigma G \gamma_j G \Sigma \gamma_j} \right), \quad (\text{B.2})$$

and the rotation matrix reads

$$\mathbf{U}_j(\mu_0, \mu_0) = \begin{pmatrix} 1 & \frac{G G \gamma_j^- - \gamma_j}{G \Sigma \gamma_j} \\ \frac{\Sigma \Sigma \gamma_j^- + \gamma_j}{\Sigma G \gamma_j} & 1 \end{pmatrix} (\alpha_s(\mu_0)). \quad (\text{B.3})$$

The diagonalization of the evolution equation at an arbitrary scale can be now obtained by the use of evolution

$$\mathbf{U}_j(\mu, \mu_0) = \mathbf{E}_j(\mu, \mu_0) \mathbf{U}_j(\mu_0, \mu_0) \mathbf{E}_j^{-1}(\mu, \mu_0) \quad (\text{B.4})$$

where \mathbf{E}^{-1} is the inverse of the evolution operator (120) and

$$\mathbf{E}_j(\mu, \mu_0) = \begin{pmatrix} \exp \left\{ - \int_{\mu_0}^{\mu} \frac{d\mu'}{\mu'} \gamma_j^+(\alpha_s(\mu')) \right\} & 0 \\ 0 & \exp \left\{ - \int_{\mu_0}^{\mu} \frac{d\mu'}{\mu'} \gamma_j^-(\alpha_s(\mu')) \right\} \end{pmatrix} \quad (\text{B.5})$$

is the evolution operator in the $\{+, -\}$ basis.

C Momentum fraction representation versus conformal moments

In the momentum fraction representation the Compton form factors are represented as convolution of the coefficient function with the corresponding GPD. In the singlet sector in which quark (${}^{\Sigma}\mathcal{O}$) and gluon (${}^{\mathcal{G}}\mathcal{O}$) operators mix under renormalization, we might introduce the vector notation:

$${}^{\Sigma}\mathcal{F}(\xi, \Delta^2, \mathcal{Q}^2) = \int_{-1}^1 \frac{dx}{\xi} \mathbf{C}(x/\xi, \mathcal{Q}^2/\mu^2, \alpha_s(\mu)|\xi) \mathbf{F}(x, \eta = \xi, \Delta^2, \mu^2). \quad (\text{C.1})$$

Here the column vector

$$\mathbf{F} = \begin{pmatrix} {}^{\Sigma}F \\ {}^{\mathcal{G}}F \end{pmatrix}, \quad F = \{H, E, \tilde{H}, \tilde{E}\} \quad (\text{C.2})$$

contains the GPDs, and the row one, defined as $\mathbf{C} = ({}^{\Sigma}C, (1/\xi){}^{\mathcal{G}}C)$, consists of the hard scattering part that to LO accuracy reads

$$\frac{1}{\xi} \mathbf{C}(x/\xi, \mathcal{Q}^2/\mu^2, \alpha_s(\mu)|\xi) = \left(\frac{1}{\xi - x - i\epsilon}, 0 \right) + \mathcal{O}(\alpha_s). \quad (\text{C.3})$$

We remark that the ξ dependence in ${}^{\Sigma}C$ and ${}^{\mathcal{G}}C$ enters only via the ratio x/ξ . Note also that the u -channel contribution in the quark entry (C.3) has been reabsorbed into the symmetrized quark singlet distribution

$${}^{\Sigma}F(x, \eta, \Delta^2, \mu^2) = \sum_{q=u,d,\dots} [{}^qF(x, \eta, \Delta^2, \mu^2) \mp {}^qF(-x, \eta, \Delta^2, \mu^2)]. \quad (\text{C.4})$$

Here the second term in the square brackets with $-(+)$ -sign for H, E (\tilde{H}, \tilde{E})-type GPDs is for $x > \eta$ related to the s -channel exchange of an antiquark. The gluon GPDs have definite symmetry property under the exchange of $x \rightarrow -x$: ${}^{\mathcal{G}}H$ and ${}^{\mathcal{G}}E$ are even, while ${}^{\mathcal{G}}\tilde{H}$ and ${}^{\mathcal{G}}\tilde{E}$ are odd.

C.1 Evaluation of conformal moments

The convolution formula (C.1) has already at LO the disadvantage that it contains a singularity at the cross-over point between the central region ($-\eta \leq x \leq \eta$) and the outer region ($\eta \leq x \leq 1$), i.e., for $x = \xi = \eta$. Its treatment is defined by the $i\epsilon$ prescription, coming from the Feynman propagator. The GPD is considered smooth at this point, but will generally not be holomorphic [88]. The fact that both regions are dual to each other, up to a so-called D -term contribution [120], makes the numerical treatment even more complicated. This motivated our development of a more suitable formalism in [98].

To make contact with the conformal OPE, we expand the hard-scattering amplitude in terms of Gegenbauer polynomials with indices 3/2 and 5/2 for quarks and gluons, respectively, and introduce the conformal GPD moments, which formally leads to

$$^s\mathcal{F}(\xi, \Delta^2, \mathcal{Q}^2) = 2 \sum_{j=0}^{\infty} \xi^{-j-1} \mathbf{C}_j(\mathcal{Q}^2/\mu^2, \alpha_s(\mu)) \mathbf{F}_j(\xi, \Delta^2, \mu^2). \quad (\text{C.5})$$

The expansion coefficients \mathbf{C}_j can be calculated by the projection:

$$\begin{aligned} \mathbf{C}_j(\mathcal{Q}^2/\mu^2, \alpha_s(\mu)) &= \frac{2^{j+1}\Gamma(j+5/2)}{\Gamma(3/2)\Gamma(j+4)} \\ &\times \frac{1}{2} \int_{-1}^1 dx \mathbf{C}(x, \mathcal{Q}^2/\mu^2, \alpha_s(\mu)|\xi=1) \begin{pmatrix} (j+3)[1-x^2]C_j^{3/2} & 0 \\ 0 & 3[1-x^2]^2C_{j-1}^{5/2} \end{pmatrix} (x). \end{aligned} \quad (\text{C.6})$$

Note that we have here rescaled the integration variable with respect to ξ and that the integral runs only over the rescaled central region. The conformal moments of the singlet GPDs are defined as

$$\mathbf{F}_j(\eta, \Delta^2, \mu^2) = \frac{\Gamma(3/2)\Gamma(j+1)}{2^j\Gamma(j+3/2)} \frac{1}{2} \int_{-1}^1 dx \eta^{j-1} \begin{pmatrix} \eta C_j^{3/2} & 0 \\ 0 & (3/j) C_{j-1}^{5/2} \end{pmatrix} \left(\frac{x}{\eta}\right) \mathbf{F}(x, \eta, \Delta^2, \mu^2). \quad (\text{C.7})$$

Here j is an odd (even) non-negative integer for the (axial-)vector case.

In order to make use of the NLO $\overline{\text{MS}}$ results given in the momentum fraction representation, for quark part we determine the corresponding conformal moments using the results from Ref. [137]. In particular, the conformal moments (128) for the axial-vector case can be read off from Eq. (3.32) in Ref. [137], where the normalization factor $(2j+3)/(j+1)(j+2)$ must be removed and the remaining expression multiplied by the color factor C_F . The conformal moments (127) for the vector case one can easily recover from the hard-scattering amplitude given in Ref. [154], Eqs. (14) and (15). Thereby one has only to evaluate the difference between the vector and axial-vector results

$$\Sigma_C^{V(1)}(x, \mathcal{Q}/\mu^2) - \Sigma_C^{A(1)}(x, \mathcal{Q}/\mu^2) = -\frac{C_F}{x} \ln(1-x). \quad (\text{C.8})$$

Employing Tab. 8 in App. C of Ref. [137], we find, after removing the normalization factor $2(2j+3)/(j+1)(j+2)$, that the difference for the conformal moments is $C_F/(j+1)(j+2)$.

C.2 Conformal moments for the gluon part

Following the method for computing moments with respect to conformal partial waves (with the index k) in the quark sector that was explained in detail in App. C of Ref. [137], we here give the necessary results for the gluon sector.

We introduce the notation similar to the one used in Ref. [137]

$$\langle G(x) \rangle_{k-1}^{(5/2)} \equiv \int_0^1 dx G(x) \frac{x^2(1-x)^2}{N_{k-1}^{5/2}} C_{k-1}^{5/2}(2x-1), \quad (\text{C.9})$$

with

$$N_{k-1}^{5/2} = \frac{k(k+3)}{N_k^{3/2}} \quad N_k^{3/2} = \frac{(k+1)(k+2)}{4(2k+3)}. \quad (\text{C.10})$$

It follows trivially that $\langle G(1-x) \rangle_{k-1}^{(5/2)} = (-1)^{k-1} \langle G(x) \rangle_{k-1}^{(5/2)}$, and one can easily make the correspondence to definitions of conformal moments given in (C.6):

$$\mathbb{G}C_k = \frac{2^{k+1}\Gamma(k+5/2)}{\Gamma(3/2)\Gamma(k+4)} 48 N_{k-1}^{5/2} \langle \mathbb{G}C(2x-1) \rangle_{k-1}^{(5/2)} \quad (\text{C.11})$$

It is convenient to use the following expression for the Gegenbauer polynomials:

$$\frac{x^2(1-x)^2}{N_{k-1}^{5/2}} C_{k-1}^{5/2}(2x-1) = (-1)^{k-1} \frac{12(2k+3)}{k(k+1)} \sum_{i=0}^{k+1} (-1)^i \binom{k+1}{i} \binom{k+i+1}{i+2} x^{i+2}. \quad (\text{C.12})$$

The evaluation of the conformal moments, i.e., in our case the evaluation of the expressions

$$\left\langle \frac{g(x)}{x} \right\rangle_{k-1}^{(5/2)} = (-1)^{k-1} \frac{12(2k+3)}{k(k+1)} \sum_{i=0}^{k+1} (-1)^i \binom{k+1}{i} \binom{k+i+1}{i+2} \int_0^1 x^{i+1} g(x), \quad (\text{C.13})$$

and

$$\left\langle \frac{g(x)}{1-x} \right\rangle_{k-1}^{(5/2)} = \frac{12(2k+3)}{k(k+1)} \sum_{i=0}^{k+1} (-1)^i \binom{k+1}{i} \binom{k+i+1}{i+2} \int_0^1 x^{i+1} g(1-x), \quad (\text{C.14})$$

consists then in calculating the Mellin moments and performing the summation. The Mellin moments for the functions we encounter and most of the nontrivial sums we are left with can be found in [150].

In Table 5 we summarize the conformal moments of the functions relevant to our calculation.

References

- [1] A. Mueller, editor, *Perturbative Quantum Chromodynamics*, World Scientific, Singapore, 1989.
- [2] S. J. Brodsky, M. Burkardt and I. Schmidt, Nucl. Phys. **B441**, 197 (1995), [hep-ph/9401328].
- [3] A. D. Martin, W. J. Stirling and R. S. Thorne, Phys. Lett. **B636**, 259 (2006), [hep-ph/0603143].

Table 5: The conformal moments of some relevant functions.

$\left\langle \frac{1}{1-x} \right\rangle_{k-1}^{(5/2)}$	$\frac{1}{12N_{k-1}^{5/2}}$
$\left\langle \frac{\ln(1-x)}{1-x} \right\rangle_{k-1}^{(5/2)}$	$\frac{1}{12N_{k-1}^{5/2}} \left[1 - S_1(k-1) - S_1(k+3) \right]$
$\left\langle \frac{\ln(1-x)}{x} \right\rangle_{k-1}^{(5/2)}$	$\frac{-1}{12N_{k-1}^{5/2}} \left[\frac{1}{k} - \frac{1}{k+1} + \frac{1}{k+2} - \frac{1}{k+3} \right]$
$\left\langle \frac{\ln(1-x)}{x^2} \right\rangle_{k-1}^{(5/2)}$	$\frac{1}{12N_{k-1}^{5/2}} \left[(-1)^k - \frac{2}{(k+1)(k+2)} \right]$
$\left\langle \frac{\ln^2(1-x)}{x^2} \right\rangle_{k-1}^{(5/2)}$	$\frac{1}{12N_{k-1}^{5/2}} \frac{2}{(k+1)(k+2)} [2S_1(k) + 2S_1(k+2) - 3]$

[4] S. Alekhin, JETP Lett. **82**, 628 (2005), [hep-ph/0508248].

[5] J. Pumplin *et al.*, JHEP **07**, 012 (2002), [hep-ph/0201195].

[6] M. Glück, E. Reya and A. Vogt, Eur. Phys. J. **C5**, 461 (1998), [hep-ph/9806404].

[7] E. Leader, A. V. Sidorov and D. B. Stamenov, Phys. Rev. **D73**, 034023 (2006), [hep-ph/0512114].

[8] J. Blümlein and H. Bottcher, Nucl. Phys. **B636**, 225 (2002), [hep-ph/0203155].

[9] M. Glück, E. Reya, M. Stratmann and W. Vogelsang, Phys. Rev. **D63**, 094005 (2001), [hep-ph/0011215].

[10] T. Gehrmann and W. J. Stirling, Phys. Rev. **D53**, 6100 (1996), [hep-ph/9512406].

[11] W. T. Giele and S. Keller, Phys. Rev. **D58**, 094023 (1998), [hep-ph/9803393].

[12] S. Forte, L. Garrido, J. I. Latorre and A. Piccione, JHEP **05**, 062 (2002), [hep-ph/0204232].

[13] J. C. Rojo, *The Neural network approach to parton distribution functions*, PhD thesis, 2006, hep-ph/0607122.

[14] G. Lepage and S. Brodsky, Phys. Rev. **D22**, 2157 (1980).

- [15] S. Brodsky and G. Lepage, Phys. Rev. **D24**, 1808 (1981).
- [16] A. Efremov and A. Radyushkin, Phys. Lett. **B94**, 245 (1980).
- [17] A. Duncan and A. Mueller, Phys. Rev. **D21**, 1636 (1980).
- [18] V. Chernyak and A. Zhitnitsky, Nucl. Phys. **B246**, 52 (1984).
- [19] N. Isgur and C. L. Smith, Phys. Rev. Lett. **52**, 1080 (1984).
- [20] N. Isgur and C. L. Smith, Phys. Lett. **217B**, 535 (1989).
- [21] A. Radyushkin, Acta Physica Polonica **B15**, 403 (1984).
- [22] I. I. Balitsky, V. M. Braun and A. V. Kolesnichenko, Nucl. Phys. **B312**, 509 (1989).
- [23] V. Braun and I. Filyanov, Z. Phys. **C 48**, 239 (1990).
- [24] D. Müller, D. Robaschik, B. Geyer, F.-M. Dittes and J. Hořejši, Fortschr. Phys. **42**, 101 (1994), [hep-ph/9812448].
- [25] F.-M. Dittes, B. Geyer, D. Müller, D. Robaschik and J. Hořejši, Phys. Lett. **209B**, 325 (1988).
- [26] X. Ji, Phys. Rev. Lett. **78**, 610 (1997), [hep-ph/9603249].
- [27] X. Ji, Phys. Rev. **D55**, 7114 (1997), [hep-ph/9609381].
- [28] A. Radyushkin, Phys. Lett. **B380**, 417 (1996), [hep-ph/9604317].
- [29] S. Brodsky, L. Frankfurt, J. Gunion, A. Mueller and M. Strikman, Phys. Rev. **D50**, 3134 (1994), [hep-ph/9402283].
- [30] ZEUS, J. Breitweg *et al.*, Eur. Phys. J. **C6**, 603 (1999), [hep-ex/9808020].
- [31] H1, C. Adloff *et al.*, Eur. Phys. J. **C13**, 371 (2000), [hep-ex/9902019].
- [32] ZEUS, J. Breitweg *et al.*, Eur. Phys. J. **C12**, 393 (2000), [hep-ex/9908026].
- [33] A. Radyushkin, Phys. Lett. **B385**, 333 (1996), [hep-ph/9605431].
- [34] J. Collins, L. Frankfurt and M. Strikman, Phys. Rev. **D56**, 2982 (1997), [hep-ph/9611433].
- [35] LHPC, P. Hägler *et al.*, Phys. Rev. **D68**, 034505 (2003), [hep-lat/0304018].
- [36] LHPC, P. Hägler *et al.*, Eur. Phys. J. **A24S1**, 29 (2005), [hep-ph/0410017].

- [37] LHPC and SESAM, P. Hägler *et al.*, Phys. Rev. Lett. **93**, 112001 (2004), [hep-lat/0312014].
- [38] QCDSF, M. Göckeler *et al.*, Phys. Rev. Lett. **92**, 042002 (2004), [hep-ph/0304249].
- [39] QCDSF, M. Göckeler *et al.*, Phys. Lett. **B627**, 113 (2005), [hep-lat/0507001].
- [40] R. G. Edwards *et al.*, PoS **LAT2006**, 121 (2006), [hep-lat/0610007].
- [41] X. Ji, W. Melnitchouk and X. Song, Phys. Rev. **D56**, 5511 (1997), [hep-ph/9702379].
- [42] M. Diehl, T. Feldmann, R. Jakob and P. Kroll, Nucl. Phys. **B596**, 33 (2001), [hep-ph/0009255].
- [43] S. J. Brodsky, M. Diehl and D. S. Hwang, Nucl. Phys. **B596**, 99 (2001), [hep-ph/0009254].
- [44] S. Scopetta and V. Vento, Eur. Phys. J. **A16**, 527 (2003), [hep-ph/0201265].
- [45] S. Boffi, B. Pasquini and M. Traini, Nucl. Phys. **B649**, 243 (2003), [hep-ph/0207340].
- [46] H.-M. Choi, C.-R. Ji and L. S. Kisslinger, Phys. Rev. **D64**, 093006 (2001), [hep-ph/0104117].
- [47] B. C. Tiburzi and G. A. Miller, Light front Bethe-Salpeter equation applied to form factors, generalized parton distributions and generalized distribution amplitudes, hep-ph/0205109, 2002.
- [48] L. Theussl, S. Noguera and V. Vento, Eur. Phys. J. **A20**, 483 (2004), [nucl-th/0211036].
- [49] S. Ahmad, H. Honkanen, S. Liuti and S. K. Taneja, Phys. Rev. **D75**, 094003 (2007), [hep-ph/0611046].
- [50] M. Diehl, Phys. Rept. **388**, 41 (2003), [hep-ph/0307382].
- [51] A. V. Belitsky and A. V. Radyushkin, Phys. Rept. **418**, 1 (2005), [hep-ph/0504030].
- [52] J. Ralston and B. Pire, Phys. Rev. **D66**, 111501 (2002), [hep-ph/0110075].
- [53] M. Burkardt, Phys. Rev. **D62**, 071503 (2000), [hep-ph/0010082].
- [54] M. Burkardt, Int. J. Mod. Phys. **A18**, 173 (2003), [hep-ph/0207047].
- [55] M. Diehl, Eur. Phys. J. **C25**, 223 (2002), [hep-ph/0205208].
- [56] A. V. Belitsky and D. Müller, Nucl. Phys. **A711**, 118 (2002), [hep-ph/0206306].
- [57] A. V. Belitsky, X. Ji and F. Yuan, Phys. Rev. **D69**, 074014 (2004), [hep-ph/0307383].

- [58] M. Guidal and M. Vanderhaeghen, Phys. Rev. Lett. **90**, 012001 (2003), [hep-ph/0208275].
- [59] A. V. Belitsky and D. Müller, Phys. Rev. Lett. **90**, 022001 (2003), [hep-ph/0210313].
- [60] A. V. Belitsky and D. Müller, Phys. Rev. **D68**, 116005 (2003), [hep-ph/0307369].
- [61] S. J. Brodsky, D. Chakrabarti, A. Harindranath, A. Mukherjee and J. P. Vary, Phys. Lett. **B641**, 440 (2006), [hep-ph/0604262].
- [62] S. J. Brodsky, D. Chakrabarti, A. Harindranath, A. Mukherjee and J. P. Vary, Phys. Rev. **D75**, 014003 (2007), [hep-ph/0611159].
- [63] A. Airapetian *et al.* (HERMES Coll.), Phys. Rev. Lett. **87**, 182001 (2001), [hep-ex/0106068].
- [64] S. Stepanyan *et al.* (CLAS Coll.), Phys. Rev. Lett. **87**, 182002 (2001), [hep-ex/0107043].
- [65] H1, C. Adloff *et al.*, Phys. Lett. **B517**, 47 (2001), [hep-ex/0107005].
- [66] ZEUS, S. Chekanov *et al.*, Phys. Lett. **B573**, 46 (2003), [hep-ex/0305028].
- [67] H1, A. Aktas *et al.*, Eur. Phys. J. **C44**, 1 (2005), [hep-ex/0505061].
- [68] A. V. Belitsky, D. Müller and A. Kirchner, Nucl. Phys. **B629**, 323 (2002), [hep-ph/0112108].
- [69] L. Frankfurt, W. Koepf and M. Strikman, Phys. Rev. **D54**, 3194 (1996), [hep-ph/9509311].
- [70] S. V. Goloskokov and P. Kroll, Eur. Phys. J. **C42**, 281 (2005), [hep-ph/0501242].
- [71] D. Y. Ivanov, L. Szymanowski and G. Krasnikov, JETP Lett. **80**, 226 (2004), [hep-ph/0407207].
- [72] HERMES, A. Airapetian *et al.*, Phys. Rev. **D75**, 011103 (2006), [hep-ex/0605108], hep-ex/0605108.
- [73] HERMES, Z. Ye, Transverse target-spin asymmetry associated with DVCS on the proton and a resulting model-dependent constraint on the total angular momentum of quarks in the nucleon, hep-ex/0606061, 2006.
- [74] CLAS, S. Chen *et al.*, Phys. Rev. Lett. **97**, 072002 (2006), [hep-ex/0605012].
- [75] Jefferson Lab Hall A, C. M. Camacho *et al.*, Phys. Rev. Lett. **97**, 262002 (2006), [nucl-ex/0607029], nucl-ex/0607029.
- [76] D. Müller and A. Kirchner, Eur. Phys. J. **C32**, 347 (2003), [hep-ph/0302007].

- [77] A. Belitsky and D. Müller, Phys. Lett. **B417**, 129 (1997), [hep-ph/9709379].
- [78] L. Mankiewicz, G. Piller, E. Stein, M. Vanttinen and T. Weigl, Phys. Lett. **B425**, 186 (1998), [hep-ph/9712251].
- [79] X. Ji and J. Osborne, Phys. Rev. **D 57**, 1337 (1998), [hep-ph/9707254].
- [80] X. Ji and J. Osborne, Phys. Rev. **D58**, 094018 (1998), [hep-ph/9801260].
- [81] A. Belitsky and D. Müller, Phys. Lett. **B486**, 369 (2000), [hep-ph/0005028].
- [82] A. V. Belitsky and D. Müller, Nucl. Phys. **B537**, 397 (1999), [hep-ph/9804379].
- [83] A. Belitsky, A. Freund and D. Müller, Nucl. Phys. **B574**, 347 (2000), [hep-ph/9912379].
- [84] A. V. Belitsky, A. Freund and D. Müller, Phys. Lett. **B493**, 341 (2000), [hep-ph/0008005].
- [85] A. Freund and M. McDermott, Phys. Rev. **D65**, 074008 (2002), [hep-ph/0106319].
- [86] A. V. Vinnikov, Code for prompt numerical computation of the leading order GPD evolution, hep-ph/0604248, 2006.
- [87] L. Schoeffel, private communication, 2006.
- [88] A. Radyushkin, Phys. Rev. **D56**, 5524 (1997), [hep-ph/9704207].
- [89] A. Belitsky, B. Geyer, D. Müller and A. Schäfer, Phys. Lett. **B 421**, 312 (1998), [hep-ph/9710427].
- [90] M. Polyakov and A. Shuvaev, On 'dual' parametrizations of generalized parton distributions, hep-ph/0207153, 2002.
- [91] V. Guzey and T. Teckentrup, Phys. Rev. **D74**, 054027 (2006), [hep-ph/0607099].
- [92] A. Shuvaev, Phys. Rev. **D60**, 116005 (1999), [hep-ph/9902318].
- [93] J. D. Noritzsch, Phys. Rev. **D62**, 054015 (2000), [hep-ph/0004012].
- [94] I. Balitsky and V. Braun, Nucl. Phys. **B311**, 541 (1989).
- [95] N. Kivel and L. Mankiewicz, Nucl. Phys. **B557**, 271 (1999), [hep-ph/9903531].
- [96] A. Manashov, M. Kirch and A. Schäfer, Phys. Rev. Lett. **95**, 012002 (2005), [hep-ph/0503109].

- [97] M. Kirch, A. Manashov and A. Schäfer, Phys. Rev. **D72**, 114006 (2005), [hep-ph/0509330].
- [98] D. Müller and A. Schäfer, Nucl. Phys. **B739**, 1 (2006), [hep-ph/0509204].
- [99] A. Belitsky, D. Müller, L. Niedermeier and A. Schäfer, Phys. Lett. **B437**, 160 (1998), [hep-ph/9806232].
- [100] A. Belitsky, D. Müller, L. Niedermeier and A. Schäfer, Nucl. Phys. **B546**, 279 (1999), [hep-ph/9810275].
- [101] D. Müller, Phys. Lett. **B634**, 227 (2006), [hep-ph/0510109].
- [102] K. Kumerički, D. Müller, K. Passek-Kumerički and A. Schäfer, Phys. Lett. **B648**, 186 (2007), [hep-ph/0605237].
- [103] Z. Chen, Nucl. Phys. **B525**, 369 (1997), [hep-ph/9705279].
- [104] A. Belitsky, D. Müller, L. Niedermeier and A. Schäfer, Nucl. Phys. **B593**, 289 (2001), [hep-ph/0004059].
- [105] P. Hoodbhoy and X. Ji, Phys. Rev. **D58**, 054006 (1998), [hep-ph/9801369].
- [106] M. Diehl, Eur. Phys. J. **C19**, 485 (2001), [hep-ph/0101335].
- [107] M. Diehl, T. Gousset, B. Pire and J. P. Ralston, Phys. Lett. **B411**, 193 (1997), [hep-ph/9706344].
- [108] J. Bjorken and S. Drell, *Relativistic Quantum Mechanics* (McGrawHill Book Company, New York, 1964).
- [109] P. Roman, *Introduction to Quantum Field Theory* (Wiley, New York, 1969).
- [110] S. Ferrara, R. Gatto and A. Grillo, Phys. Lett. **36B**, 124 (1971), 38B, 188 (E).
- [111] S. Ferrara, R. Gatto and A. Grillo, Phys. Lett. **38B**, 333 (1972).
- [112] S. Ferrara, R. Gatto and A. Grillo, Phys. Rev. **D5**, 3102 (1972).
- [113] S. Ferrara, A. Grillo and G. Parisi, Nucl. Phys. **B54**, 552 (1973).
- [114] D. Müller, Phys. Rev. **D58**, 054005 (1998), [hep-ph/9704406].
- [115] V. M. Braun, G. P. Korchemsky and D. Müller, Prog. in Part. and Nucl. Phys. **51**, 312 (2003), [hep-ph/0306057].

- [116] X. Ji, J. Phys. **G24**, 1181 (1998), [hep-ph/9807358].
- [117] F. Carlson, *Sur une classe de séries de Taylor*, PhD thesis, Uppsala University, 1914.
- [118] R. J. Eden, P. V. Landshoff, P. J. Olive and J. C. Polkinghorne, *The Analytic S-Matrix* (Cambridge University Press, 1966), p. 126.
- [119] O. V. Teryaev, Analytic properties of hard exclusive amplitudes, hep-ph/0510031.
- [120] M. V. Polyakov and C. Weiss, Phys. Rev. **D60**, 114017 (1999), [hep-ph/9902451].
- [121] A. Belitsky, D. Müller, A. Kirchner and A. Schäfer, Phys. Rev. **D64**, 116002 (2001), [hep-ph/0011314].
- [122] O. V. Teryaev, Phys. Lett. **B510**, 125 (2001), [hep-ph/0102303].
- [123] M. J. Creutz, S. D. Drell and E. A. Paschos, Phys. Rev. **178**, 2300 (1969).
- [124] M. Damashek and F. J. Gilman, Phys. Rev. **D1**, 1319 (1970).
- [125] C. A. Dominguez, C. Ferro Fontan and R. Suaya, Phys. Lett. **B31**, 365 (1970).
- [126] G. Schierholz, Phys. Rev. **D10**, 1261 (1974).
- [127] S. J. Brodsky, F. E. Close and J. F. Gunion, Phys. Rev. **D5**, 1384 (1972).
- [128] S. J. Brodsky, F. E. Close and J. F. Gunion, Phys. Rev. **D8**, 3678 (1973).
- [129] M. Bander, Phys. Rev. **D5**, 3274 (1972).
- [130] Y. Frishman, Phys. Rept. **13**, 1 (1974).
- [131] J. M. Cornwall, D. Corrigan and R. E. Norton, Phys. Rev. Lett. **24**, 1141 (1970).
- [132] J. M. Cornwall, D. Corrigan and R. E. Norton, Phys. Rev. **D3**, 536 (1971).
- [133] F.-M. Dittes and A. Radyushkin, Phys. Lett. **134B**, 359 (1984).
- [134] M. Sarmadi, Phys. Lett. **143B**, 471 (1984).
- [135] S. Mikhailov and A. Radyushkin, Nucl. Phys. **B254**, 89 (1985).
- [136] D. Müller, Phys. Rev. **D49**, 2525 (1994).
- [137] B. Melić, D. Müller and K. Passek-Kumerički, Phys. Rev. **D68**, 014013 (2003), [hep-ph/0212346].

- [138] A. Belitsky and A. Schäfer, Nucl. Phys. **B527**, 235 (1998), [hep-ph/9801252].
- [139] B. Melić, B. Nžić and K. Passek, Phys. Rev. **D65**, 053020 (2002), [hep-ph/0107295].
- [140] G. Curci, W. Furmanski and R. Petronzio, Nucl. Phys. **B175**, 27 (1980).
- [141] E. B. Zijlstra and W. L. van Neerven, Nucl. Phys. **B383**, 525 (1992).
- [142] E. Zijlstra and W. van Neerven, Nucl. Phys. **B417**, 61 (1994); *ibid.* **B426**, 245 (1994) (E); *ibid.* **B773**, 105 (2007) (E).
- [143] S. Moch, J. A. M. Vermaseren and A. Vogt, Nucl. Phys. **B688**, 101 (2004), [hep-ph/0403192].
- [144] W. L. van Neerven and A. Vogt, Nucl. Phys. **B568**, 263 (2000), [hep-ph/9907472].
- [145] M. Gluck, E. Reya and A. Vogt, Z. Phys. **C48**, 471 (1990).
- [146] W. Vogelsang, Nucl. Phys. **B475**, 47 (1996), [hep-ph/9603366].
- [147] R. Mertig and W. van Neerven, Z. Phys. **C70**, 637 (1996), [hep-ph/9506451].
- [148] A. Vogt, S. Moch and J. A. M. Vermaseren, Nucl. Phys. **B691**, 129 (2004), [hep-ph/0404111].
- [149] J. Blümlein and S. Kurth, Phys. Rev. **D60**, 014018 (1999), [hep-ph/9810241].
- [150] J. A. M. Vermaseren, Int. J. Mod. Phys. **A14**, 2037 (1999), [hep-ph/9806280].
- [151] J. Blümlein and S.-O. Moch, Phys. Lett. **B614**, 53 (2005), [hep-ph/0503188].
- [152] D. Maitre, Comput. Phys. Commun. **174**, 222 (2006), [hep-ph/0507152].
- [153] W. L. van Neerven and A. Vogt, Nucl. Phys. **B588**, 345 (2000), [hep-ph/0006154].
- [154] A. Belitsky, D. Müller, L. Niedermeier and A. Schäfer, Phys. Lett. **B474**, 163 (2000), [hep-ph/9908337].
- [155] A. V. Belitsky and D. Müller, Nucl. Phys. **B527**, 207 (1998), [hep-ph/9802411].
- [156] A. P. Bakulev and N. G. Stefanis, Nucl. Phys. **B721**, 50 (2005), [hep-ph/0503045].
- [157] K. Goeke, M. Polyakov and M. Vanderhaeghen, Prog. Part. Nucl. Phys. **47**, 401 (2001), [hep-ph/0106012].
- [158] M. Diehl, T. Feldmann, R. Jakob and P. Kroll, Eur. Phys. J. **C39**, 39 (2005), [hep-ph/0408173].

- [159] M. Guidal, M. V. Polyakov, A. V. Radyushkin and M. Vanderhaeghen, Phys. Rev. **D72**, 054013 (2005), [hep-ph/0410251].
- [160] C. F. Perdrisat, V. Punjabi and M. Vanderhaeghen, Prog. Part. Nucl. Phys. **59**, 694 (2007), [hep-ph/0612014].
- [161] W. Melnitchouk, R. Ent and C. Keppel, Phys. Rept. **406**, 127 (2005), [hep-ph/0501217].
- [162] E. P. Wigner, *Group Theory and its Application to the Quantum Mechanics of Atomic Spectra* (Academic Press, New York, 1959).
- [163] M. Diehl, T. Gousset, B. Pire and O. Teryaev, Phys. Rev. Lett. **81**, 1782 (1998), [hep-ph/9805380].
- [164] S. D. Drell and T.-M. Yan, Phys. Rev. Lett. **24**, 181 (1970).
- [165] QCDSF, M. Gockeler *et al.*, Nucl. Phys. Proc. Suppl. **140**, 399 (2005), [hep-lat/0409162].
- [166] D. Müller, *Pomeron dominance in deeply virtual Compton scattering and the femto holographic image of the proton*, hep-ph/0605013.
- [167] A. P. Szczepaniak and J. T. Londergan, Phys. Lett. **B643**, 17 (2006), [hep-ph/0604266].
- [168] A. Donnachie and H. G. Dosch, Phys. Lett. **B 502**, 74 (2001), [hep-ph/0010227].
- [169] A. Freund, M. McDermott and M. Strikman, Phys. Rev. **D67**, 036001 (2003), [hep-ph/0208160].
- [170] M. Capua, S. Fazio, R. Fiore, L. Jenkovszky and F. Paccanoni, Phys. Lett. **B645**, 161 (2007), [hep-ph/0605319].
- [171] F. James, *Minuit reference manual, version 94.1* (CERN, 1994).
- [172] S. Forte, Int. J. Mod. Phys. **A21**, 769 (2006), [hep-ph/0509371].
- [173] A. Shuvaev, K. Golec-Biernat, A. Martin and M. Ryskin, Phys. Rev. **D60**, 014015 (1999), [hep-ph/9902410].
- [174] H1, S. Aid *et al.*, Nucl. Phys. **B470**, 3 (1996), [hep-ex/9603004].
- [175] S. Alekhin, Phys. Rev. **D68**, 014002 (2003), [hep-ph/0211096].
- [176] H1, C. Adloff and Others, Phys. Lett. **B483**, 23 (2000), [hep-ex/0003020].

- [177] ZEUS, S. Chekanov *et al.*, Eur. Phys. J. **C24**, 345 (2002), [hep-ex/0201043].
- [178] M. Strikman and C. Weiss, Phys. Rev. **D69**, 054012 (2004), [hep-ph/0308191].
- [179] L. Frankfurt, M. Strikman and C. Weiss, Ann. Rev. Nucl. Part. Sci. **55**, 403 (2005), [hep-ph/0507286].
- [180] I. V. Anikin and O. V. Teryaev, Phys. Rev. D **76**, 056007 (2007), arXiv:0704.2185 [hep-ph].
- [181] M. Diehl and D. Y. Ivanov, Eur. Phys. J. C **52**, 919 (2007), arXiv:0707.0351 [hep-ph].
- [182] M. V. Polyakov, *Tomography for amplitudes of hard exclusive processes*, arXiv:0707.2509 [hep-ph].